Understanding igneous processes through zircon trace element systematics: prospects and pitfalls

Marín Ósk Hafnadóttir

Dissertations in Geology at Lund University,
Master's thesis, no 376
(45 hp/ECTS credits)

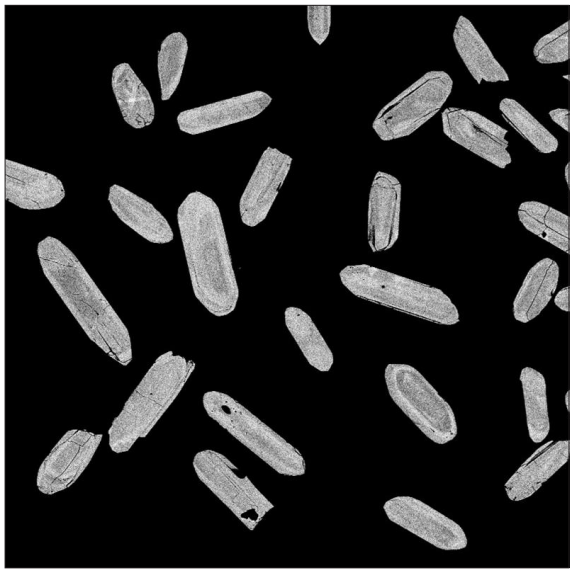

Department of Geology
Lund University
2014

Understanding igneous processes through zircon trace element systematics: prospects and pitfalls

Master's thesis

Marín Ósk Hafnadóttir

Department of Geology
Lund University
2014

Contents

Cover Picture: A few zircon grains from sample ASGH030A. Picture by Marín Ósk Hafnadóttir.

Understanding igneous processes through zircon trace element systematics: prospects and pitfalls

MARÍN ÓSK HAFNADÓTTIR

Hafnadóttir, M.Ó., 2014: Understanding igneous processes through zircon trace element systematics: prospects and pitfalls. *Dissertations in Geology at Lund University*, No. 376, 109 pp. 45 hp (45 ECTS credits).

Abstract: Zircon were extracted from five granitoids in the Birimian terrane in Ghana, and detrital zircon were sampled from six locations in Central West Greenland. Of these, one population is derived from the Palaeoproterozoic Prøven Igneous Complex. The remaining five populations are derived from the Archean basement in Central West Greenland. Zircon populations were analyzed with the LA-ICP-MS technique for *in situ* trace element abundances in order do assess igneous processes from the zircon compositions. Zircon populations are variably LREE enriched, which stems from secondary processes, and a screening process was implemented to identify altered zircon. Screening is based on increased Lanthanum, Uranium and Thorium concentrations within the zircon as well as low Ce-anomalies. Remaining trace element data demonstrated that the zircon populations were generated in continental crust magmas, as the populations have higher U/Yb and generally lower Y concentrations than oceanic zircon. Additionally, the U/Yb is relatively constant from the Hadean to the Palaeoproterozoic, which may indicate an earlier onset of plate tectonics than commonly depicted. Negative Eu-anomalies and Sr concentrations within zircon grains provide constraints on plagioclase fractionation in the source and consequently depth of melting. The Archean zircon generally have none to less negative Eu-anomalies and higher Sr concentrations than zircon from the Prøven Igneous Complex and Birimian terrane, as well as Hadean zircon from the Jack Hills and Mount Narryer in Australia. This difference might be ascribed to plagioclase fractionation in the source of the Hadean and Palaeoproterozoic rocks. Generally, Archean rocks do not display plagioclase fractionation signatures due to genesis at depths where plagioclase is not stable. However, a large portion of the Archean population overlaps with the other populations indicating plagioclase fractionation. This may be due to them being derived from magmas that were generated at shallower depths than generally portrayed for Archean rocks. To constrain the source depth, garnet was a feasible phase, as it is stable at greater depths than plagioclase. An attempt to find garnet signatures in zircon, however, proved futile, as zircon has higher partition coefficients than garnet for the elements garnet and zircon co-incorporate.

Keywords: Zircon, Ghana, West Greenland, Archean, Palaeoproterozoic, Hadean, Birimian, hydrothermal alteration, plagioclase fractionation

Supervisor: Anders Scherstén

Marín Ósk Hafnadóttir, Department of Geology, Lund University, Sölvegatan 12, SE-223 62 Lund, Sweden.
E-mail: marinoskh@gmail.com

Att förstå magmatiska processer genom spårelementsystematik i zirkon: möjligheter och fällor

MARÍN ÓSK HAFNADÓTTIR

Hafnadóttir, M.Ó., 2014: Att förstå magmatiska processer genom spårelementsystematik i zirkon: möjligheter och fällor. *Examensarbeten i geologi vid Lunds universitet*, Nr. 376, 109 sid. 45 hp (45 ECTS credits).

Sammanfattning: Zirkon från magmatiska bergarter extraherades från fem granitoider i Birimianterrängen i Ghana., och detritala zirkoner provtogs från sex platser i centrala Västgrönland. Av dessa härrör en population från palaeoproterozoikum i Prøvens magmatiska komplex. De återstående fem detritala populationerna härrör från Arkeiska källor i Västgrönland. Zirkon-populationerna analyserades med LA-ICP-MS-teknik för in situ-bestämning av spårämnen för att utvärdera hur magmatiska processer kan spåras i zirkonsammansättningen. Zirkonpopulationerna är berikade i LREE i varierande grad, vilket härrör från sekundära processer, varpå en sållningsprocess genomfördes för att identifiera förändrade zirkoner. Urvalet grundas på förhöjd lantan-, uran- och toriumkoncentrationer i zirkon, samt låga Ce-anomalier. Kvarvarande spårelementdata visade att zirkon-populationerna genererades i kontinentala magmor, eftersom dessa populationer har högre U/Yb och generellt lägre Y-koncentrationer än oceaniska zirkoner. Vidare är U/Yb relativt konstant från Hadean till Palaeoproterozoisk tid, vilket kan tyda på att plattektonik började tidigare än vad som allmänt antas. Negativa Eu-anomalier och Sr-koncentrationer i zirkon indikerar plagioklasfraktionering i källan och därmed djup av uppsmältning . De arkeiska zirkonerna har i allmänhet ingen mindre negativ Eu-anomalier och högre Sr-koncentrationer än zirkon från den Prøvens magmatiska komplex och Birimianterrängen, liksom Hadeiska zirkoner från Jack Hills och Mount Narryer i Australien. Denna skillnad kan tillskrivas plagioklasfraktionering i källan av hadeiska och proterozoiska bergarter. Generellt visar arkeiska bergarter inte tecken på plagioklasfraktionering då de bildats på djup där plagioklas inte är stabilt. En stor del av den arkeiska populationen överlappar med andra populationer, vilket indikerar plagioklasfraktionering. Detta kan tyda på att en del magmor bildades på grundare djup än vad som allmänt antas för arkeiska bergarter. Granat är ett mineral som är stabilt vid större djup, och ingår i restitmaterialet vid uppsmältning. Ett försök att hitta granatsignaturer i zirkon visade sig dock fruktlöst eftersom zirkon har högre fördelningskoefficienter för de elementer som är kompatibla i både granat och zirkon.

Nyckelord: Zirkon, Ghana, Västgrönland, Arkeikum, Palaeoproterozoikum, Hadean, Birimian, hydrotermal-omvandling, plagioklasfraktionering

Handledare: Anders Scherstén

Ämnesinriktning: Berggrundsgeologi

Marín Ósk Hafnadóttir, Geologiska institutionen, Lunds universitet, Sölvegatan 12, 223 62 Lund, Sverige.
E-post: marinoskh@gmail.com

1 Introduction

1.1 Previous work

Zircon commonly occurs as an accessory mineral in igneous rocks; mainly those of intermediate to felsic composition (Ballard et al. 2002). Zircon typically incorporates significant amounts of various minor- and trace elements, e.g. Rare-Earth Elements (REE), U, Th, and Hf. It is therefore an important trace mineral with a number of important applications in petrology. It has proven itself as a trustworthy U-Pb geochronometer (Hoskin & Schaltegger 2003) and is widely used in Lu/Hf, Sm/Nd and oxygen isotope research (Kinny & Maas 2003, Valley 2003). The zircon crystal lattice is robust and zircon is the only known preserved remnant from the Hadean. For this reason alone, it is important to understand the link between zircon isotope and trace element chemistry as this is currently the only link to the understanding of the early Earth evolution.

Zircon with mantle affinities, (kimberlites) have distinguishable chemical signatures; low concentrations of trace elements, e.g. REE+Y, Th, U, and low HREE amounts (Heaman et al. 1990, Belousova et al. 1998). Heaman et al. (1990) also discriminated zircons from carbonatites and nepheline syenites based on their low Hf contents, and mafic zircons based on their high concentrations of Sc, fractionated chondrite normalized REE patterns (high Lu/Sm), high Th/U and low Hf contents. However, many have reported difficulties in discriminating differences in zircon that originate from felsic rocks. Maas et al. (1992) note that there is no single distinct zircon geochemical characteristic that may ascribe felsic origin to Mount Narryer and Jack Hills detrital zircon (3.9-4.2 Ga), although the combination of data available indicates that they are. There is significant overlap in REE patterns and concentrations between and within zircon populations from various granitoids, making numerous attempts of discrimination futile (Heaman et al. 1990, Hoskin & Ireland 2000, Hoskin et al. 2000). Hoskin & Ireland (2000) suggest this may be because at zircon saturation point in a melt, the melt may be considered broadly granitic.

Distribution of REE between zircon and melt has been inferred from calculated partition coefficients but has proven difficult - especially for light REE (LREE) - as the values calculated cover a much too large scale (Hanchar & van Westrenen 2007) to provide consistency. Partition of REE into zircon depends on various features, such as melt composition, other crystallizing phases, volatility and temperature. As zircons may crystallize over a large time span within an evolving melt, a single population may thus present a large intrasample variation (Grimes et al. 2009).

Grimes et al. (2007) has created a method of discrimination between oceanic and continental zircon, based on Uranium, Ytterbium and Yttrium concentrations and ratios. Also, light REE Europium and Cerium have been used to infer feldspar phase stability in the source melt, and oxidation state and temperature of the melt, respectively (e.g. Kemp & Hawkesworth 2003, Ballard et al. 2002, Pettke et al. 2005, Claiborne et al. 2010, Trail et al. 2012). This work continues along that ilk. The aim is to observe any systematic trace element signatures in various zircon populations and to see if these can be linked to specific igneous processes. If so, these signatures might serve to shed light on how and where zircon, and especially detrital zircon, originated.

1.2 Zircon

Zircon ($ZrSiO_4$) is a tetragonal orthosilicate (Finch & Hanchar 2003). Its structure involves chains of ZrO_8 that share edges and corners with SiO_4 (Fig. 1).

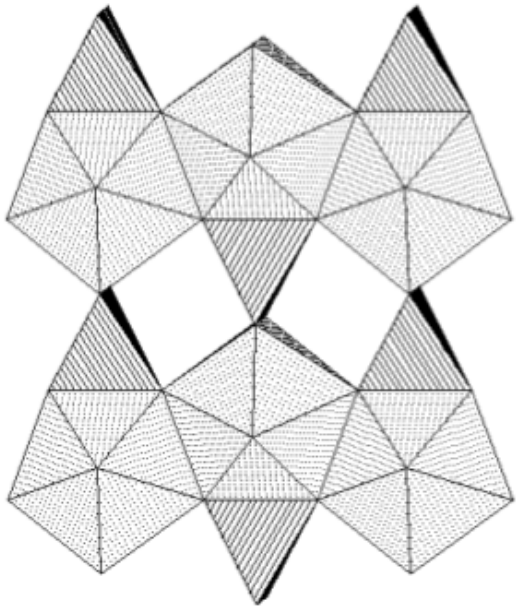

Fig. 1. The zircon structure. ZrO_8 (grey shaded) are joined together to form chains. These chains are linked together by SiO_4 (striped). (Image from Finch & Hanchar 2003).

Zircon is rarely pure. There are numerous elements that substitute for Zr^{4+} (0.84 Å) and Si^{4+} (0.26 Å), either by simple- or coupled substitution. Hf^{4+} substitutes readily for Zr^{4+}, due to very similar ionic radius and the same valence state (Fig. 2), and thus sometimes exceeds 3 wt.% in zircon. This is an example of simple substitution. U^{4+} and Th^{4+} substitute for Zr^{4+} in the same way (Shannon 1976, Hoskin & Schaltegger 2003). Coupled substitutions in zircons are dominated by the so-called 'xenotime' substitution: $(Y+REE)^{3+} + P^{5+} \rightarrow Zr^{4+} + Si^{4+}$. This is the main mechanism by which REE are incorporated into zircon (Hoskin & Schaltegger 2003). Other means of REE incorporation must be in effect, however. If the 'xenotime' substitution was the sole mechanism, the ratio between REE and P would be ~1. Nevertheless, REE:P is usually larger than that (Speer 1982, Hinton

& Upton 1991, Hoskin et al. 2000, Hanchar et al. 2001). The compatibility of REE^{3+} (La through Lu) increase with decreasing ionic radius; La has a VIII-coordinated radius of 1.160 Å whereas Lu has 0.977 Å. Thus the heavy REE (Tb-Lu) more closely correspond to Zr^{4+} 0.84 Å ionic radius than the LREE (La-Gd) and are present in zircon in larger quantities (Fig. 2) (Hoskin & Schaltegger 2003).

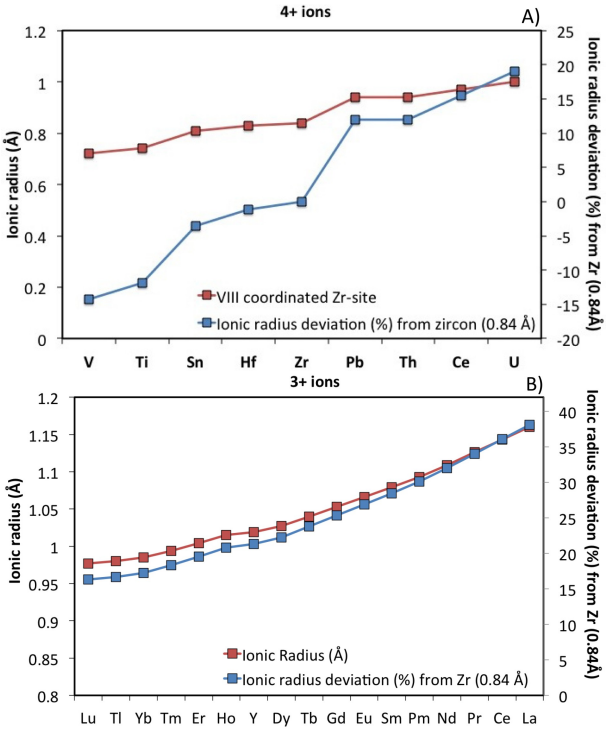

Fig. 2. Diagrams showing the ionic radius of 4+ and 3+ ions and percent deviation from Zr ionic radius of 0.84 Å. The larger the ionic radius relative to the 0.84 Å of zircon, the more difficult the substitution process. According to diagram A) Hf should readily substitute for Zr, as is observed. Heavier REE also substitute more readily for Zr than LREE (diagram B). Also Ce^{4+} deviates less from Zr than Ce^{3+}, with regard to ionic radius and valence state, and thus Ce^{4+} substitutes more readily for Zr than Ce^{3+}.

Exceptions to this are Ce and Eu. Eu can form a reduced species with a valence state of +2 in addition to the normal REE valency of +3 (Drake 1975). The valence state of Eu^{2+} and its much too large ionic radius (1.25 Å), make Eu incompatible into the Zr^{4+} (0.84 Å) site (Shannon 1976, Hoskin & Schaltegger 2003). Thus Eu is usually present to a lesser degree than expected in zircon, and forms a negative anomaly relative to its neighbors, Sm and Gd. The anomaly is a function of the Eu^{2+}/Eu^{3+} in the magma but is quantified with the use of Eu/Eu*, where Eu is the actual amount of Eu in the mineral/rock. Eu* is the amount of Eu from linear interpolation of its REE neighbors; Sm and Nd (Hoskin & Schaltegger 2003).

$$\frac{Eu}{Eu^*} = \frac{Eu_N}{\sqrt{Sm_N \times Gd_N}}$$

The opposite trend occurs regarding Ce concentrations. Apart from its usual trivalent state, Ce may be present in magma in a tetravalent state. The anomaly spans from the availability of Ce^{4+} in melt coupled with zircons affinity for Ce^{4+} over Ce^{3+} (Hinton & Upton 1991, Schaltegger et al. 1999, Hoskin & Schaltegger 2003). Ce^{4+} (0.97 Å) substitutes readily for Zr^{4+} (0.84 Å) in zircon (Fig. 2) (Shannon 1976, Murali et al. 1983, Claiborne et al. 2010, Trail et al. 2012). Thus, Ce is usually present in excessive amounts relative to the adjacent La and Pr. Ce/Ce* is the quantification of a Ce-anomaly in zircon; Ce represents the Ce measured and Ce* the Ce expected to make up a smooth LREE curve (Hoskin & Schaltegger 2003).

$$\frac{Ce}{Ce^*} = \frac{Ce_N}{\sqrt{La_N \times Pr_N}}$$

REE are incompatible in numerous silicate minerals. This stems from their relatively high valence state and ionic radii. Thus, as zircon saturation point is reached, REE has become enriched in the remaining melt (Winter 2010). Theoretically, the REE abundances in zircon should thus represent the REE in the melt at the time of crystallization, given that the zircon was in equilibrium with the melt. Diseqilibrium is however more common (Watson 1996, Hoskin & Ireland 2000).

Apart from substitution into the Zr^{4+} and Si^{4+} sites, zircon may incorporate various impurities into interstitial voids. This stems from the fact that the zircon crystal structure is relatively open (Fig. 1) (Finch & Hanchar 2003). This is limited to impurities that do not pose too much stress on the crystal structure (Hanchar et al. 2001, Finch et al. 2001, Finch & Hanchar 2003). More space for impurities may be created by decay of the radioactive U and Th (Seitz 1949). The process involves emittance of both α-recoil nucleus (daughter isotope) as well as α-particle (He nucleus). These collide with their surroundings, creating disorder and displacements, into which various cations may settle (Seitz 1949, Woodhead et al. 1991, Ellsworth et al. 1994, Geisler et al. 2001, Geisler et al. 2007).

Nevertheless, zircon is generally resistant towards chemical as well as physical disturbances. It has been known to endure metamorphism and even melting of the host rock. Its closure temperature, albeit debated, has been commonly mentioned to be as high as >1000°C (Cherniak et al. 1997). Zircon is thus an excellent geochemical recorder that has yet to reach its full potential.

2 Geological settings

2.1 Mount Narryer and Jack Hills, Australia

The Yilgarn Craton in Western Australia is an extensive piece of preserved Archean crust (Mole et al. 2012; fig. 3). It is divided into numerous terranes including the Narryer Gneiss Complex, within which the oldest preserved zircons have been discovered. Comprising the northwestern part of the Yilgarn Craton, the Narryer Gneiss Complex is mainly composed of granitic gneisses; the Meeberrie (3680-3600 Ma), Eurada (3490-3440 Ma) and Dugel gneisses (3400-3300 Ma). The main gneissic fabric is due to the collision between the Narryer terrane and Murchison terrane (Myers & Williams 1985, Myers 1988, Kinny et al. 1988, Nutman et al. 1991, Nutman et al. 1993, Crowley et al. 2005; fig. 3). Other rock formations comprise only ~10% of the Narryer Gneiss Complex, and within that proportion are the Mount Narryer and Jack Hills formations (Williams and Myers 1987, Myers 1988, Kinny et al. 1990).

Mount Narryer is a 2.5 km wide, 21 km long and >2 km thick sedimentary sequence, composed mainly of quartzite and conglomerates (Iizuka et al. 2010). It has been folded and metamorphosed to granulite facies. Nevertheless, well-preserved cross-bedding and other sedimentary structures occur throughout the sequence (Crowley et al. 2005). The units that comprise the sequence were deposited between 3.28 Ga and 2.7 Ga, but detrital zircons with U/Pb ages up to 4.28 Ga have been found within the sequence (Froude et al. 1983, Compston & Pidgeon 1986, Kinny et al. 1990, Crowley et al. 2005, Pidgeon & Nemchin 2006).

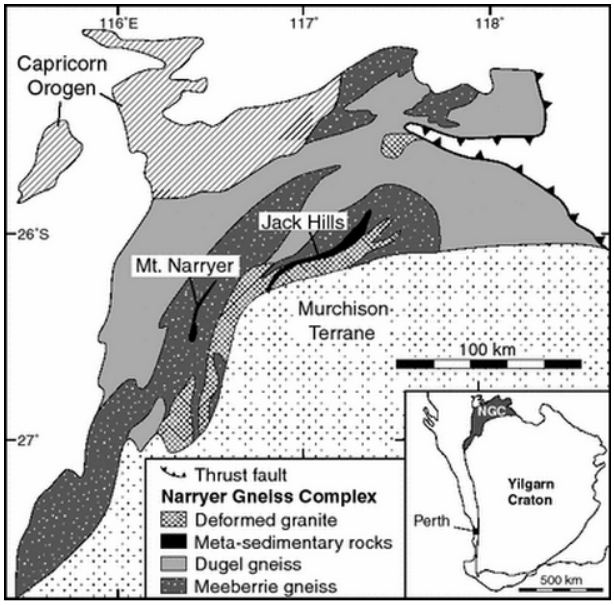

Fig. 3. A geological map of the Narryer Gneiss Complex and the locations of Mount Narryer and Jack Hills metasedimentary belts. North of the Narryer Gneiss Complex is the Capricorn Orogen, formed in in the collisional event between the Archean Pilbara Craton and Yilgarn Craton 1830-1780 Ma (Occhipinti et al. 1999, Cawood & Tyler 2004). The inlet represents western Australia and the extension of the Yilgarn Craton and Narryer Gneiss Complex. (Figure from Myers 1988, modified by Iizuka et al. 2010).

Jack Hills is likewise a narrow meta-sedimentary belt, about 70 km long. It is composed mainly of banded iron formations, chert, quartzite, sandstones and conglomerates (Crowley et al. 2005). However, only pieces of intact sedimentary stratigraphy is preserved as Jack Hills shows more deformation and disruption than Mount Narryer (Crowley et al. 2005). Deposition occurred between 3.1 Ga and 2.6 Ga (Pidgeon & Wilde 1998, Nelson 2001). Detrital zircons as old as 4.4 Ga have been discovered within the Jack Hills meta-sedimentary belt (Wilde et al. 2001).

The Mount Narryer and Jack Hills >3900 Ma zircons are the sole remnants of a now eroded crust of unknown composition.

2.2 West African Craton

The main component of West Africa is the West African Craton (WAC). It may be divided three-ways into the Reguibat Shield in the north, the Neoproterozoic to Phanerozoic Tadoueni Basin in the center and the Man Shield in the south (Fig. 4). Both Reguibat and Man Shields may be further divided into an Archean nucleus to the west and a Palaeorpoterozoic domain to the east (Ennih & Liégeois 2008). The Kedougou-Kenieba and Kayers inliers attest to the continuation of

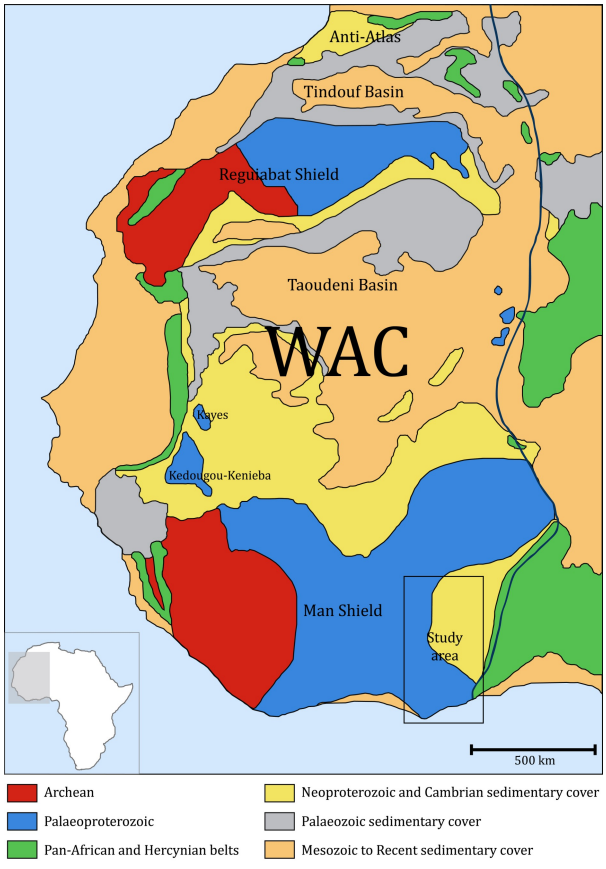

Fig. 4. Major geological units of the West African Craton. Blue line represents the eastern border of the craton. (Modified by Bára Dröfn Kristinsdóttir (unpublished thesis) from Ennih & Liégeois 2008)

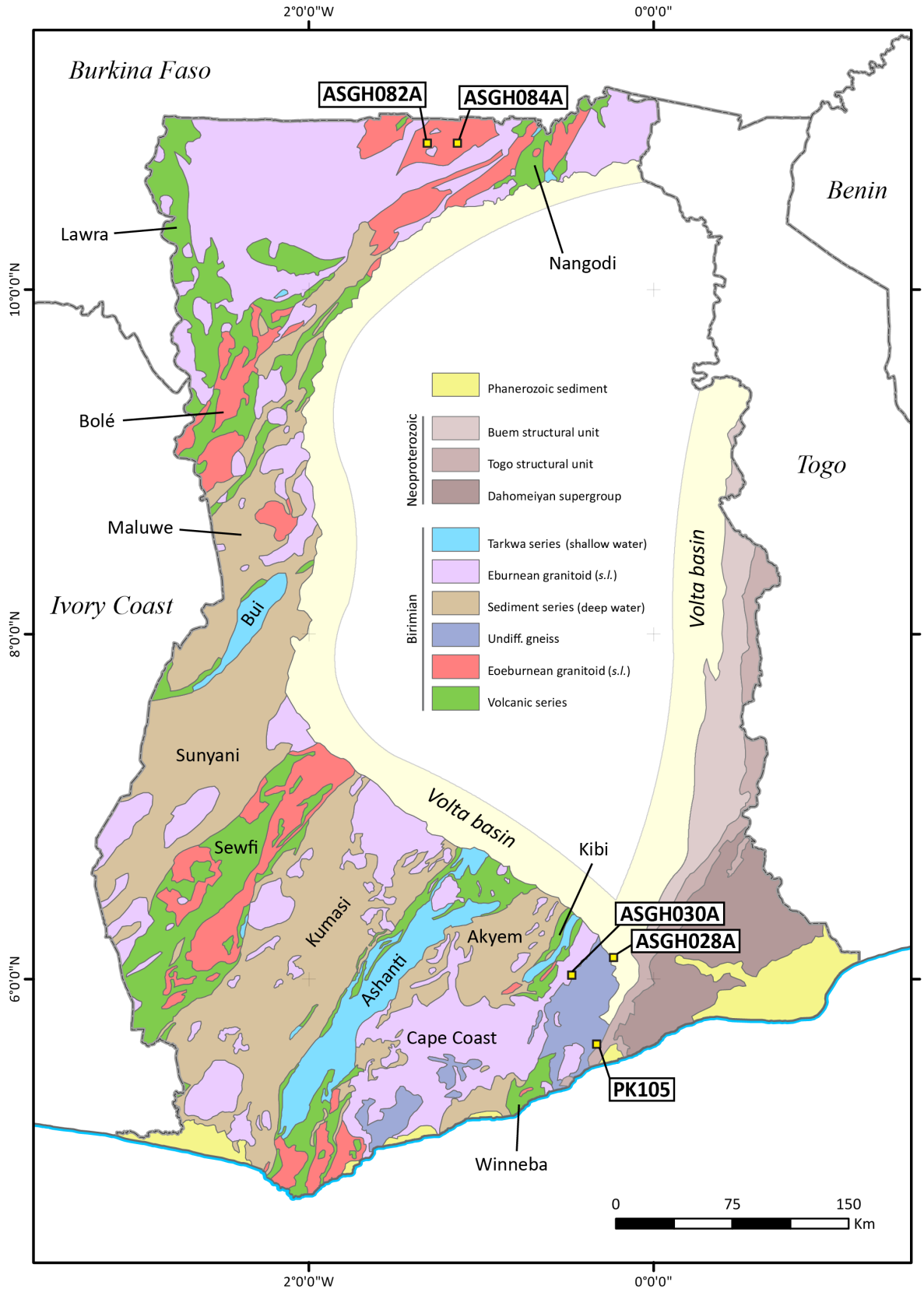

Fig. 5. Geological map of Ghana with Birimian sample locations marked. The map is projected using Ghana Metre Grid. Scale is 1:1 000 000. (Modified by Mikael Grenholm (unpublished thesis) from Agyei Duodu et al. (2009), with minor additions from Adadey et al. (2009) and changes based on data from Baratoux et al. (2011)).

the Palaeorpoterozoic domain beneath the Tadoueni Basin (Boher et al. 1992). The Archean and Palaeoproterozoic domains are separated by the Sassandra fault in the Man Shield and the Zednes fault in the Reguibat Shield (Boher et al. 1992). Pan-African and Hercynian (0.6 Ga) mobile belts envelope the WAC to the east and to the southwest (Kouamelan et al. 1997). Correlation of lithological units and age data indicate that the WAC and São Luís Craton in South America formed a single craton in Early Proterozoic (Abouchami et al. 1990, Boher et al. 1992, Feybesse et al. 2006).

2.2.1 Birimian terrane

The Palaeoproterozoic domain of the WAC is generally termed the Birimian terrane, which consists of volcanic belts separated by sedimentary basins (Leube et al. 1990, Taylor et al. 1992; fig. 5). These are mainly NE-SW trending (Leube et al. 1990). The volcanic belts are composed of tholeiitic flows, hyaloclastites and pillow lavas, overlain by calc-alkaline dacitic to rhyolitic tuffs and lavas (Attoh 1982, Leube et al. 1990, Sylvester & Attoh 1992). The sedimentary basins comprise primarily volcaniclastics, greywackes and argillitic sediments (Leube et al. 1990,
Eisenlohr & Hirdes 1992). Four felsic intrusive suites have been emplaced in the Birimian terrane in Ghana. Dixcove granitoids intrude mainly the volcanic belts. These are non-foliated, metaluminous plutons, commonly dioritic to granidioritic in composition (Leube et al. 1990). Peraluminous, granodioritic Cape Coast intrusions have been emplaced within the sedimentary basins (Leube et al. 1990) and show foliation (Taylor et al. 1992). These basin and belt granitoids are coeval (Leube et al. 1990). Rarer are the post-tectonic (Hirdes et al. 1992), peraluminous, granitic K-rich Bongo plutons that intrude the Tarkwaian sediments. Finally, the unique Winneba granite pluton is the only intrusion that shows signatures indicative of Archean contribution (Leube et al. 1990). Tarkwaian sediments unconformably rest on the Birimian terrane (Taylor et al. 1992). These are erosional products of the Birimian terrane (Davis et al. 1994). A large part of the Birimian terrane in Ghana is covered by the Late Precambrian to Paleozoic Volta basin (Leube et al. 1990).

2.2.2 Evolution of the Birimian terrane

It has proven to be an elusive task to interpret the geodynamic setting of the Birimian terrane. Leube et al. (1990) proposed a model of intracratonic rifting, based on structural evidence and the Mid-Ocean Ridge Basalt (MORB) affinity of the tholeiites of the Birimian terrane. Others have followed in the same footsteps, favouring the intracratonic basin explanation (Watkins et al. 1993, Vidal & Alric 1994, Feybesse & Milési 1994). However, many have suggested that the juvenile geochemical signatures and general lack of continental signature are indicative of formation in an oceanic environment (e.g. Abouchami et al. 1990). Abouchami et al. (1990) and Lompo (2009) suggested intraoceanic plume activity. Boher et al. (1992), however, explained the calc-alkaline rocks with subduction activity. Furthermore, the rocks of Haute-Comoé in Ivory Coast have MORB and Island Arc Basalt (IAB) characteristics which Vidal & Alric (1994) interpreted to be due to them being of back-arc basin origin. Soumaila et al. (2004) place the Nigerian Diagorou-Darbani greenstone belt in a back-arc basin environment, based on geochemical analysis of mafic rocks. Dampare et al. (2008) follow along that ilk with their geochemical analysis of the Ghanaian Ashanti belt. Furthermore, they find intra-oceanic island arc and fore-arc signatures. Numerous studies have likewise placed the Birimian greenstone belts in an island arc setting. Sylvester & Attoh (1992) note close resemblances between the Birimian terrane and modern, immature island arcs. Additionally, Salah et al. (1996) depicted evolution from island arc to a volcanic arc at a continental margin, based on geochemical evidence. Sediments from the upper Birimian terrane in Djibo greenstone belt, Burkina Faso, show source signatures indicative of continental margin being supplied by a volcanic arc. Isotopic data (Dia et al. 1997) provide further support for the arc setting.

However the Birimian volcanic belts and sedimentary basins were formed, they underwent deformation, metamorphism to greenschist facies and granitoid emplacement during the Eburnean Orogenic event at ~2.13-1.98 (Hirdes et al. 1992, Boher et al. 1992, Hirdes & Davis 1998, Feybesse et al. 2006). The Birimian zircons in this work were retrieved from basin and belt granitoids emplaced during the Eburnean event.

2.3 Nuussuaq Basin, West Greenland

The detrital zircons of Archean age were retrieved from the extensive Nuussuaq Basin in Central West Greenland (Fig. 6). This basin is a part of a basin complex that records the opening of the Labrador Sea in the Cretaceous to Paleocene. The basin is composed of deposits that range from fan-delta sandstones to deep sea anoxic shales. These deposits register an early Cretaceous rifting phase as well as a late Cretaceous rifting episode, with accompanying subsidence and uplift. Latest deposits in Nuussuaq Basin include volcanics that testify to sea-floor spreading and continental break-up (Scherstén et al. 2007).

2.4 Prøven Igneous Complex, West Greenland

The northeast segment of the Laurentian craton is composed of several Palaeoproterozoic collisional orogens. Thereof is the Nagssugtoqidian-Rinkian Orogen, into which the Prøven Igneous Complex (PIC) intrudes, along with the Palaeoproterozoic metasediments of the Karrat Group (Thrane et al. 2005; fig. 7). The PIC intrusion is over 100 km in diameter and is located in the Central West Greenland. The main body is opx-bearing granite and is foliated, increasing from

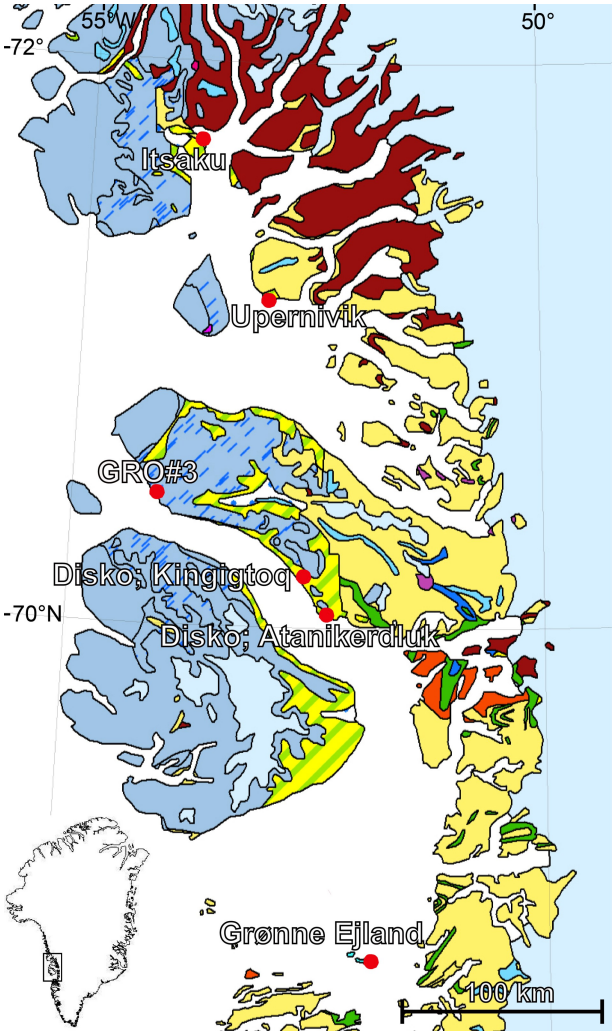

Fig. 6. Geological map of the Central West Greenland and sample locations of the West Greenland detrital zircons. Map scale is 1:2500000. (Modified after Escher & Pulvertaft (1995))

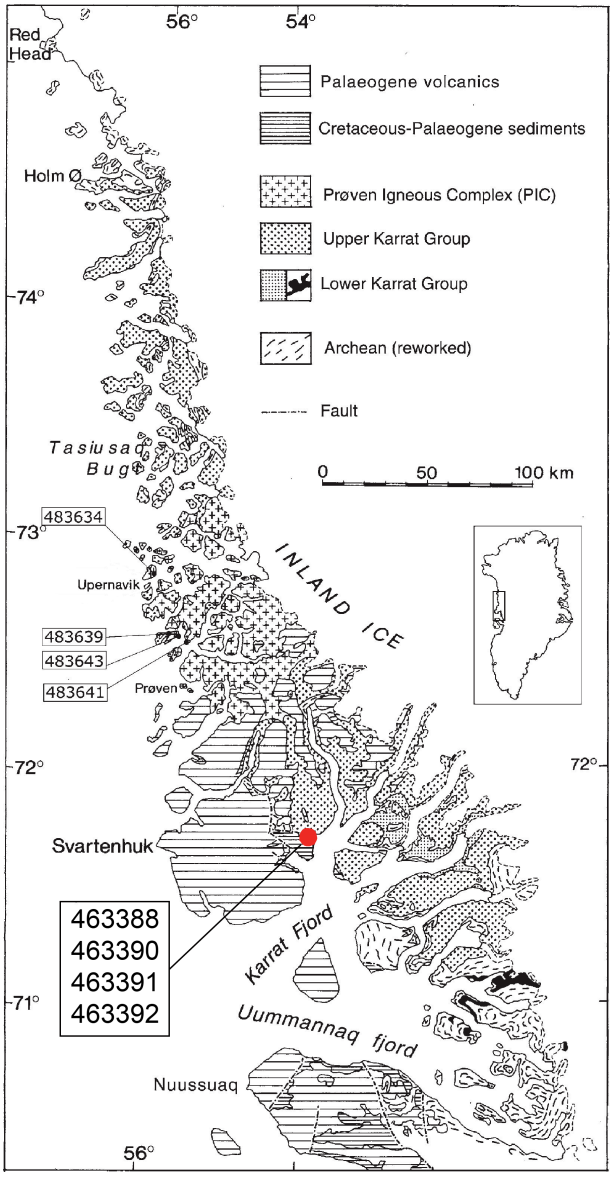

Fig. 7. Geological sketch map of Prøven Igneous Complex and surrounding area. Samples 483634, 483639, 483643 and 483641 are whole rock samples used in this work, whereas 463388, 463390-463392 represent host rocks of detrital PIC zircon used in this work. (Image from Henderson and Pulvertaft 1987).

weak in the center to strong in outer contacts. Ages reported range from 1860±25 Ma (whole rock Rb-Sr, Kalsbeek 1981) to 1869±9 Ma (zircon U-Pb, Thrane et al. 2005).

Many have proposed that the PIC formed in a subduction-related setting of convergence and collision (Grocott and Pulvertaft 1990, Hoffman 1990, Van Kranendonk et al. 1993, Scott 1999). A newer study by Thrane et al. (2005), however, proposes that collision processes of the Nagssugtoqidian-Rinkian Orogen initiated delamination of Archean continental crust. Upwelling asthenosphere filled the newly vacant space, warmed the Archean lower continental crust which in turn partially melted and subsequently the PIC was created (Thrane et al. 2005).

2.5 Mid-Atlantic Ridge, Southwest Indian Ridge and East Pacific Rise

Oceanic zircons were retrieved from the Mid-Atlantic Ridge, Southwest Indian Ridge and East Pacific Rise spreading centres (Fig. 8). Host rocks range from gabbros to tonalites (Coogan & Hinton 2006, Grimes et al. 2007). These data will be used for comparison with other zircon data in this thesis.

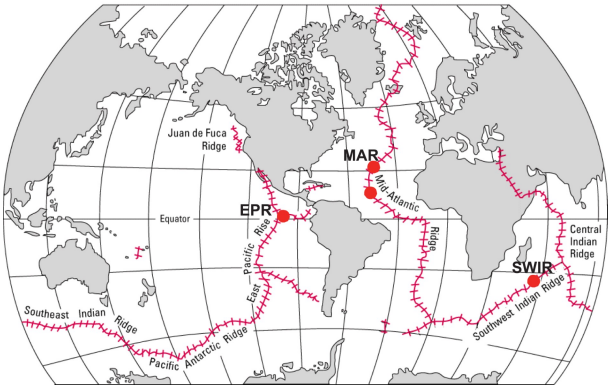

Fig. 8. Sample locations of Mid-Atlantic Ridge (MAR), Southwest Indian Ridge (SWIR) and East Pacific Rise (EPR) zircon marked with red filled circles. (Base image from USGS 1999).

3 Analytical methods

3.1 Zircon extraction and sample preparation

The Birimian samples were coarsely crushed and then milled in a Cr-steel swing mill for ~15 seconds to create a rock powder. West Greenland samples are from the Geological Survey of Denmark and Greenland (GEUS) collections. These were separated with a gold pan. Sediments and water are poured into a heightened container from which they flow down sponge-lined steps. The sponges detain the heavy minerals which are collected.

Each sample was mixed with water and put on a Wilfley table to separate heavier minerals from lighter (modified from Söderlund & Johansson 2002). The tail of heavier minerals was collected. Since zircon has specific gravity of 4.6-4.7 $^{g}/_{cm}$ (Deer, Howie & Zussman 1992) it will stay in the heavy mineral fraction. The heavy-mineral fraction was transferred to a petri dish and a magnetic pencil was used to remove magnetic minerals. Zircon was handpicked under a binocular microscope, using forceps and pipettes. Between 107 and 231 grains were handpicked from each Birimian sample.

The zircon grains were placed on double-sided tape mounts and sent to NORDSIM in Stockholm, where the mounts were cast into epoxy resin and polished to expose cross-sections of each zircon grain.

3.2 SE and BSE imaging

The mounts were carbon-coated. This serves as bettering of image quality as it increases conductivity on the sample surface and decreases electric charging effects (Goldstein 1992). Secondary electron (SE) images and back-scattered electron (BSE) images were obtained for the samples from Ghana using a scanning electron microscope (SEM); a standard Hitachi S-4300N, at the Department of Geology, Lund University. None were obtained for the West Greenland zircon.

In principal, a beam of primary electrons is focused onto the sample surface. These energize the atoms in the sample, which are in turn emitted as secondary electrons, a process called elastic scattering (Goldstein 1992). This beam-sample interaction causes another process, inelastic scattering, where a portion of these primary electrons are scattered back from the sample surface. A detector collects these radiation signals coming from the sample, which are in turn projected onto a screen as easily interpretable images. The back-scattered electrons offer a way of compositional interpretation, as the number of back-scattered electrons increases with atomic number. Areas with higher average atomic number will therefore appear brighter on the image (Goldstein 1992).

Secondary electron overview image of either 500 µm or 1 mm resolution, depending on sample size, was obtained for every Birimian samples and 5-7 back-scattered images of different areas within every sample. Magnification was kept as low as possible, or 300 µm, without losing visibility of possible compositional features and cracks and to avoid burning of the sample.

3.3 Laser ablation trace element analyses

Analyzes were done at the Geological Survey of Denmark and Greenland (GEUS) in Copenhagen. Trace element concentrations within individual zircons were determined using the a New Wave 213 laser ablation (LA) unit that is coupled to a Thermo Element 2 sector-field inductively coupled mass spectrometer (SF-ICP-MS).

This technique can be coarsely divided into two parts; the laser ablation system and the inductively coupled plasma mass spectrometer. The laser ablation system introduces a beam of high intensity photons, the laser, which are directed and focused onto the sample. For the Birimian analysis, the laser spot diameter was 25µm for most zircon grains and 40 µm for a few. Upon impact with the solid material the energy of the laser converts into heat, causing the sample to vaporize and various particles, i.e. particulates, ions and atoms, to be emitted. Carrier gas, usually a Helium-Argon mixture, transports these particles, the aerosol, to the inductively coupled plasma (Košler & Sylvester 2003).

The plasma is formed within three coaxial tubes, called the torch. Argon gas flows between the two outer tubes of the torch and the gas containing the

sample flows through the innermost tube. At the end of the torch is a Copper coil, which is connected to a radio-frequency power generator. This generator applies its power to the coil, creating a magnetic field within the Argon gas, which is supplied with free oscillating electrons generated from a spark from an electrically powered lighter. These electrons collide with the magnetic field causing heating of the Argon to temperatures existing on the Sun, ~8000 K, and the gas to ionize. The ionized gas is called plasma and when the aerosol is introduced into the plasma, the aerosol atoms form ions that are sucked into the mass spectrometer (Longerich & Diegor 2001, Košler & Sylvester 2003).

The ions need to be separated based on mass to charge ratio before they reach the detector. In the sector field ICP-MS ions are directed into a high vacuum tube system where a magnetic field is created by electromagnets. The magnetic field forces the stream of ions to bend as a function of their mass and the intensity of the magnetic field. A double-focusing SF-ICP-MS, which was used in this work, has an additional electrostatic analyzer that further separates ions based on their kinetic energy. In order to record ions of different m/c, the magnetic intensity can be varied over time, or it could be kept constant while varying the voltage implemented on the electrostatic analyzer. If the magnetic intensity or voltage is not appropriate for the mass to charge ratio (m/c) of the ion, it is deflected too much or too little, hits the wall of the tube and never reaches the detector. Therefore the intensity of the magnetic field or voltage to the electrostatic analyzer is varied over time to record ions of different m/c (Longerich & Diegor 2001, Taylor 2001).

This method has been used on zircon for little over two decades but has been greatly refined in recent years. Most elements can be analyzed, with detection limits down to the ppm level (Rollinson 1993, Hoskin & Schaltegger 2003). Elements are measured sequentially and at very high speed and thus this method has the advantage of being rapid (Rollinson 1993, Košler et al. 2002, Hoskin & Schaltegger 2003, Kinny & Maas 2003). Precision is generally very good (5-15%) (Hoskin & Schaltegger 2003), as well as the accuracy (Rollinson 1993), but one should bear in mind that accuracy gives results in accordance with the quality of standards used (Hanchar & Watson 2003).

3.4 Potential pitfalls in laser ablation analyses

The LA-SF-ICP-MS has its shortcomings. Here, two possible pitfalls will be mentioned. As the laser drills into the crystal, it might encounter inclusions that were not observable through the image analysis (Fig. 9). These inclusions will contribute their main elements to the time-resolved spectra (Hoskin & Schaltegger 2003). Apatite ($Ca_5(PO_4)_3(OH,F,Cl)$), for example, is a common inclusion in zircon crystals (Jennings et al. 2011). If one measures the zircon for calcium (Ca) and phosphorus (P) and that zircon contains a larger inclusion that the laser encounters, the results given would be too high and non-representative of the zircon (Fig. 10). Monazite ($(Ce,La,Th)PO_4$), xenotime (YPO_4), K-feldspar ($(Ka,Na)AlSi_3O_4$), plagioclase ($NaAlSi_3O_8 - CaAl_2Si_2O_8$) and biotite ($K(Fe, Mg)_3AlSi_3O_{10}(F,OH)_2$) are also common inclusions in zircon (Dennen & Shields 1956, Deer, Howie & Zussman 1992)

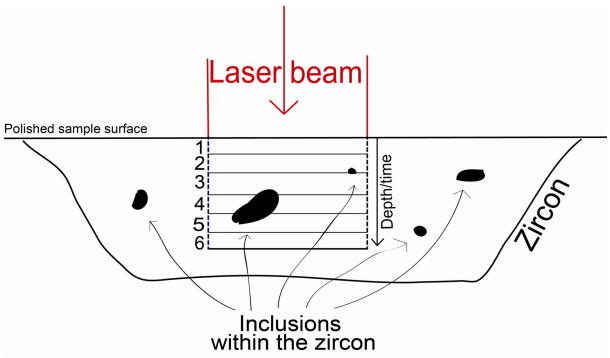

Fig. 9. The laser beam ablating a zircon crystal. Each number represents an interval of ablation and thus elemental amount analysis. Note that this is a simplistic view, 30 intervals is more realistic.

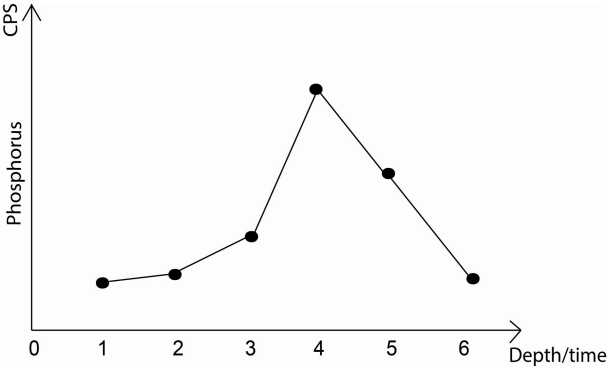

Fig. 10. A closer look at one of the elements measured, phosphorus (P). X-axis represents the intervals of measurement (see fig. 9) and Y-axis represents counts per second (CPS), from which absolute amounts can be calculated. The first interval measured (1; see X-axis) shows phosphorus concentrations representative of the zircon. The second interval (2) shows vague phosphorus increase, as well as interval 3. In interval 4 and 5 the phosphorus amount spikes and skews the data significantly. Interval 6 shows normal zircon phosphorus amount again. As phosphorus is one of the main elements constituting apatite, it is very possible that the laser may have encountered an apatite inclusion.

The other downside of the laser ablation system is that it is destructive. For very small crystals, one might not be able to analyze it again as the former ablation process will have destroyed it (Thomas et al. 2003).

3.5 ^{206}Pb-^{207}Pb age evaluations

The U-Pb dating method is important within the field of geochronology, especially when dealing with material of Precambrian age (Kramers et. al. 2009). The theory behind this method can be explained relatively simply, however, many complexities have arisen and some have not yet been resolved (Kramers et al. 2009). For the purposes of this thesis it will make do with the simplistic explanation and approach.

Lead has four natural stable isotopes; ^{204}Pb, ^{206}Pb, ^{207}Pb and ^{208}Pb. Zircon grains incorporate only the non-radiogenic ^{204}Pb, but at a minimal rate (Davis et al. 2003). Pb occurs in three valence states; Pb^{o}, Pb^{4+} and Pb^{2+}. Pb^{o} and Pb^{2+} have ionic radii too large to be compatible in the octahedral site in zircon, which has the optimal radius of its usual occupant, the 0.84Å Zr^{4+} ion. The valence states are also lower (Watson et al. 1997, Harley and Kelly 2007). The Pb^{4+} ion, on the other hand, has the effective ionic radius of 0.94Å (Shannon 1976) and the same valence state as the zirconium ion, making it seem compatible into the octahedral site. However, as Pb^{4+} is only stable at higher temperatures and conditions of highly elevated oxygen fugacity (Watson et. al. 1997), Pb^{4+} is rarely incorporated into the zircon lattice.

The lead measurable in zircons is thus mainly the result of radioactive decay of uranium and thorium; elements that zircon incorporates to some extent as they share the same valence state as Zr^{4+} and their effective ionic radius is not too large to inhibit incorporation (ionic radii: 1.00Å and 1.05Å (Shannon 1976)) (Hoskin & Schaltegger 2003). ^{235}U, ^{238}U and ^{232}Th decay to the daughter isotopes ^{206}Pb, ^{207}Pb and ^{208}Pb. Analyzing for these isotopes, as well as the non-radiogenic ^{204}Pb, enables calculations of ages (Harley & Kelly 2007).

As only two of the four lead isotopes, ^{206}Pb and ^{207}Pb, were measured for the Birimian zircons, due to time and mass range limitations, only approximate age calculations could be done. To make use of the lead data retrieved, age evaluations were calculated to screen the data for anomalous age domains in each zircon. Obtained ages should be taken with caution and only serve as approximate age guides. The following equation (Faure 1986) was solved for ^{235}U using various ages (t) until the $^{207}Pb/^{206}Pb$ of the zircon in question was obtained. λ represents the decay constants of the U isotopes (Steiger & Jäger 1977).

$$\left(\frac{^{207}Pb}{^{206}Pb}\right) = \frac{^{235}U}{^{238}U}\left(\frac{e^{\lambda_2 t}-1}{e^{\lambda_1 t}-1}\right)$$

$$\lambda_1 = {}^{238}U = 1.55125\times10^{-10}$$

$$\lambda_2 = {}^{235}U = 9.8485\times10^{-10}$$

4 Zircon host rock

4.1 Birimian rock descriptions and whole rock analyses

Rock samples, ASGH028A, ASGH030A, ASGH082A and ASGH084A were provided by Dr. Anders Scherstén, who collected them during fieldwork in Ghana in 2009. PK 105 was provided by Dr. Anders Scherstén but collected by Dr. Per Kalvig at the Denmark and Greenland Geological Survey (GEUS).

4.1.1 PK105

Sample PK 105, a biotite-hornblende bearing granite, was retrieved from the Suhum Basin. It is the oldest of the samples analysed for ages, 2232 Ma (Anders Scherstén, unpublished data). No field images exist.

PK105 is coarse- and uneven grained. No fabric is observable. The sample consists mainly of quartz, K-feldspar, plagioclase, hornblende and biotite (Fig. 11a-b). The quartz displays undulose extinction and bulging grain boundaries. The K-feldspar rarely displays alteration, however plagioclase commonly exhibits cloudy, alteration bands. Biotite is commonly altered whereas hornblende is not. Not common but present are magnetite, small epidote grains within feldspar, zircon, and secondary muscovite and calcite along grain boundaries and in fractures (Fig. 11c-d). This sample is generally well preserved with local alteration areas.

Whole rock analysis reveals LREE enrichment relative to HREE (Fig. 14), with $(La/Yb)_N$ being 38.23. Sr/Y is 29.9. Y and Yb are 8.1 ppm and 0.76 ppm respectively. Eu/Eu* is 0.83 whereas Ce/Ce* is 1.01. The sum of REE is 165.49 ppm.

4.1.2 ASGH028A

This coarse-grained biotite-granite sample (Fig. 11g) has an age of 2130 Ma (Anders Scherstén, unpublished data) and originates in a quarry in the the Suhum Basin, close to the the Volta Basin.

ASGH028A is uneven grained with grain sizes ranging from small to large. No fabric is visible. Muscovite and biotite is common, as well as quartz, plagioclase, K-feldspar (Fig. 11e-f). Halos around biotite are fairly common as well as alteration. Plagioclase is commonly altered. Quartz exhibits undulose extinctions and bulging grain boundaries. Secondary epidote is present. Nevertheless, the sample is fairly well preserved.

It is LREE enriched and HREE depleted (Fig. 14), with $(La/Yb)_N$ of 12.07. Eu/Eu* is a negative 0.81. Ce/Ce* 0.998. Sr/Y is 23.3. Concentration of Y is 15.8 ppm and Yb is 1.48 ppm. The sum of REE is 116.15 ppm.

4.1.3 ASGH030A

Sample ASGH030A was retrieved from the northern Kibi-Winneba belt. The outcrop exhibits local shearing, with common mafic enclaves. Well preserved lenses of isotropic biotite-granite are present and ASGH030A was retrieved from such a lens (Fig. 12c-d). No age has been obtained for it nor from any other

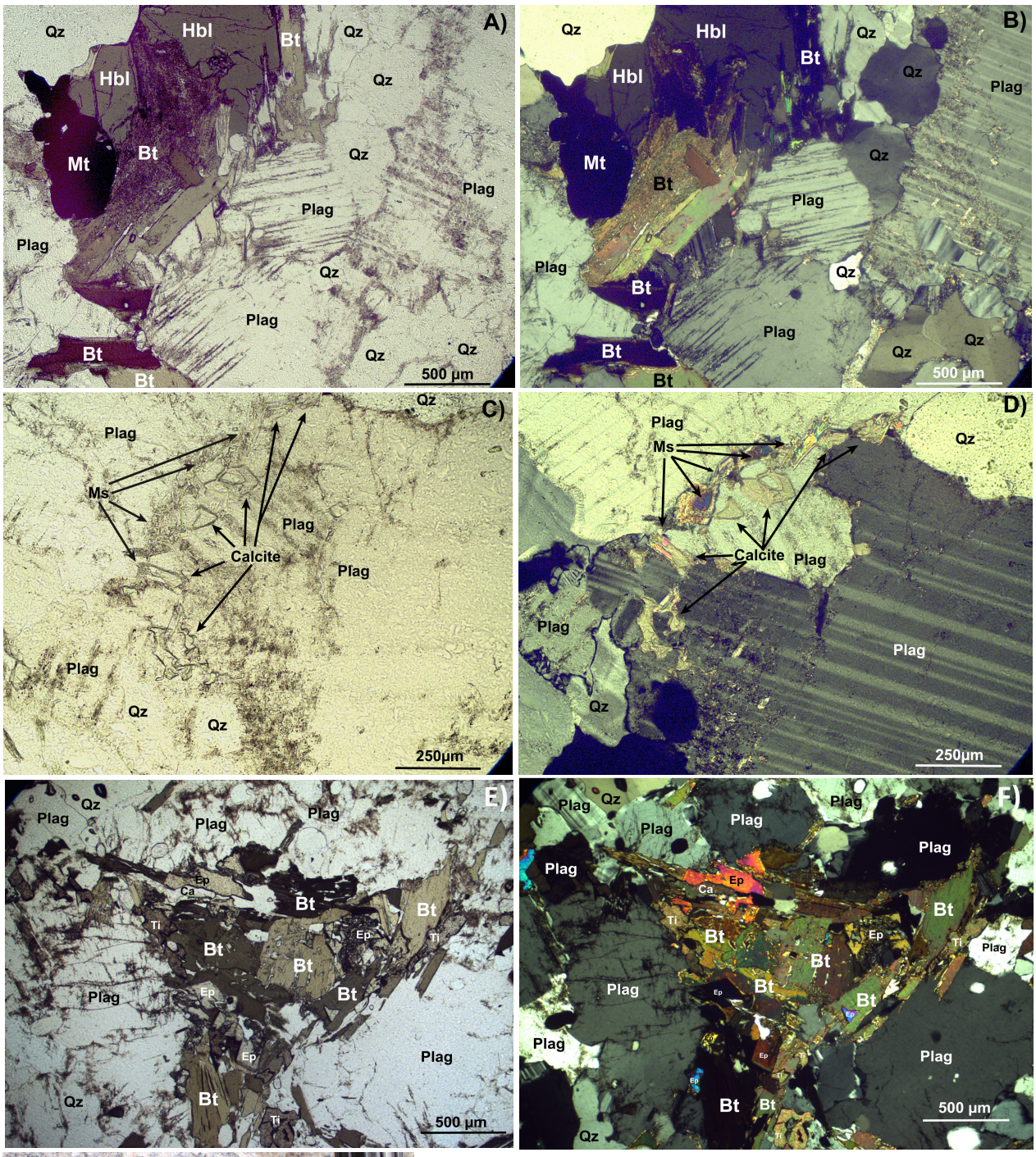

Fig. 11. Samples PK105 and ASGH028A. **A)** A plain-polarized microscope image showing common minerals found in PK105; quartz (Qz), plagioclase (Plag), hornblende (Hbl) and biotite (Bt). In addition magnetite (Mt) is present in the image. **B)** Image A) cross-polarized. **C)** A plain-polarized microscope image showing secondary muscovite (Ms) and calcite (Ca) occurring along a fracture in plagioclase and at grain boundaries in PK105. **D)** Image C) cross-polarized **E)** Thin section image of ASGH028A, in plain-polarized light, showing quartz (Qz), plagioclase (Plag), biotite (Bt), epidote (Ep), titanite (Ti), calcite (Ca) and secondary muscovite (Ms). **F)** Image C) cross-polarized. Note the bands within the large plagioclase grain on the left, the irregular grain boundaries and disturbances in biotite. These are due to alteration. **G)** Hand specimen of ASGH028A. (Field images courtesy of Anders Scherstén).

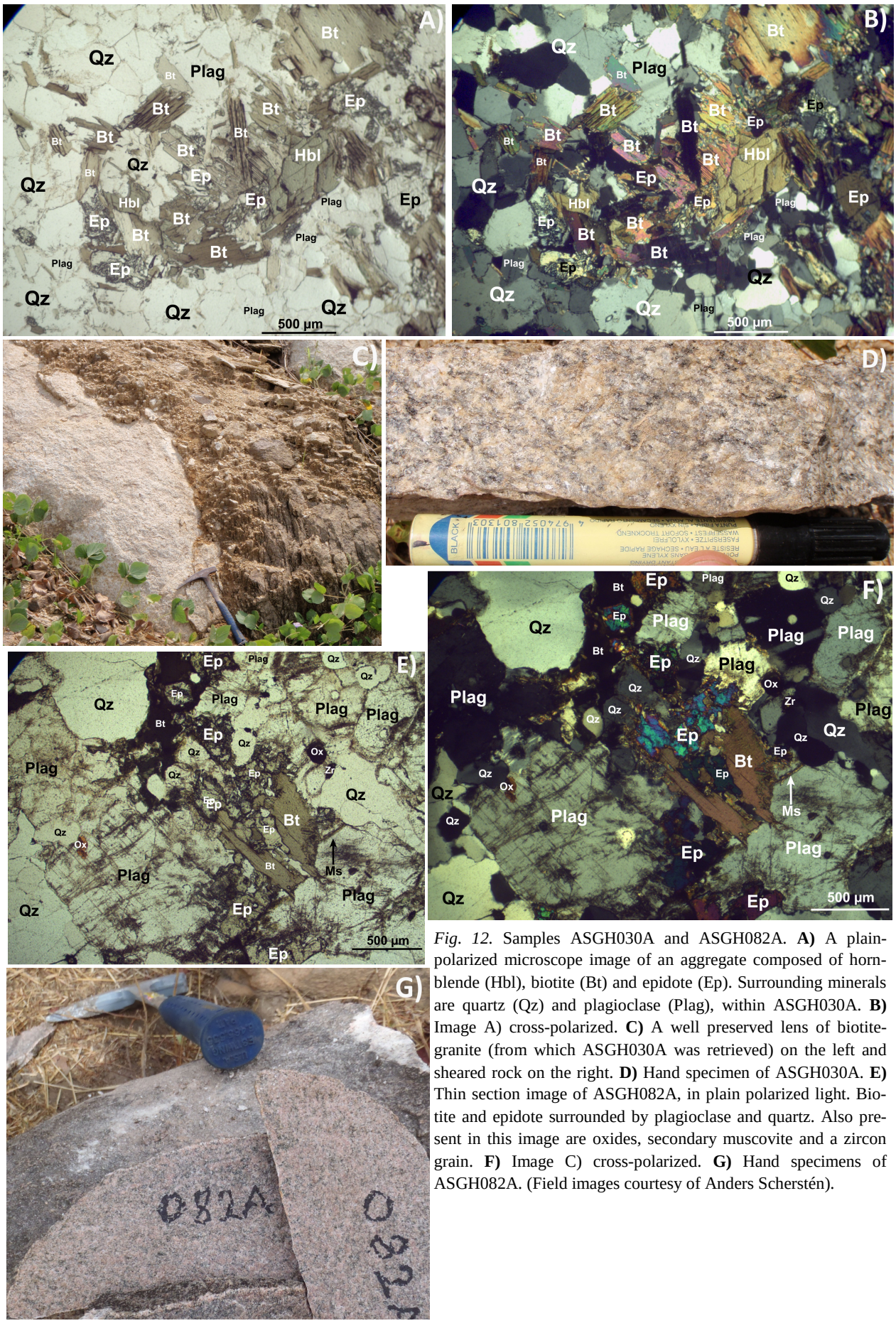

Fig. 12. Samples ASGH030A and ASGH082A. **A)** A plain-polarized microscope image of an aggregate composed of hornblende (Hbl), biotite (Bt) and epidote (Ep). Surrounding minerals are quartz (Qz) and plagioclase (Plag), within ASGH030A. **B)** Image A) cross-polarized. **C)** A well preserved lens of biotite-granite (from which ASGH030A was retrieved) on the left and sheared rock on the right. **D)** Hand specimen of ASGH030A. **E)** Thin section image of ASGH082A, in plain polarized light. Biotite and epidote surrounded by plagioclase and quartz. Also present in this image are oxides, secondary muscovite and a zircon grain. **F)** Image C) cross-polarized. **G)** Hand specimens of ASGH082A. (Field images courtesy of Anders Scherstén).

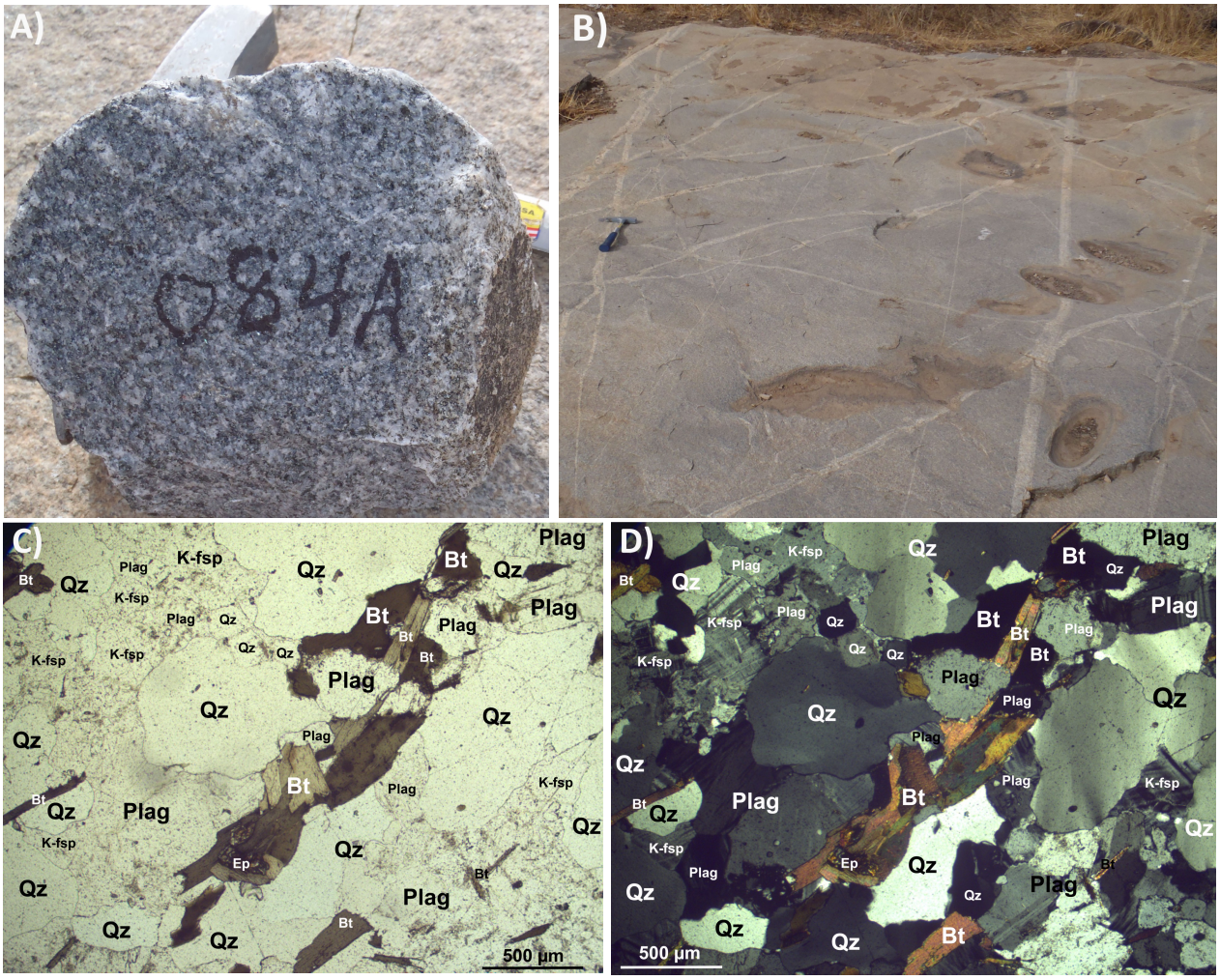

Fig. 13. Sample ASGH084A. **A)** Hand specimen of sample ASGH084A. **B)** The outcrop where ASGH084A was collected. The rock is cross-cut by pegmatitic dykes. **C)** Thin section image of ASGH084A, in plain-polarized light. Biotite surrounded by quartz, K-feldspar and plagioclase. Epidote is also present. **D)** Image C) cross-polarized. (Field images courtesy of Anders Scherstén).

sample in the northern Kibi-Winneba belt. A sample from the southern Kibi-Winneba belt, ASGH001A, has an age of 2090±60Ma. Occasional simple twin K-feldspar, may be orthoclase.

This sample is porphyritic, with small to large quartz grains and large, slightly altered microcline phenocrysts. The quartz occasionally exhibits undulose extinction and bulging grain boundaries. K-feldspar and plagioclase are common as well as biotite (Fig. 12a-b). The biotite is occasionally altered but generally it is relatively well preserved. It appears in aggregates, occasionally with well preserved hornblende. Plagioclase is not uncommonly altered. Less common minerals include sphene, epidote, zircon and secondary muscovite on biotite and in fractures.

The sample shares the LREE enrichment relative to HREE (Fig. 14) with the other samples; it has a $(La/Yb)_N$ of 44.95. Eu/Eu* is 1.11, so it is positive but vague. Ce/Ce* is 0.976. Sr/Y is a relatively high 218.0. Y amounts to 5.2 and Yb is 0.39 ppm. The sum of REE is 111.37 ppm.

4.1.4 ASGH082A

This sample is a biotite-hornblende (Fig. 12e-g) bearing granite from northern Ghana. It has been dated at 2156 Ma (Anders Scherstén, unpublished data).

This sample is fairly even- and fine grained. Biotite determines fabric. Minerals present are quartz, plagioclase, K-feldspar, biotite and epidote (Fig. 12e-f). The quarts exhibits undulose extinction and bulging grain boundaries. The K-feldspar and plagioclase are frequently altered, but K-feldspar to a less degree than plagioclase. Biotite is occasionally altered and commonly exhibits halos. Also visible are iron oxides, zircon, sphene and secondary muscovite growing along grain boundaries and in fractures.

It is LREE enriched relative to HREE (Fig. 14); it has a $(La/Yb)_N$ of 6.81, but to a much lesser extent than the other samples. Eu/Eu* is 0.53, so it is very negative. Ce/Ce* is 0.994. Sr/Y is a mere 5.0. Y and Yb amount to 30.0 ppm and 2.92 ppm, respectively. The sum of REE is 151.47 ppm.

4.1.5 ASGH084A

This sample is a biotite-tonalite (Fig. 13a-b) from northern Ghana. It has been dated at 2156 Ma (Anders Scherstén, unpublished data).

ASGH084A is fine- to medium grained, uneven grained and has fabric defined by biotite. It is generally well preserved. Other minerals include quartz, K-feldspar and plagioclase (Fig. 13c-d). Quartz exhibits undulous extinction and bulging grain boundaries. The plagioclase is commonly altered but K-feldspar less so. Halos commonly surround biotite but biotite is otherwise fairly well preserved. Less common minerals present are zircon, iron oxides and secondary muscovite along grain boundaries and on biotite.

It is LREE enriched relative to HREE (Fig. 14), but to a lesser extent than the other samples, with $(La/Yb)_N$ of 12.26. Eu/Eu* is 0.55, so it is very negative. Ce/Ce* is 0.930. Sr/Y 11.8. Concentrations of Y and Yb are 11.3 ppm and 1.22 ppm, respectively.The sum of REE is 95.29 ppm.

4.2 West Greenland

No whole rock samples were collected in the field, neither for the Archean zircons or Prøven Igneous zircon. However, Thrane et al. (2005) provide whole rock information on the Prøven Igneous Complex.

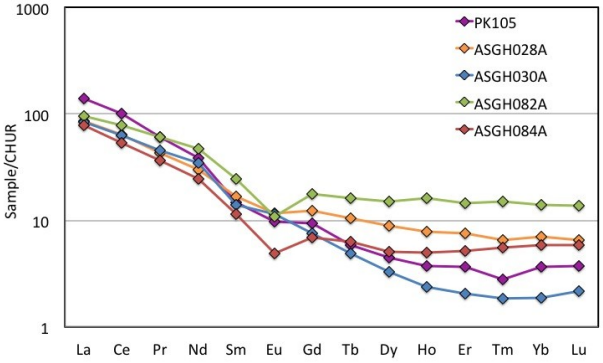

Fig. 14. Chondrite-normalized REE curves for the whole rock analyses of the Birimian samples.

5 Results

5.1 West Greenland zircon (Archean)

This population consists of 412 zircons and is HREE enriched relative to LREE (Fig. 15). $(Lu/Gd)_N$ ranges from 0.5 to 63.9 (med. 14.6). $(Sm/La)_N$ varies from 2.0-1294 (med. 38 ppm), showing almost little to moderate steepness of the LREE profile. ∑LREE varies between 2.6-2333 ppm (med. 54.8 ppm). ∑HREE varies between 34.4-4485 ppm, med. 451.5 ppm. The Ce/Ce* anomaly is highly variable, ranging from 1.1 to 495.3 (med. 12.2). The Europium anomaly (Eu/Eu*) is negative and varies from 0.09 to 1.97 (med. 0.55). The Th/U ranges from 0.14-3.75 (med. 0.71).

Ages range from 2502-3852 Ma (Anders Scherstén, unpublished data).

5.2 Prøven Igneous Complex zircon

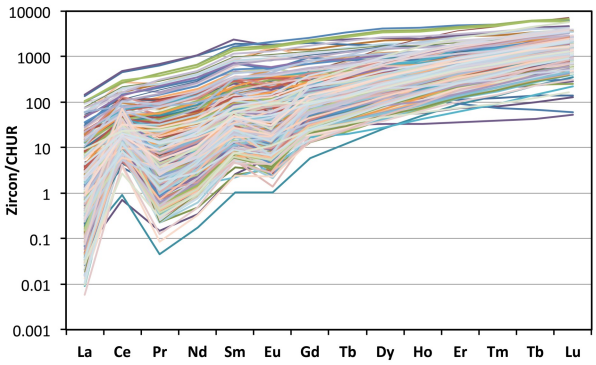

Fig. 15. REE profiles of Archean detrital zircons from West Greenland.

The number of zircons analysed is 144. They are HREE enriched relative to LREE (Fig. 16). $(Lu/Gd)_N$ ranges from 3.0 to 25.8 (med. 12.1). $(Sm/La)_N$ varies from 0.32-317.6 (med. 21.3), showing almost no steepness of the LREE profile to moderate steepness. ∑LREE varies between 15-1356 ppm (med. 44). ∑HREE varies between 182-2524 ppm, med. 352 ppm. The Ce/Ce* anomaly is highly variable, ranging from 1.0 to 92.4 (med. 6.4). The Europium anomaly (Eu/Eu*) is negative and varies from 0.02 to 2.9 (med. 0.46). The Th/U ranges from 0.4-1.5 (med. 0.6).

Ages range from 1829-1985 Ma (Anders Scherstén, unpublished data).

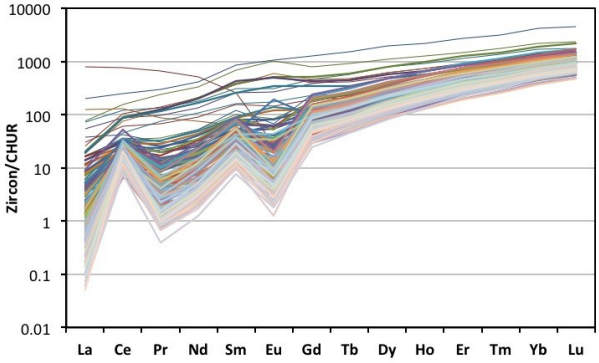

Fig. 16. REE profiles of zircons from the Prøven Igneous Complex.

5.3 Birimian PK105

5.3.1 External morphology and internal structure

The population consists of 31 grains that range in size from 45-99 µm in the long dimension, with two individual grains of 120 µm and 153 µm. Aspect ratios range from 1.5:1 to 4.6:1, with the median of 2:1. About half of the population has smoothed ends, making it fairly difficult to determine external morphology but it seems to be governed by {110} prisms and {101} pyramids (Pupin 1980). Only 7 specimens show any signs of growth zoning and it is faint and/or localized. This is due to low resolution of the SEM images; 300 µm. Overgrowths or reaction rims seem to be present in 12 grains, but these are usually thin and vaguely observable. Another 11 zircons may also

have reaction rims/overgrowths but it is inconclusive. 20 zircons have observable fractures. 18 fractures fell within the ablation pit and thereof were 5 fractures rather large. See Fig. 17.

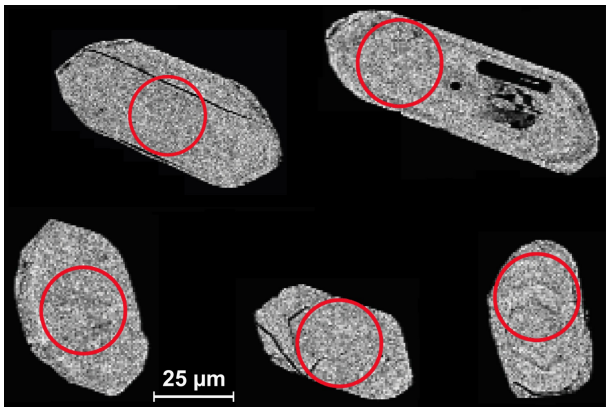

Fig. 17. Five zircon examples from PK105. Red circles represent spot location and size (25 µm).

5.3.2 Geochemistry

REE profile ranges from the typical positive slope, with HREE enriched relative to LREE, to a flat profile (Fig. 18). $(Lu/Gd)_N$ varies between 1.6-22.7 (med. 6.6), showing vague to moderate steepness of the HREE. $(Sm/La)_N$ ranges from 0.4-7.0. This shows a negative slope of the LREE profile to only minor positive slope. In comparison $(Sm/La)_N$ between 22 and 110 are typical for magmatic zircon (Hoskin 2005). The general lack of LREE slope thus represents severe LREE enrichment. ∑LREE [La-Gd] is 117-2610 ppm (med. 755 ppm). ∑HREE [Tb-Lu], varies between 488-1291 ppm (med. 671 ppm). PK 105 has a Ce/Ce* anomaly ranging from a negative 0.98 to a positive 4.0 (med. 1.5). The Eu/Eu* anomaly varies from the negative 0.54 to the positive 6.4 (med. 1.4), and the majority show a positive anomaly. Zircons with a positive anomaly have rarely been observed (Maas et. al. 1992). The Th/U varies from 0.35 to 1.69 (med. 0.52).

Age evaluations gave ages between 2050-2500 Ma.

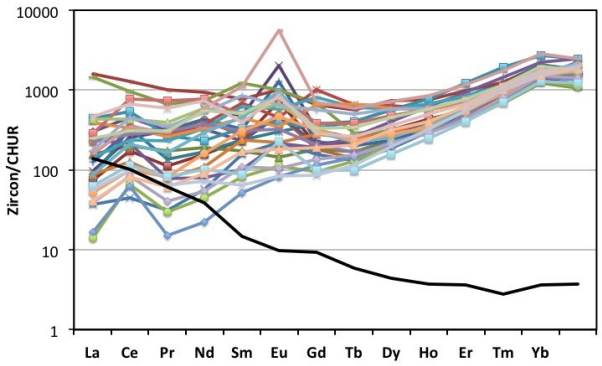

Fig. 18. PK105 zircon REE profiles. Black line represents the PK105 whole rock profile.

5.4 Birimian ASGH028A

5.4.1 External morphology and internal structure

This population of 35 zircons has aspect ratios of 0.9:1 to 3.4:1 (median: 2:1) and the length of the grains ranges from 41 to 90 µm. Due to smoothed ends and at least 16 zircons having overgrowths/reaction rims, determining crystal morphology was challenging. However, as with PK105, the morphology seems to be mainly {110} prisms and {101} pyramids, but additionally with {211} pyramids (Pupin 1980). Fractures are fairly common, they are present in 21 grains. Growth zoning is only vaguely and/or locally visible in 5 zircons. This is due to low resolution of the SEM images; 300 µm. See Fig. 19.

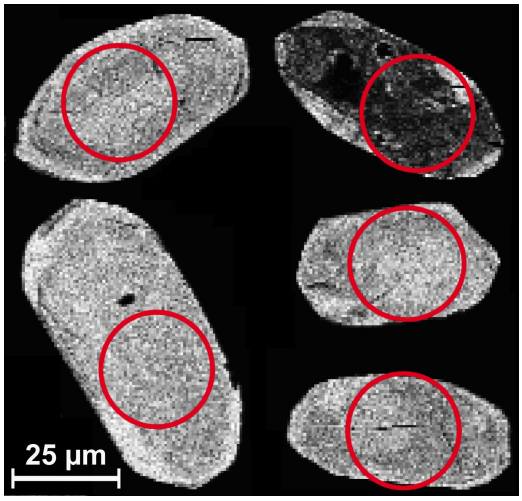

Fig. 19. Five zircon examples from ASGH028A. Red circles represent spot location and size (25 µm).

5.4.2 Geochemistry

$(Lu/Gd)_N$ ranges from 2.7 to 27.1 (med. 8.7). $(Sm/La)_N$ varies between 0.9-10.0 (med. 1.4). This goes to show that, although not as severe as PK105, LREE enrichment is also present (Fig. 20). ∑LREE varies between 38.3-9955 ppm. ∑HREE varies between 546-8524 ppm, med. 1436 ppm. The Ce/Ce* anomaly is low, only ranging from 0.36 to 2.90. The Europium anomaly (Eu/Eu*) is negative and varies from 0.22 to 0.52 (med. 0.4), apart from one positive value of 1.43. Th/U range from 0.2-1.7 (med. 0.52).

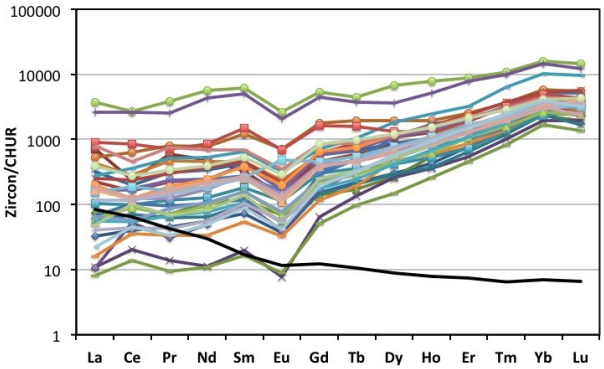

Fig. 20. ASGH028A zircon REE profiles. Black line represents the ASGH028A whole rock profile.

Age evaluations resulted in an interval of 1910 -2450 Ma for this sample.

5.5 Birimian ASGH030A

5.5.1 External morphology and internal structure

This sample consists of 35 analyzed zircons. They vary in length, the shortest being 54 µm and the longest 141 µm. Aspect ratios range from 1.6:1 to 5.9:1. The morphology is governed by {100} prisms and {101} pyramids, with the supplementary bipyramid {301} (Pupin 1980, Caironi et. al. 1996). The majority of zircons contain observable fractures, of which 9 fall within the ablation pit. All but 5 specimens show vague growth zoning - vague because of low resolution - with thick and few bands. Overgrowths/reaction rims are rare. See Fig. 21.

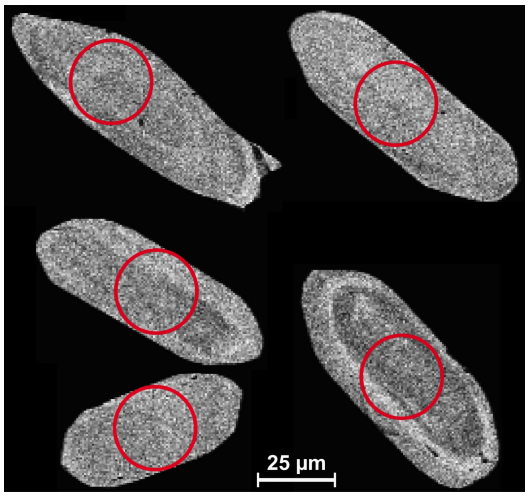

Fig. 21. Five zircon examples from ASGH030A. Red circles represent spot location and size (25 µm).

5.5.2 Geochemistry

This sample is HREE enriched relative to LREE (Fig. 22). $(Lu/Gd)_N$ ranges from 9.1 to 45.5 (med. 27.5). $(Sm/La)_N$ varies from 0.6-112.7 (med. 8.3) showing indeed some LREE enrichment but less extensive than in previous samples. ∑LREE varies between 25-542 ppm (med. 72 ppm). ∑HREE varies between 769-4028 ppm, med. 1419 ppm. The Ce/Ce* anomaly is variable, ranging from 1.1 to 20.6. The Europium anomaly (Eu/Eu*) is negative and varies from 0.25 to 0.63 (med. 0.45). The Th/U ranges from 0.1-5.7 (med. 0.4).

Age evaluations resulted in a rather scattered age interval; 1740-2530 Ma.

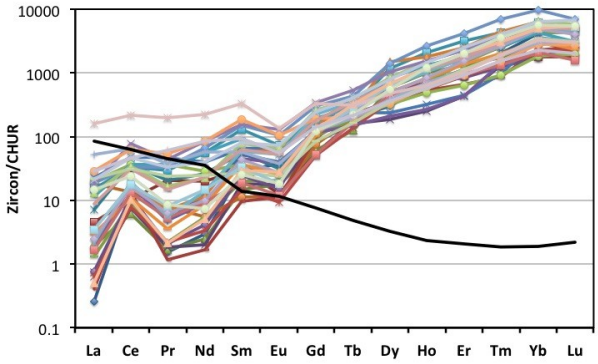

Fig. 22. ASGH030A zircon REE profiles. Black line represents the ASGH030A whole rock profile.

5.6 Birimian ASGH082A

5.6.1 External morphology and internal structure

This sample comprises 27 zircons. They range in size, in the long dimension, from 48-96 µm (med. 60 µm). Aspect ratios vary from 1.6:1 to 2.6:1 (med. 1.9:1). The morphology is governed by {100} prisms but determining pyramid morphology proved challenging due to smoothed ends. It seems, however, that the zircon grains are governed by {101} pyramids (Pupin 1980). Half of the population is fractured, but the fractures fall within the ablation pit in only 5 specimens. Very faint growth zoning is visible in 21 zircon grains but would be clearer in a higher resolution SEM image. Overgrowths/reaction rims are rare. See Fig. 23.

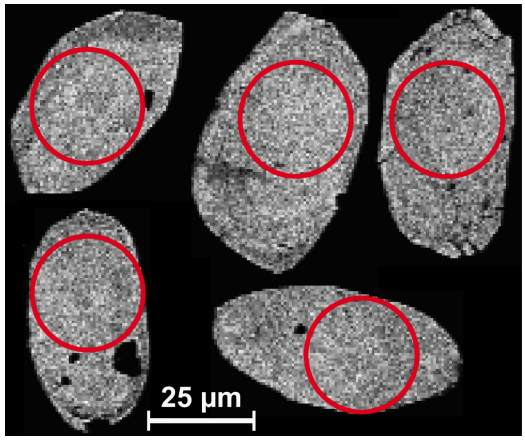

Fig. 23. Five zircon examples from ASGH082A. Red circles represent spot location and size (25 µm).

5.6.2 Geochemistry

$(Lu/Gd)_N$ ranges from 4.7 to 37.6 (med. 15.7), showing little to moderate steepness of the HREE section of the REE profile. $(Sm/La)_N$ varies from 1.1-

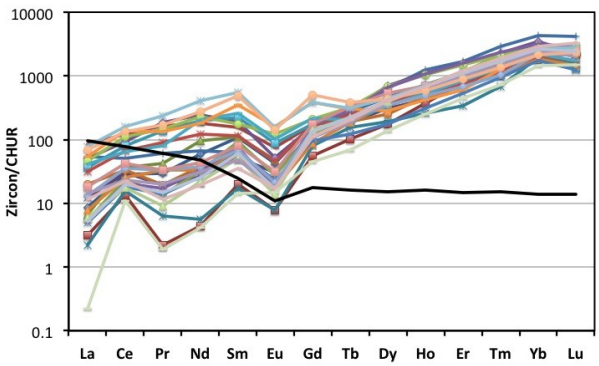

Fig. 24. ASGH082A zircon REE profiles. Black line represents the ASGH082A whole rock profile.

65.0 (med. 6.4), showing almost little to moderate steepness of the LREE profile (Fig. 24). ∑LREE varies between 27-642 ppm (med. 110 ppm). ∑HREE ranges from 530-1794 ppm, med. 1045 ppm. The Ce/Ce* anomaly ranges from 0.9 to 17.0 (med. 1.7). The Europium anomaly (Eu/Eu*) is negative and varies from 0.15 to 0.63 (med. 0.29). The Th/U ranges from 0.25-0.66 (med. 0.42).

Ages 1800-2420 Ma were retrieved with age evaluations.

5.7 Birimian ASGH084A

5.7.1 External morphology and internal structure

The population consists of 38 zircon grains. The shortest grain measured 51 µm in the long dimension and the longest 107 µm (med. 65 µm). Aspect ratios range from 1.4:1 to 3.1:1 (med. 1.9:1). The morphology is governed by {110} prisms, and {101} and{101}= {211} pyramids. Of 21 zircon grains that are fractured in some way, only 9 zircons contained fractures within the ablation pit. All but 5 zircons have vague growth zoning and overgrowths/reaction rims are rare. Low resolution SEM imaging hinders proper visibility of growth zoning. See Fig. 25.

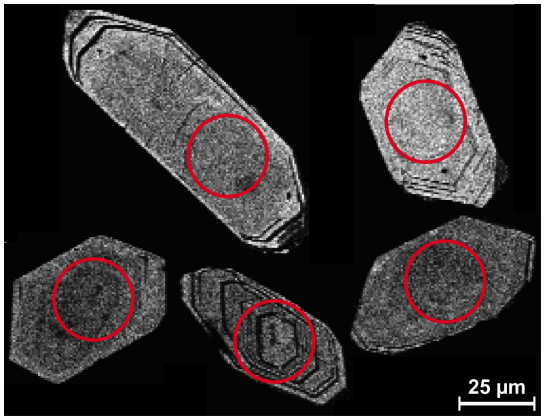

Fig. 25. Five zircon examples from ASGH084A. Red circles represent spot location and size (25 µm).

5.7.2 Geochemistry

$(Lu/Gd)_N$ ranges from 0.63 to 46.9 (med. 12.2). $(Sm/La)_N$ varies from 0.41-28.8 (med. 8.9), showing negative to a moderate positive slope of the LREE profile (Fig. 26). ∑LREE varies between 14.1-6594 ppm (med. 308). ∑HREE varies between 114-1801 ppm, med. 528 ppm. The Ce/Ce* anomaly is highly variable, ranging from 1.1 to 14.4 (med. 1.7). The Europium anomaly (Eu/Eu*) is negative and varies from 0.42 to 0.98 (med. 0.6). The Th/U ranges from 0.55-1.93 (med. 1.07).

Age evaluations resulted in values varying from 1780 Ma to 2570 Ma.

6 Discussions

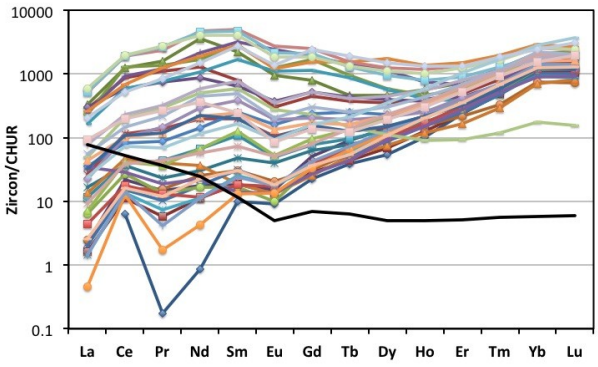

Fig. 26. ASGH084A zircon REE profiles. Black line represents the ASGH084A whole rock profile.

6.1 LREE enrichment in Birimian zircon

6.1.1 Element partitioning into zircon

A high proportion of the Birimian zircon populations are variably enriched in LREE. LREE enrichment is also present in the Jack Hills and Mount Narryer zircon population, West-Greenland Archean zircon Archean and zircon from the Prøven Igneous Complex (PIC). The LREE enrichment of the Birimian samples is generally larger and therefore the focus will be on them.

To visualize the magnitude of LREE enrichment with regard to their partitioning into zircon, the ionic radii were plotted against the predicted partition coefficients of Whitehouse and Kamber (2002) as well as observed partition coefficients (see Table 1). Ideally, the partition coefficients should follow the predicted partition coefficients parabola. However, the LREE deviate substantially upwards from the parabola (Fig. 27), as well as HREE for ASGH030A. These high apparent partition coefficients reflect overabundance of the REE (Whitehouse & Kamber 2002) in relation to known bulk rock concentrations.

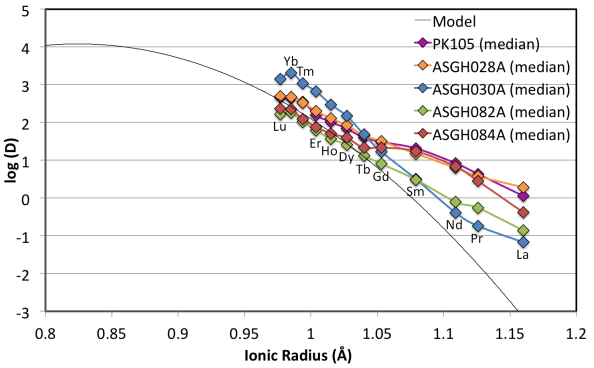

Fig. 27. Partition coefficients (log(D)) against ionic radius (Å). Parabola represents predicted partition coefficients of trivalent cations substituting for Zr^{4+} (Whitehouse & Kamber 2002). Plotted are the observed partition coefficients of the Birimian samples. Eu and Ce were omitted, as Eu yields lower apparent partition coefficients relative to its neighbours, and Ce yields higher apparent partition coefficients relative to its neighbours.

Table. 1. Modelled and observed partition coefficients of REE substituting for Zr^{4+}. The model values are calculated from sample GGU 125540 (Whitehouse & Kamber 2002) and the observed values represent median values of each sample.

		PK105	ASGH028A	ASGH030A	ASGH082A	ASGH084A
	Model	Observation	Observation	Observation	Observation	Observation
La	0.019	1.14	1.89	0.0692	0.139	0.379
Ce	0.0109	2.77	1.91	0.294	0.429	1.73
Pr	0.0551	4.31	3.77	0.182	0.543	2.83
Nd	0.249	8.37	6.28	0.442	0.792	6.94
Sm	2.71	26.7	15.0	3.20	3.07	17.4
Eu	6.84	47.2	11.4	2.98	2.51	19.6
Gd	16.2	30.6	31.9	16.9	8.07	21.8
Tb	36.3	39.6	45.0	48	13.2	21.4
Dy	76.3	68.5	84.3	148	25.6	39.4
Ho	117	104	129	300	36.6	51.0
Er	247	156	201	664	61.6	75.9
Tm	389	356	337	1092	104	122
Yb	569	440	475	2077	182	225
Lu	780	467	500	1421	164	233

6.1.2 'Xenotime' substitution

The excessive abundances of LREE in the samples cannot readily be accounted for solely by 'xenotime' substitution. For the samples in this work, the (REE+Y)/P ranges from 0.3-337 (Fig. 28). There is a negative correlation between the (REE+Y)/P ratios and P concentrations. The grains with the highest P concentrations (above 1000 ppm) have the lowest (REE+Y)/P. These grains contain known apatite inclusions.

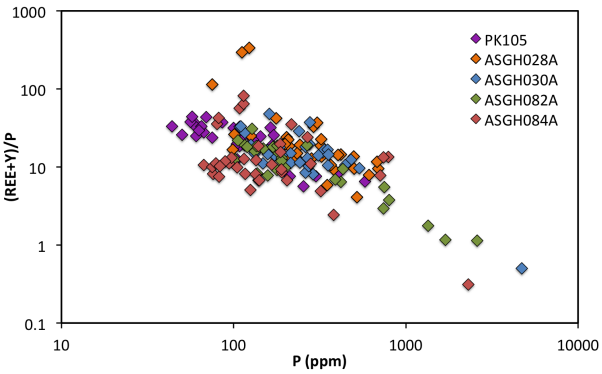

Fig. 28. (REE+Y)/P against P concentrations for the samples in this work.

6.1.3 Analytical errors

Early on in this work, it was suspected that the data was corrupt due to an unknown analytical error. The LA-ICP-MS was first excluded as the culprit. It could not have been poorly standardized, as the analyses were conducted in two sessions, a week apart, with no discrepancy between data. Most importantly 612 and 614 NIST glasses yield reasonable results (Fig. 29a-b). Data reduction problems (e.g. software issues) were excluded after similar results were obtained using Iolite (Hellstrom et al. 2008, Paton et al. 2011) as well as SILLS (Guillong et. al. 2008) softwares.

6.1.4 Metamorphism

Metamorphism has been known to rid zircon grains of structurally non-crucial cations with ionic radii dissimilar to Zr^{4+}. Thus they contain relatively lesser amounts of LREE than magmatic zircons. This also

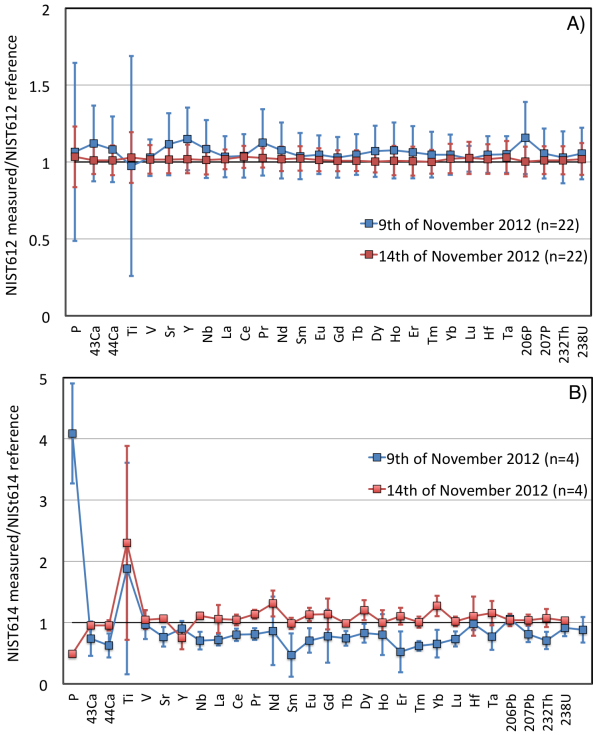

Fig. 29. The deviation of elements in NIST glasses measured from NIST reference material. Reference values are from Jochum et. al. 2008. The dates represent the time when the analyses took place. **A)** The NIST 612 glasses analysed on the 9th of November yield values 0.97 to 1.16 times reference material (med. 1.05). The NIST 612 glasses analysed on the 14th of November yield very good results. All elements yield values almost identical to the reference values (med. 1.0). **B)** The NIST 614 analyses on the 9th of November yield values 0.47 to 1.06 times the reference values (med. 0.8). The NIST 614 glasses analysed on the 14th of November yield results 0.8 to 1.3 times reference material (med. 1.1).

involves flushing of Th^{4+} relative to U^{4+}, as the ionic radius of Th^{4+} (1.05 Å) differs more from Zr^{4+} (0.84 Å) than U^{4+} (1.0 Å) (Ahrens 1965, Shannon 1976, Hoskin & Black 2000). This results in a lower Th/U (<0.07) relative to magmatic zircons (Rubatto 2002). Other commonly mentioned characteristics of metamorphic zircons are Hf enrichment (Hoskin & Schaltegger 2003) and roundness of the grains (Hoskin & Black 2000). None of the zircons show any of these characteristics. However, rim overgrowth, a feature that has been observed in zircons that have been affected by metamorphism (Hoskin & Schaltegger 2003), does appear in zircons of samples PK105 and ASGH028A. However, using a 25 micron diameter of the laser beam, these could in most cases be avoided.

6.1.5 Inclusions

What could not be avoided, however, due to the nature of the drilling of the laser beam, are subsurface inclusions. In order to identify potential inclusions, mixing curves were calculated for different minerals. Titanite

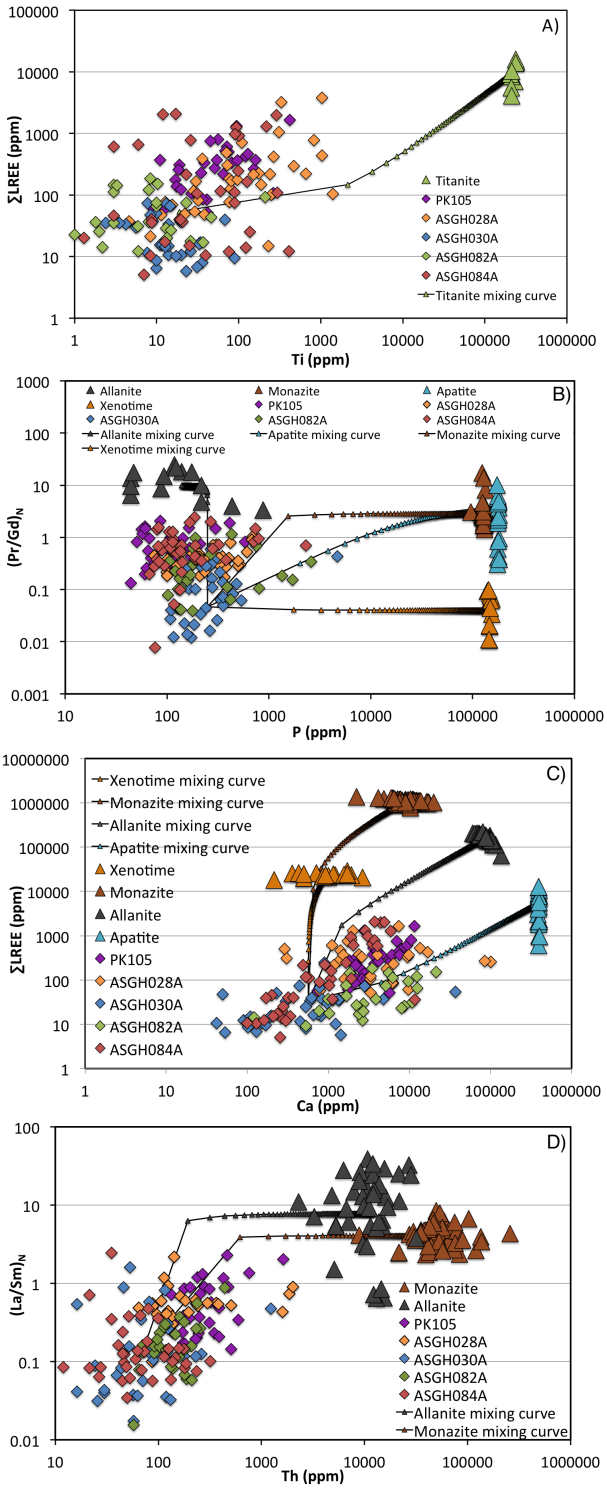

Fig. 30. Inclusion discrimination diagrams. **A)** Titanite against LREE concentrations. Plotted are samples of this research and titanite (Tiepolo et al. 2004, Anand & Balakrishnan 2011). **B)** P versus light to middle REE enrichment (expressed as $Pr/Gd)_N$. Plotted are samples of this research, allanite (Hickling et al. 1970, Gregory et al. 2007, Gregory et al. 2012), monazite (Villaseca et al. 2003), apatite (Belousova et al. 2001) and xenotime (Villaseca et al. 2003). **C)** Ca versus LREE concentrations. Plotted are the samples of this research, xenotime (Villaseca et al. 2003), monazite (Villaseca et al. 2003), allanite (Hickling et al. 1970, Gregory et al. 2007, Gregory et al. 2012) and apatite (Belousova et al. 2001). **D)** The versus the degree of LREE enrichment (expressed as $(La/Sm)_N$). Plotted are data of this research, allanite (Hickling et al. 1973, Gregory et al. 2007, Gregory et al. 2012) and monazite (Villaseca et al. 2003).

($CaTiOSiO_5$) is a mineral known to incorporate REE in significant amounts (Ward et al. 1992, Bea 1996, Tiepolo et. al. 2002) and occurs as inclusions in zircon (Hoskin et. al. 2000). Some data from PK105 and ASGH028A do show increased amounts of titanium along with the LREE enrichment (Fig. 30a). Apart from possibly one grain from ASGH028A, the samples have an overabundance of LREE for a given Ti-concentration, which deviates away from the titanite mixing curve, indicating that titanite inclusions cannot explain the high LREE enrichment. Xenotime, known to incorporate REE (Bea 1996), seems to be absent (Fig. 30b-c) but apatite, also a common REE incorporator (Bea 1996), is present in a few grains (Fig. 30b-c). Monazite, a REE incorporator that has a preference for LREE (Bea 1996), was more problematic to determine. Fig. 30b does not show any clear indicator of monazite presence and Fig. 30c does not show any indicators of monazite inclusions at all. Fig. 30d counteracts these observations, as a number of zircons, especially zircons from sample PK105, seem to stretch towards the monazite composition. A portion of these zircons has Th concentrations too low to follow the mixing curve. There may therefore be another explanation for this pattern. Allanite ($(LREE,Ca)_2(Al,Fe)_3(SiO_4)_3(OH)$) (McFarlane & McCulloch 2007) is found as an accessory mineral in various granitoids (Bea 1996). It has, however, been rarely reported as inclusions in zircon (Spandler et al. 2004, Braga & Masonne 2008, Marsh et al. 2012). Fig. 30b does indicate presence of allanite inclusions, as most of the zircons trend towards the allanite composition. But, as with monazite, there is inconsistenty between figures as the trends on Fig. 30c –d do not follow the allanite mixing curves.

With only a handful of apparent apatite inclusions present and no other trends consistently following mixing curves, inclusions cannot account for the severe LREE enrichment observed and are thus excluded as the reason for it.

6.1.6 Hydrothermal alteration

LREE enrichment has, however, been reported in numerous zircon populations affected by hydrothermal alteration (Geisler et al. 2003, Hoskin 2005, Rayner et al. 2004, Grimes et al. 2009). This LREE enrichment is often accompanied by an increase in Ca (Geisler et al. 2003, Rayner et al. 2005, Grimes et al. 2009). The Birimian samples bear these characteristics (Fig. 30c). The Ti increase (Fig. 30a) may be explained by hydrothermal alteration, as well as the Th increase (Fig. 30d) and likewise Nb enrichment that is prominent in samples PK105 and ASGH028A, and the U enrichment that is present in all samples (Geisler et al. 2003, Rayner et al. 2004, Hoskin 2005, Grimes et al. 2009).

To further support this theory, the discrimination diagrams of Hoskin (2005), were used. PK105, ASGH028A and a zircons from the other samples cluster within the hydrothermal field (Fig. 31a). There is significant scatter, however, in fig. 31b but nevertheless PK105 and ASGH028A plot within the hydrothermal field along with a number of zircons from ASGH082A and ASGH084A. Even a high number of zircons that plot outside the hydrothermal field, plot within an area that has been associated with hydrothermal activity as well (Grimes et al. 2009; porous field, fig. 31a-b). These zircons are characterized by micro-porosity and hydrothermally-indicative geochemistry, but morphology resembles magmatic zircons (Grimes et. al. 2009). Only a handful of zircons fall within the magmatic field, a fact that one has to bear in mind throughout this work.

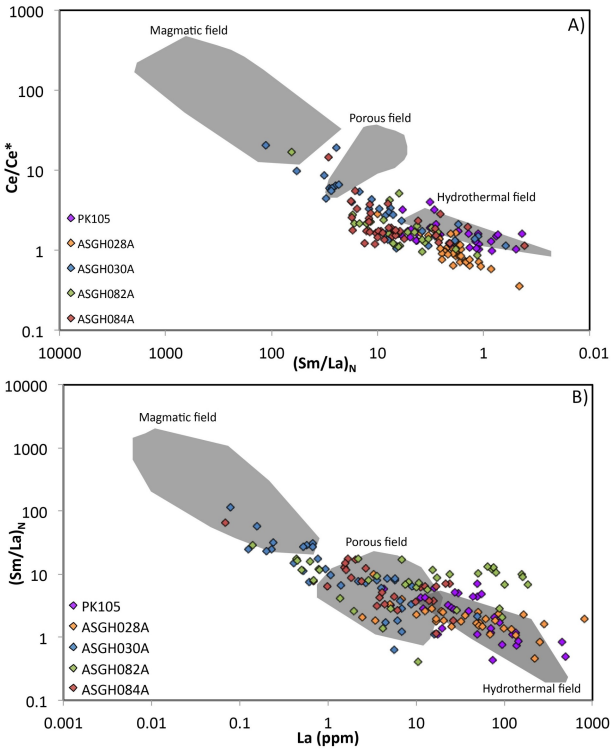

Fig. 31. Discrimination diagrams for magmatic and hydrothermal zircons. Adapted from Hoskin 2005. Plotted are Birimian samples of this research and data from Ballard et al. 2002, Geisler et al. 2003, Hoskin 2005 and Grimes et al. 2009. **A)** (Sm/La_N) versus Ce-anomaly (Ce/Ce*). Magmatic zircons have generally higher Ce-anomaly and lower LREE content (expressed by higher $(Sm/La)_N$ ratios) than hydrothermal zircons. **B)** La concentrations against $(Sm/La)_N$. Magmatic zircons plotted have generally lower LREE concentrations (expressed by higher $(Sm/La)_N$ ratios than hydrothermal zircons

6.1.7 Radiation damage

This element enrichment has been explained by hydrothermal fluids causing cation exchange within the crystal lattice of the zircon (Rayner et al. 2004). A preliminary requirement for this exchange has been speculated to be lattice damage, caused by radioactive decay of U and Th (Woodhead et al. 1991, Geisler et al. 2001). Energetic α-particles and less energetic α-nuclei are emitted in this process and destroy the lattice in their emission path (Seitz 1949, Ellsworth et al. 1994). A damaged lattice contains increased amounts of space (Seitz 1949) for cation exchange and the hydrothermal fluids providing those cations accelerate lattice recovery (Geisler et al. 2001, 2003). Higher amounts of U and Th increase the lattice damage (Marsellos & Garver 2010), and thus the higher concentrations of U and Th may be a primary feature and not an artefact of hydrothermal alteration. Fig. 32, a discrimination diagram for radiation damage (Whitehouse & Kamber 2002), shows a positive correlation between increasing U+Th concentrations and LREE enrichment (expressed as $(La/Gd)_N$). The same zircons show signs of radiation damage as well as hydrothermal alteration (Fig. 31), PK105 and ASGH028A being the most severely damaged.

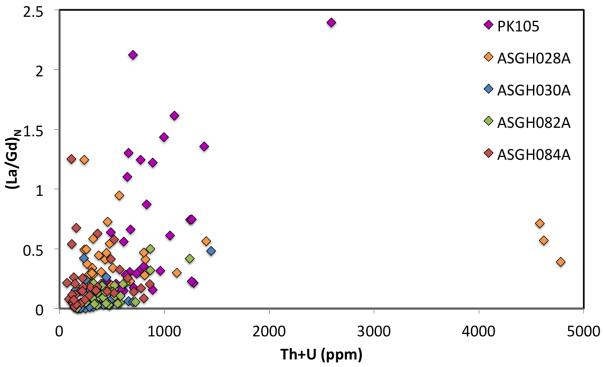

Fig. 32. Combined U and Th concentrations against the LREE enrichment (expressed as $(La/Gd)_N$) of the Birimian samples. Proxy for radiation damage. The steeper the trend, the more damaged the zircon (Whitehouse & Kamber 2002).

Radiation damage and subsequent hydrothermal alteration are thus the most plausible explanation for the apparent LREE enrichment. Because of the severity of LREE enrichment, PK105 will be omitted in some diagrams and interpretations.

6.1.8 Screening proposal

It is evident that before interpreting zircon geochemistry, especially detrital zircon geochemistry, some screening is necessary to avoid the incorporation of grains with abundant inclusions or grains that are hydrothermally altered. Metamorphic origin may be assessed with the Th/U, Hf concentrations, external morphology and internal structures (Hoskin & Black 2000, Hoskin & Schaltegger 2003). Coupling the P vs. (REE+Y)/P diagram (Fig. 28) with the P vs. $(Pr/Gd)_N$ plot (Fig. 30b) rather successfully depicts the presence of apatite inclusions. The Th vs. $(La/Sm)_N$ (Fig. 30d) has frequently been used to indicate the presence of monazite inclusions and may also be used in the case of possible allanite inclusions. However, coupling that with P vs. $(Pr/Gd)_N$ and Ca vs. ∑LREE increases the

reliability of interpretations (Fig. 30b-c). The same goes for xenotime within the Ca vs. ∑LREE and P vs. $(Pr/Gd)_N$ diagrams (Fig. 30b-c). Titanite inclusions may be determined with the Ti vs. ∑LREE concentrations (Fig. 30a). If inclusions may not explain the geochemistry, hydrothermal alteration may. The discrimination diagrams of Hoskin (2005) (Fig. 31a-b) serve to determine hydrothermal alteration. However, coupling them with the radiation diagram of Whitehouse & Kamber (2002) (Fig. 32), a commonly mentioned prerequisite to hydrothermal alteration, further supports any interpretation in that matter.

6.2 Source implications

6.2.1 Oceanic crust versus continental crust

Grimes et al. (2007) suggested that it is possible to discriminate between oceanic and continental zircon on the basis of the U/Yb and Y concentrations within zircon. The Y vs. U/Yb discrimination diagram has shown to have a >80% success rate in depicting whether zircon is derived from continental or oceanic crust. This is highly beneficial for detrital zircon studies, but problematic if detrital zircons are few and/or not representative of the population (Grimes et al. 2007).

Zircon grains from the Palaeoproterozoic Prøven Igneous Complex in Greenland, and the Palaeoproterozoic Birimian terrane in WAC plot within the continental field (Fig. 33), as was expected. The West Greenland Archean zircon and Jack Hills & Mount Narryer Hadean zircon also plot within the continental field. The modern oceanic MAR, SWIR and EPR zircon make up the oceanic field.

Generally, the U/Yb is controlled by difference in element solubility. Incompatible elements such as U, are readily soluble in fluids and thus subsequently enriched in the continental crust relative to oceanic

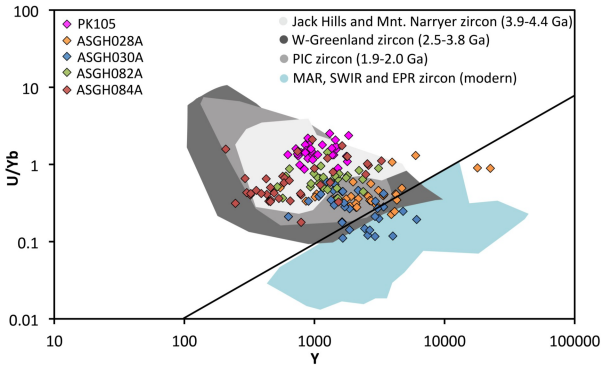

Fig. 33. Discrimination diagram that distinguishes oceanic crust zircon from continental crust zircon. The diagonal line separates the two environments. The data of this work plot within the continental field. (Oceanic MAR, SWIR and EPR zircon data obtained from Coogan & Hinton (2006) and Grimes et al. (2007). Hadean zircon data obtained from Maas et al. (1992), Wilde et al. (2001), Crowley et al. (2005) and Cavosie et al. (2006)).

crust (Fig. 34) and especially the upper mantle. The continental crust is less enriched in less incompatible elements, such as Y and Yb, relative to the oceanic crust (Fig. 34; Grimes et al. 2007). U and Yb have high partition coefficients in zircon and similar at that. Zircon also has an affinity for Y, but to a lesser extent (Bea et al. 1994). The concentrations in zircon are therefore controlled by the availability of these elements in the melt. Zircon should thus reflect the igneous environment it grew in, and thus have higher U/Yb and lower Y concentrations if derived from continental crust than if derived from MORB.

The U/Yb of the Palaeoproterozoic Birimian zircon and Prøven Igneous Complex may with fair confidence be explained by this continental crust differentiation process, as described above, as it had al-

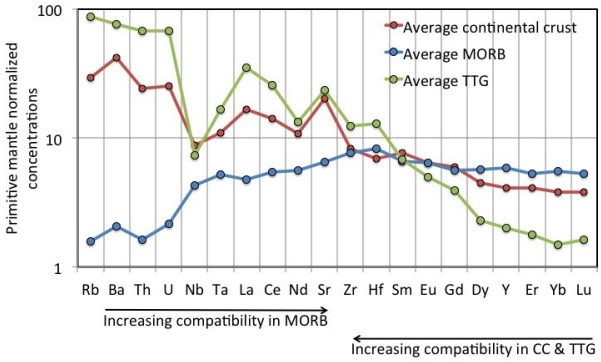

Fig. 34. Comparison of average continental crust (CC) concentrations (Kelemen et al. 2003), average Mid-Ocean Ridge Basalt (MORB) concentrations (Klein 2003) and average Tonalite-Trondhjemite-Granodiorite (TTG) concentrations (Moyen and Martin 2012) for various trace elements. Compatibility of elements increases from left to right. MORB is depleted in incompatible elements and slightly enriched in compatible elements. CC is enriched in incompatible elements but slightly depleted in compatible elements.

ready started by then (Bennett 2003). However, to ascribe this explanation to the U/Yb of West Greenland Archean zircon and even the Jack Hills and Mount Narryer zircon, the process must have started before the formation of host rocks. Hf and Nd isotope data from >3.6 Ga crustal gneiss suites and juvenile granite zircons and mafic lavas that have higher Nb/Th values than primitive mantle do indicate that it had started >4 Ga (Bennett 2003, Hawkesworth et al. 2010) and even as early as >4.45 Ga (Grimes et al. 2007).

Plotting the zircon age against U/Yb reveals that it has stayed constant through time (Fig. 35) and again places zircons from the Hadean, Archean and Palaeoproterozoic under the same hat; the continental crust. A number of authors have indeed inferred granitic magmas as the source of the Hadean zircons from various data (Maas et al. 1992, Crowley et al. 2007, Grimes et al. 2007). The relatively constant U/Yb may thus be implying that there has been no change in the processes behind the creation of the continental crust

and thus that plate tectonics may have started earlier than 3.2-3.0 Ga as postulated by some (e.g. Condie & Benn 2006, Næraa et al. 2012). This is a rather large statement for the U/Yb of zircons from only four environments and thus the data set must be increased.

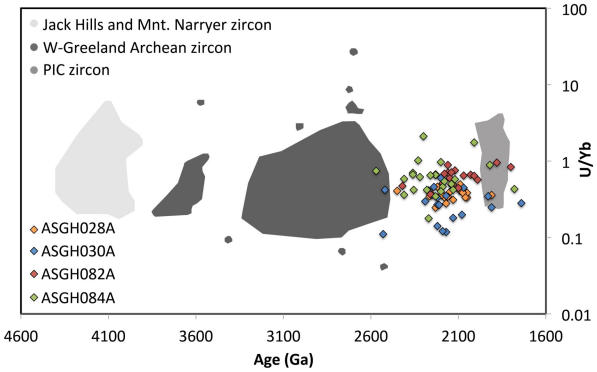

Fig. 35. Age vs. U/Yb ratios. Ages were obtained with U-Pb methods. No significant change in U/Yb can be observed from 4.4 Ga to 1.9 Ga.) See Fig. 33 for Hadean zircon references).

6.2.2 Phase stability

Phase stability has been utilised to infer pressures and/or temperatures of the environment melts originated in. Garnet and plagioclase play a large role in that context. Garnet has high partition coefficients for HREE in rock types ranging from tholeiite to rhyolite (Sisson & Bacon 1992, Green et al. 2000). It is commonly used as a barometer as it starts fractionating in melts at 9-10 kbars at 700°C and 15 kbars at 1000°C (Moyen & Martin 2012). Garnet fractionation has been ascribed to the middle and lower crust (Huang et al. 2013). Partition coefficients for HREE in plagioclase feldspars are however low opposed to its Eu^{2+} and Strontium (Sr) partition coefficients (Nagasawa 1971). Plagioclase feldspar can be stable at temperatures up to 1100°C in dehydrated systems whereas in hydrated systems it becomes unstable at temperatures and pressures below the garnet stability field (Moyen & Martin 2012). Plagioclase fractionation has thus been related to shallow to mid crustal depths (Kemp & Hawkesworth 2003) and subsequent low pressures. Coupled with garnet, these may serve to constrain the pressure at which melt is originated. The possibility of seeing these signatures in zircon may serve the same purpose in detrital zircon.

6.2.2.1 Plagioclase

The Eu^{2+}, so incompatible in zircon, is very compatible in plagioclase feldspar ($NaAlSi_3O_8$ – $CaAl_2Si_2O_8$), as it has the same valence state and a similar ionic radius to Ca^{2+} (1.14 Å) (Shannon 1976, Deer et al. 1993). Fractionation of plagioclase feldspar will thus deplete the melt in Eu^{2+} and thus zircon even more during partial melting or fractional crystallisation (Kemp & Hawkesworth 2003). This is particularly true for felsic magmas in the upper continental crust and increases with increasing fractionation. A similar principle applies to Sr. Sr forms a divalent ion with an ionic radius of 1.32 Å, which is very similar to Ca^{2+} (1.14 Å) and Eu^{2+}. Therefore Sr will fractionate into plagioclase feldspar and leave the remaining melt depleted in Sr and consequently zircon (Shannon 1976, Kemp & Hawkesworth 2003). Feldspar fractionation thus gives rise to increasingly negative Eu-anomalies and that should correlate with decreasing amounts of Sr in zircon.

Discrimination diagrams (Fig. 36) highlight the difference between the modern oceanic MAR, SWIR and EPR zircon and West Greenland Archean zircon, on one hand, and PIC and Birimian zircon, - and interestingly, Hadean zircon, on the other hand. The fact that oceanic zircon has generally lower Eu-anomalies and Sr concentrations (Fig. 36b-c) may be ascribed to its environment, where magmas are less fractionated.

Relative to the West Greenland Archean zircon and the oceanic zircon, the PIC, Birimian and Hadean zircon trend towards a lower Sr/Nd, larger negative Eu/Eu* and lower Sr/Eu* (Fig. 36). This trend is consistent with plagioclase feldspar fractionation in the source and is expected from the Birimian ASGH084A, ASGH082A and the PIC zircon, since their whole rock compositions display negative Sr- and Eu anomalies. In addition, the emplacement temperature for PIC falls into plagioclase stability field, at 850°C (Thrane et al. 2005). It should be mentioned that sample ASGH028A has lower Sr/Nd than expected, due to LREE enrichment. Also, sample ASGH084A deviates visibly from other Birimian zircon (Fig. 36a-b) for the the same reason. It lowers the Sr/Nd and Sr/Eu* values and decreases the Eu-anomaly and also serves to explain the lack of gradient, common for other samples, in fig. 36c.

Fig. 36c shows an anti-correlation between Ce/Ce* and Eu/Eu*; with increasing Ce-anomalies and negative Eu-anomalies. Interestingly, the zircon populations show fractionation trends away from their respective whole rock compositions, both with regards to Eu/Eu and Ce/Ce*. The trend, or lack thereof, of the LREE enriched ASGH028A (Fig. 36c) shows that the Ce-anomaly decreases with increasing LREE content (Maas et al. 1992, Pettke et al. 2005).

The amount of Ce^{4+} in melt, and consequently zircon, increases with increasing oxygen fugacity (fO_2) and decreasing crystallisation temperatures (Ballard et al. 2002, Pettke et al. 2005, Claiborne et al. 2010, Trail et al. 2012). The trend in fig. 36c thus indicates plagioclase feldspar fractionation during fractional crystallisation that is coupled with progressive oxidation. This might seem paradoxical, as negative Eu-anomalies have also commonly been associated with reducing conditions (Hoskin & Schaltegger 2003).

Trail et. al. (2012) experimental data suggests, however, that Eu^{2+} and Ce^{4+} can coexist at all terrestrial oxygen fugacities in silicate melts and fur-

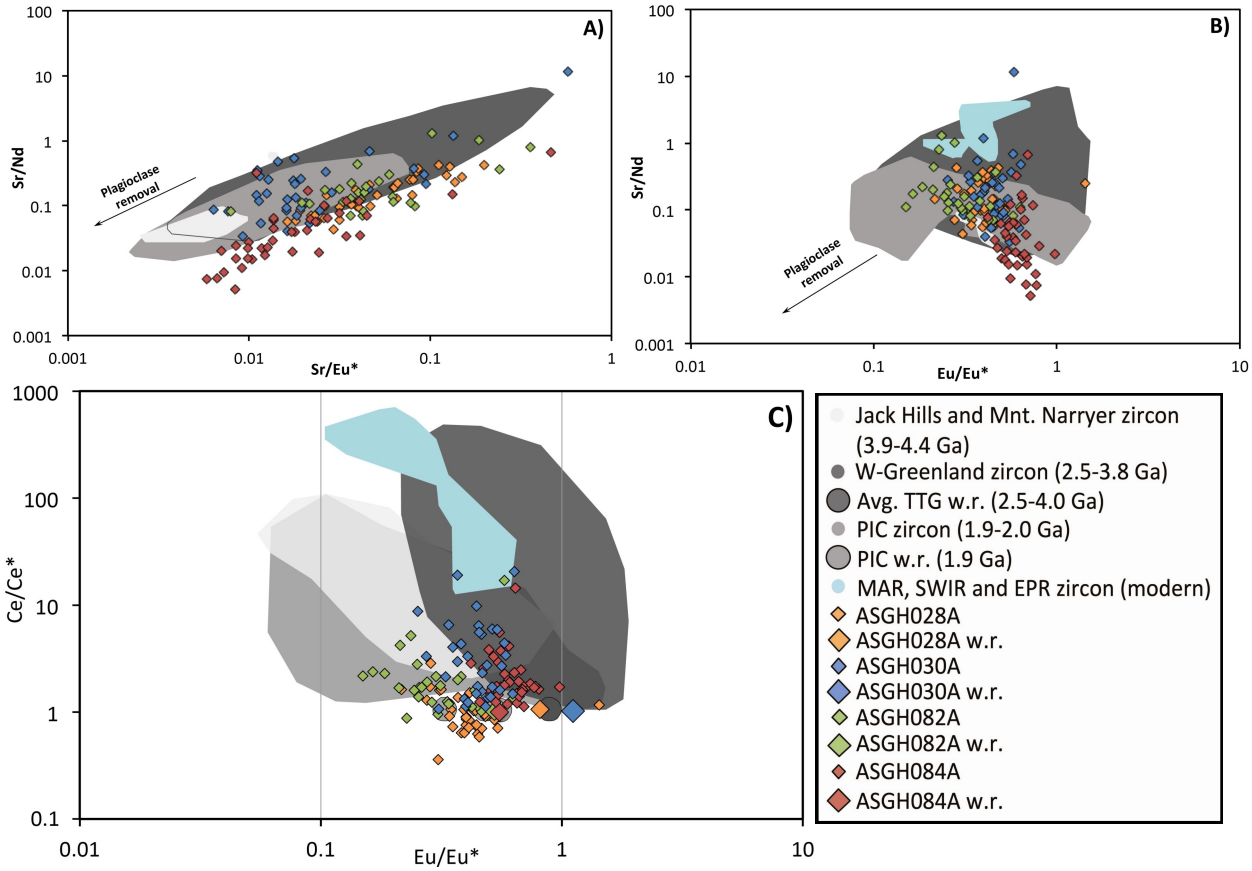

Fig. 36. **A)** Plagioclase fractionation is indicated by lower Sr/Eu* and Sr/Nd ratios. **B)** Plagioclase fractionation is indicated by larger negative Eu-anomalies and lower Sr/Nd ratios. **C)** Plagioclase fractionation is indicated by larger negative Eu-anomalies. Zircon populations tend to trend away from their host rock composition. **(**See fig. 33 for Hadean and ocean zircon references. Additional Hadean data from Iizuka et al. 2006.)

ther state that because Eu^{2+} is also dependent on oxygen fugacity, feldspar fractionation is not necessarily required to create a Eu-anomaly in zircon.

In addition, increasing Ce-anomalies in zircon may not necessarily be controlled only by increasing oxidation. Crystallisation of other phases in which $LREE^{3+}$ are compatible, but Ce^{4+} is not, may leave zircon as the only phase with kinship for Ce^{4+}. Ce^{4+} becomes concentrated in melt resulting in increased availability of Ce^{4+} for zircon (Claiborne et al. 2010).

The high Ce-anomalies observed in the West Greenland Archean zircon, coupled with lower Eu-anomalies, may indicate that oxygen fugacity holds less control on the Eu^{2+} in magmas than Ce^{4+}. Given that no feldspar fractionation occurred in the source rock, this contradicts the trend in the PIC and Hadean zircon, which do not deviate much from the Archean zircon with regard to the Ce-anomalies but have larger negative Eu-anomalies. However, plagioclase feldspar fractionation explains this trend perfectly. Indeed, Zhang et al. (2010) and Burnham & Berry 2012 note that feldspars control the Eu contents over the oxidation state.

There are indicators of plagioclase fractionation other than decreased Sr concentrations and negative Eu-anomalies. PIC and Birimian (minus AS-GH030A) whole rock data reveals increased amounts of Nb, Ta and HREE compared to the West Greenland Archean zircon, thus indicating that the magma was within the feldspar stability field. Perhaps the simplest explanation is the best one and feldspar fractionation occurred in the source of the Brimian (minus AS-GH030A) and PIC zircon populations.

6.2.2.2 Overlap

However, there is a prominent overlap between the West Greenland Archean zircon, and PIC and Birimian zircon in all three diagrams (Fig. 36). This is a surprising feature since it may suggest that feldspar fractionation occurred also in the source of some of the West Greenland detrital zircon. The Archean crust is composed mainly of Tonalite-Trondhjemite-Granodiorite (TTG) rock suites. It may therefore be assumed that the source rock of the West Greenland Archean zircons is TTG. TTGs have long been associated with generation at pressures that place them below the plagioclase feldspar stability field and thus the plagioclase fractionation signature is unexpected.

TTGs are felsic intrusive rocks very common in the Archean but otherwise rare (Moyen & Martin 2012). There is a common consensus that TTGs derive from a hydrous mafic source but the geodynamic envi-

ronment remains controversial and probably cannot be ascribed to one single setting (Moyen & Martin 2012). Broadly speaking, three theories prevail for the origin of Archean TTG rocks. TTGs that contain comparably high amounts of HREE have often been related to plateau processes. Upwelling in the mantle causes the base of the oceanic crust to heat up and generate high-HREE TTGs. The high amount of HREE is interpreted to reflect a garnet-free source and thus a lower pressure and depth of the TTG source environment (Martin & Moyen 2012). Contrasting this upwelling process, another process called downwelling may also generate TTGs, however these contain medium amounts of HREE. The mantle or the base of oceanic crust delaminates and sinks into the mantle (Kröner & Layer 1992). The increased pressure causes devolatilisation of these mafic fragments and subsequent melting. When this melt interacts with the mantle it may yield subduction zone-like magmas and thus TTGs (Martin & Moyen 2012). Both theories require a stagnant lithosphere; a single rigid, plate that covers the entire surface (Moresi & Solomatov 1998, Martin & Moyen 2012). The third and most commonly assumed hypothesis requires the lithosphere to be mobile, much like it is today. In this model TTGs formed in subduction zones.

The available compositions of TTG rocks near the retrieval locations (Kalsbeek 2001, Steenfelt et al. 2005, Szilas et al. 2013) of the zircons bear geochemical characteristics of high HREE TTGs, and thus upwelling processes. The REE profile is almost identical, as well as the K_2O/Na_2O, TiO_2, Fe_3O_2, Cr and Ni concentrations. Most other element concentrations and ratios fall in the field between medium HREE and high HREE TTGs. The significant overlap present in the diagrams thus may be explained by plagioclase fractionation in the source of some of the West Greenland Archean zircon. It implies that the zircon originated at lower pressures than is commonly depicted for TTGs and thus perhaps in an upwelling setting origin.

6.2.2.3 Garnet

Garnet fractionation has been inferred from e.g. REE diagrams, high Sr/Y and La/Yb of rocks. It is indicated by low Y and Yb concentrations and high Sr/Y and La/Yb (Fig. 37a and c), as it depletes the melt in

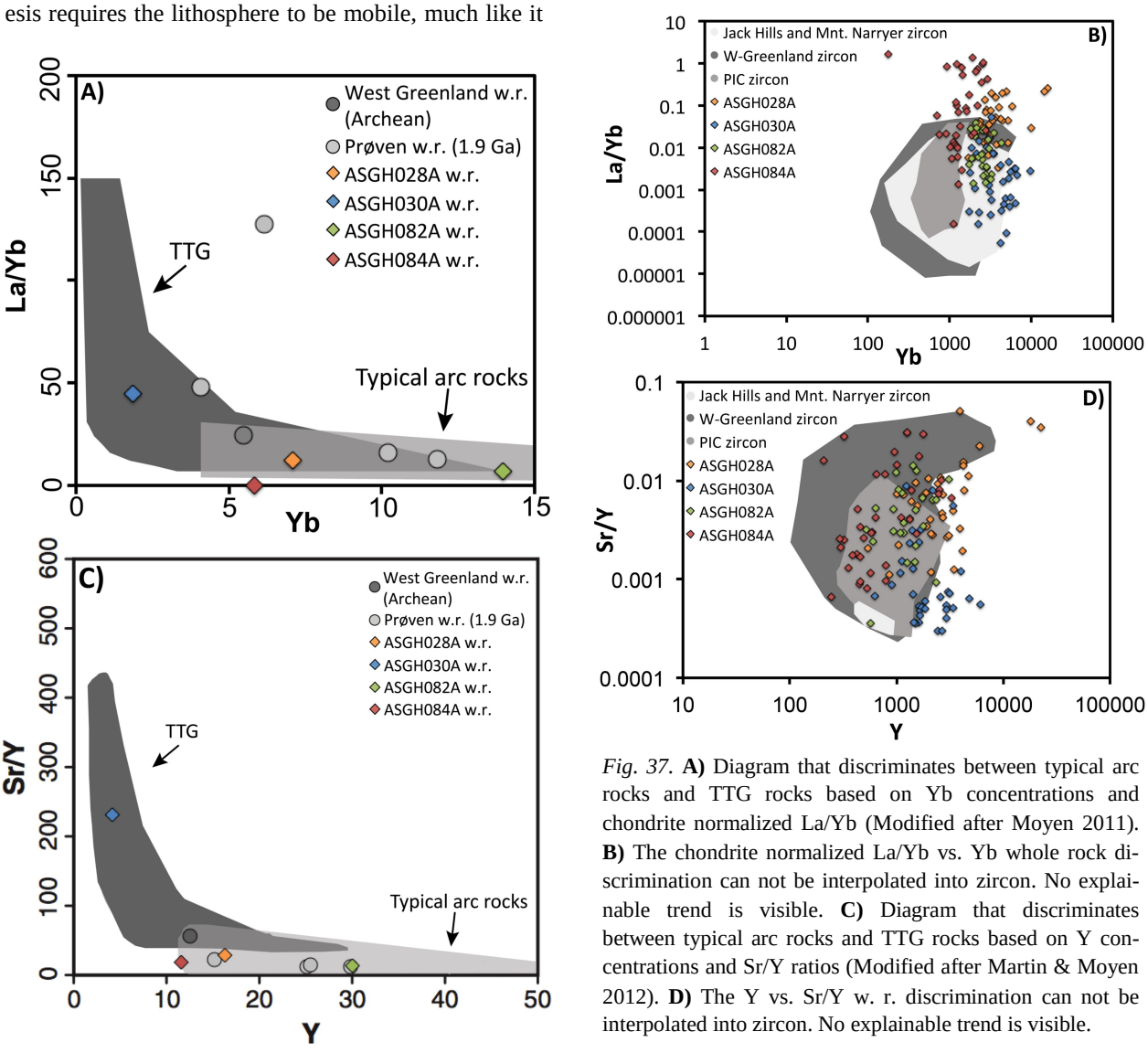

Fig. 37. **A)** Diagram that discriminates between typical arc rocks and TTG rocks based on Yb concentrations and chondrite normalized La/Yb (Modified after Moyen 2011). **B)** The chondrite normalized La/Yb vs. Yb whole rock discrimination can not be interpolated into zircon. No explainable trend is visible. **C)** Diagram that discriminates between typical arc rocks and TTG rocks based on Y concentrations and Sr/Y ratios (Modified after Martin & Moyen 2012). **D)** The Y vs. Sr/Y w. r. discrimination can not be interpolated into zircon. No explainable trend is visible.

HREE (Zhang et al. 2010). The only sample that falls into the garnet fractionation field is w.r. ASGH030A (Fig. 37a and c) indicating a deeper crustal source than other populations plotted. This garnet fractionation signature is not present in zircon. In fact, no trends are visible in the zircon images (Fig. 37b and d). Rubatto & Hermann (2007) provide the explanation for the lack of trends in fig. 37b and d. The zircon/garnet HREE partitioning is controlled by temperature. At 1000°C the zircon/garnet is ~1 but at ≤850°C the zircon/garnet is >1. Thus garnet is relatively incompetent in competing for HREE relative to zircon.

7 Conclusions

- Birimian sample PK105 is extensively enriched in LREE, as well as, but to a lesser degree, ASGH028A. Other Birimian samples are also variably enriched in LREE. This is caused by radiation damage and subsequent hydrothermal alteration as indicated by lower Ce-anomalies and increased La, U and Th concentration. Analytical errors, metamorphism, inclusions were excluded as the cause of this LREE enrichment.

- The usefulness of zircon as a discriminant tool of igneous processes is sensitive to secondary processes (e.g. alteration), which may skew the signal zircon sends. It is therefore pertinent to carefully screen the zircon populations as outlined here to avoid second order effects.

- Metamorphic effects may be determined based on low Th/U, increased Hf concentrations, external morphology and internal structures (Hoskin & Black 2000, Hoskin & Schaltegger 2003). Subsequently, screening for inclusions may be conducted. Apatite presence is depicted coupling P vs. (REE+Y)/P and P vs. $(Pr/Gd)_N$ diagrams. Th vs. $(La/Sm)_N$, P vs. (Pr/Gd)N and Ca vs. ΣLREE depicts the presence of monazite, xenotime and allanite inclusions. Ti vs. ΣLREE displays titanite inclusions. If neither metamorphism or inclusions explain LREE enrichment, hydrothermal alteration may. Coupling Th+U vs. $(La/Gd)_N$ with the La vs. $(Sm/La)_N$ and $(Sm/La)_N$ vs. Ce/Ce* diagrams of Hoskin (2005) displays hydrothermal alteration and the commonly mentioned prerequisite, radiation damage.

- The West Greenland Archean zircon, the Prøven Igneous Complex zircon and Birimian zircon fall within the continental field on a Y versus U/Yb discrimination diagram, implying that these zircons formed in magmas of continental crust affinity.

- The U/Yb of all zircon populations used in this work, remains relatively constant through time. This may imply that continental crust generating processes have remained unchanged through time and that plate tectonics might have started much earlier than the commonly postulated 3.2-3.0 Ga.

- The weak negative Eu-anomaly and lower Sr concentrations of the MAR and SWIR zircon stems from the fact that these are derived from less fractionation magmas than continental magmas.

- Signatures of plagioclase fractionation in the source of West Greenland Archean zircon are weaker than in the Prøven Igneous Complex zircon, Birimian zircon and Hadean zircon. This implies that the latter populations crystallised at shallower depths, where plagioclase was a stable phase in the source; at mid– to shallow crustal depths.

- The apparent overlap between the West Greenland Archean zircon and other continental zircon in this work demonstrates that plagioclase fractionation occurred in the source of some of the West Greenland Archean zircon. Indeed, whole rock compositions of local Archean TTGs may be classified as high-HREE TTGs. Shallower depths, within the plagioclase stability field, have been depicted for these TTGs as well as upwelling setting (Martin & Moyen 2012).

- As noted by Rubatto & Hermann (2007) an attempt to find garnet fractionation trends in zircon proved futile due to the high zircon/ garnet partition coefficient ratios, which lead to poorly resolved REE contrasts.

8 Acknowledgements

I would like to address special thanks to my supervisor, Anders Scherstén, for his endless patience, help, guidance and presence througout this project, and for improving it extensively. I would also like to thank Andreas Petersson for helping me with the zircon extraction and imaging, and with the LREE enrichment. Tonny Bernt Thomsen, at GEUS in Denmark, receives thanks for guiding me through the LA-ICP-MS analysis and data reduction, as well assisting me regarding the LREE enrichment. I would also like to thank Mikael Grenholm for allowing me to use his version of the Ghana geological map, Bernard Wood (Department of Earth Sciences, University of Oxford) for answering my e-mails, Edward Grew (School of Earth and Climate Sciences, University of Maine) for answering e-mails and providing references and Wälle

Markus (Institute of Geochemistry and Petrology, Eldgenössische Technische Hochschule Zürich) for help regarding the SILLS data reduction program. I thank Bára Dröfn Kristinsdóttir for allowing me to use her West African Craton map, for being a good listener and for being generally helpful. Finally, I thank my beloved fiancé, Tómas Andri Einarsson, for being a good listener and for caring for my well-being during this time.

9 References

Abouchami, W., Boher, M., Michard, A. & Albaréde, F.,1990: A major 2.1-Ga event of mafic magmatism in west Africa: an early state of crustal accretion. *Journal of Geophysical Research 95,* 17605-17629.

Adadey, K., Clarke, B., Théveniaut, H., Urien, P., Delor, C., Roig, J.Y., Feybesse, J.L., 2009: Geological map explanation - Map sheet 0503 B (1:100 000), CGS/BRGM/Geoman, Geological Survey Department of Ghana (GSD). No MSSP/2005/GSD/5a.

Agyei Duodu, J., Loh, G.K., Hirdes, W., Boamah, K.O., Baba, M., Anokwa, Y.M., Asare, C., Brakohiapa, E., Mensah, R.B., Okla, R., Toloczyki, M., Davis, D.W., Glück, S., 2009: Geological Map of Ghana 1:1,000,000. BGS/GGS, Accra, Ghana/ Hannover, Germany.

Ahrens, L.H., 1965: Some observations on the uranium and thorium distributions in accessory zircon from granitic rocks. *Geochimica et Cosmochimica Acta 29,* 711-716.

Anand, R., & Balakrishnan, S., 2011: Geochemical and Sm-Nd isotopic study of titanite from granitoid rocks of the eastern Dharwar Craton, southern India. *Journal of Earth System Science 120,* 237-251.

Attoh, K., 1982: Structure, gravity models, and stratigraphy of an Early Proterozoic volcanic-sedimentary belt in northeastern Ghana. *Precambrian Research 18,* 275–290.

Ballard, J.R., Palin, J.M., & Campbell, I.H., 2002: Relative oxidation states of magmas inferred from Ce(IV)/Ce(III) in zircon: Application to porphyry copper deposits of northern Chile. *Contributions to Mineralogy and Petrology 144,* 347-364.

Baratoux, L., Metelka, V., Naba, S., Jessell, M.W., Grégoire, M., Ganne, J., 2011: Juvenile Paleoproterozoic crust evolution during the Eburnean orogeny (~2.2–2.0;Ga), western Burkina Faso. *Precambrian Research 191,* 18-45.

Bea, F., 1996: Residence of REE, Y, Th and U in granites and crustal protoliths; implications for the chemistry of crustal melts. *Journal of Petrology 37,* 521-552.

Bea, F., Pereira, M.D., & Stroh, A., 1994: Mineral/ leucosome trace-element partitioning in a peraluminous migmatite (a laser ablation-ICP-MS study). *Chemical Geology 117,* 291-312.

Belousova, E.A., Griffin, W.L., & Pearson, N.J., 1998: Trace element composition and cathodoluminescence properties of southern African kimberlitic zircons. *Mineralogical Magazine 62A,* 355-366.

Belousova, E.A., Griffin, W.L., O'Reilly, S.Y., & Fisher, N.I., 2002: Apatite as an indicator mineral for mineral exploration: Trace-element compositions and their relationship to host rock type. *Journal of Geochemical Exploration 76,* 45-69.

Bennett, V.C., 2003: Compositional Evolution of the Mantle. *In* R.L. Rudnick (ed.): Treatise on Geochemistry 3, 493-519. Elsevier Ltd.

Boher, M., Abouchami, W., Michard, A., Albarede, N, & Arndt, N.T., 1992: Crustal growth in West Africa at 2.1 Ga. *Journal of Geophysical Research 97,* 345-369.

Braga, R., & Massonne, H., 2008: Mineralogy of inclusions in zircon from high-pressure crustal rocks from the Ulten Zone, Italian Alps. *Periodico Di Mineralogia 77,* 43-64.

Caironi, V., Garzanti, E., & Sciunnach, D., 1996: Typology of detrital zircon as a key to unravelling provenance in rift siliciclastic sequences (Permo-Carboniferous of Spiti, N India). *Geodinamica Acta 9,* 101-113.

Cavosie, A.J., Valley, J.W., Wilde, S.A., & E.I.M.F, 2006: Coorelated microanalysis of zircon: Trace elemement, $\delta^{18}O$, and U´Th´Pb isotopic constraints on the igneous origin of complex >3900 Ma detrital grains. *Geochemica et Cosmochimica Acta 70,* 5601-5616.

Cawood, P.A., & Tyler, I.M., 2004: Assembling and reactivating the Proterozoic Capricorn Orogen: Lithotectonic elements, orogenies, and significance. *Precambrian Research 128,* 201-218

Cherniak, D.J., Hanchar, J.M., & Watson, E.B., 1997: Rare-earth diffusion in zircon. *Chemical Geology, 134,* 289-301.

Claiborne, L.L., Miller, C.F., & Wooden, J.L., 2010: Trace element composition of igneous zircon: A thermal and compositional record of the accumulation and evolution of a large silicic batholith, Spirit

Mountain, Nevada. *Contributions to Mineralogy and Petrology 160,* 511-531.

Compston, W., & Pidgeon, R.T., 1986: Jack Hills, evidence of more very old detrital zircons in Western Australia. *Nature 321,* 766–769.

Condie, K.C., & Benn, K., 2006: Archean geodynamics: similar to or different from modern geodynamics? *In:* Benn, K., Mareschal, J.-C., Condie, K.C. (Eds.), Archean Geodynamics and Environments. AGU Geophysical Monograph, vol. 164. Washington, DC, pp. 47-60.

Coogan, L.A., & Hinton, R.W., 2006: Do the trace element compositions of detrital zircons require Hadean continental crust? *Geology 34,* 633–636.

Crowley, J.L., Myers, J.S., Sylvester, P.J., & Cox, R.A., 2005: Detrital zircon from the Jack Hills and Mount Narryer, Western Australia: Evidence for diverse >4.0 GA source rocks. *Journal of Geology 113,* 239-263.

Dampare, S.B., Shibata, T., Asiedu, D.K., Osae, S. & Banoeng-Yakubo, B., 2008: Geochemistry of Paleoproterozoic metavolcanic rocks from the southern Ashanti volcanic belt, Ghana: petrogenetic and tectonic setting implications. *Precambrian Research 162,* 403-423.

Davis, D.W., Hirdes, W., Schaltegger, U. & Nunoo, E.A., 1994: U-Pb age constraints on deposition and provenance of Birimian and gold-bearing Tarkwaian sediments in Ghana, West Africa. *Precambrian Research 67,* 89-107.

Davis, D.W., Williams, I.S., & Krogh, T.E. 2003: Historical development of zircon geochronology. *In* J. M. Hanchar & P. W. O. Hoskin (eds.): Reviews in mineralogy and geochemistry 53, 145-181. Mineralogical Society of America, Washington.

Deer, W.A., Howie, R.A. & Zussman, J., 1992: *An Introduction to the rock-forming minerals, 2nd ed.* Pearsons Education Limited. 696 pp.

Dennen, W.H. & Shields, R., 1956: Yttria in Zircon. *American Mineralogist 41,* 655-657.

Dhuime, B., Hawkesworth, C.J., Cawood, P.A., Storey, C.D., 2012: A change in the geodynamics of continental growth 3 billion years ago. *Science 335,* 1334-1336.

Dia, A., van Schmus, W.R., Kröner, A., 1997: Isotopic constraints on the age and formation of a Palaeoproterozoic volcanic arc complex in the Kedougou Inlier, eastern Senegal, West Africa. *Journal of African Earth Sciences 24,* 197- 213.

Drake, M.J., 1975: The oxidation state of europium as an indicator of oxygen fugacity. *Geochimica et Cosmochimica Acta 39,* 55-64.

Eisenlohr, B.N. & Hirdes, W., 1992: The structural development of the early Proterozoic Birimian and Tarkwaian rocks of soutwest Ghana, West Africa. *Journal of African Earth Sciences 14,* 313-325.

Ellsworth, S., Navrotsky, A., & Ewing, R.C., 1994: Energetics of radiation damage in natural zircon (ZrSiO4). *Physics & Chemistry of Minerals 21,* 140-149

Ennih, N. & Liégeois, J.-P., 2008: The boundaries of the West African craton, with special reference to the basement of the Moroccan metacratonic Anti-Atlas belt. *In* N. Ennih & J.-P. Ligeois (eds.): The boundaries of the West African craton. Geological Society, London, Special Publications 297, 1-17.

Escher, J.C., & Pulvertaft, T.C.R., 1995: Geological map of Greenland, 1:2 500 000. Copenhagen: Geological Survey of Greeland.

Faure, G., 1986: *Principles of Isotope Geology. Second edition.* John Wiley and Sons, New York, 589 pp.

Feybesse, J.-L., Miléesi, J.-P., 1994: The Archaean/ Proterozoic contact zone in West Africa: a mountain belt of décollement thrusting and folding on a continental margin related to 2.1 Ga convergence of Archaean cratons? *Precambrian Research 69,* 199–227.

Feybesse, J.-L., Billa, M., Guerrot, C., Duguey, E., Lescuyer, J.-L., Milési, J.-P. & Bouchot. V., 2006: The Paleoproterozoic Ghanian province: geodynamic model and ore controls, including regional stress modelling. *Precambrian Research 149,* 149-196.

Finch, R.J., Hanchar, J.M., Hoskin, P.W.O., & Burns, P.C., 2001: Rare-earth elements in synthetic zircon: Part 2. A single-crystal X-ray study of xenotime subsititution. *American Mineralogist 86,* 681-689.

Finch, R.J., & Hanchar, J.M., 2003: Structure and chemistry of zircon and zircon-group minerals. *In* J. M. Hanchar & P. W. O. Hoskin (eds.): Reviews in mineralogy and geochemistry 53, 1-25. Mineralogical Society of America, Washington.

Froude, D.O., Ireland, T.R., Kinny, P.D., Williams, I.S., Compston, W., Williams, I.R., & Myers, J.S., 1983: Ion microprobe identification of 4,100-4,200 Myr-old terrestrial zircons. *Nature 304,* 616-618.

Geisler, T., Ulonska, M., Schleicher, H., Pidgeon, R.T., & Van Bronswijk, W., 2001: Leaching and

differential recrystallization of metamict zircon under experimental hydrothermal conditions. *Contributions to Mineralogy and Petrology 141,* 53-65.

Geisler, T., Rashwan, A.A., Rahn, M.K.W., Poller, U., Zwingmann, H., Pidgeon, R.T., Schleicher, H. & Tomaschek, F., 2003: Low-temperature hydrothermal alteration of natural metamict zircons from the Eastern Desert, Egypt. *Mineralogical Magazine 67,* 485-508.

Geisler, T., Schaltegger, U., & Tomaschek, F., 2007: Re-equilibration of Zircon in Aqueous Fluids and Melts. *Elements 3,* 43-50.

Goldstein, J.I., Newbury, D.E., Echlin, P., Joy, D.C., Romig, Jr, A.D., Lyman, C.E., Fiori, C. & Lifshin, E., 1992: *Scanning Electron Microscopy and X-Ray Microanalysis. A Text for Biologists, Materials Scientists, and Geologists. Second Edition.* Plenum Press, New York and London.

Green, T.H., Blundy, J.D., Adam, J., & Yaxley, G.M., 2000: SIMS determination of trace element partition coefficients between garnet, clinopyroxene and hydrous basaltic liquids at 2-7.5 GPa and 1080-1200°C. *Lithos 53,* 165-187.

Gregory, C.J., Rubatto, D., Allen, C.M., Williams, I.S., Hermann, J., & Ireland, T., 2007: Allanite micro -geochronology: A LA-ICP-MS and SHRIMP U-Th-Pb study. *Chemical Geology 245,* 162-182.

Gregory, C.J., Rubatto, D., Hermann, J., Berger, A., & Engi, M., 2012: Allanite behaviour during incipient melting in the southern central alps. *Geochimica et Cosmochimica Acta 84,* 433-458.

Grimes, C.B., John, B.E., Kelemen, P.B., Mazdab, F.K., Wooden, J. L., Cheadle, M.J, Hanghøj, K., & Schwartz, J. J., 2007: Trace element chemistry of zircons from oceanic crust: A method for distinguishing detrital zircon provenance. *Geology 35,* 643 -646.

Grimes, C.B., John, B.E., Cheadle, M.J., Mazdab, F.K., Wooden, J.L., Swapp, S., & Schwartz, J.J., 2009: On the occurrence, trace element geochemistry, and crystallization history of zircon from in situ ocean lithosphere. *Contributions to Mineralogy and Petrology 158,* 757-783.

Grocott, J., Pulvertaft, T.C.R., 1990: The Early Proterozoic Rinkian Belt of Central West Greenland. *In* Lewry, J.F., Stauffer, M.R. (ed.) The Early Proterozoic Trans-Hudson Orogen of North America: Geological Association of Canada. Special Paper 37 443 –463.

Guillong, M., Meier, D.L., Allan, M.M., Heinrich, C.A. & Yardley, B.W.D., 2008: Appendix A6: SILLS: A MATLAB-based program for the reduction of laser ablation ICP-MS data of homogeneous materials and inclusions. In: P. Sylvester (editor) *Laser Ablation-ICP-MS in the Earth Sciences: Current Practices and Outstanding Issues 40,* 328-333.

Hanchar, J.M., Finch, R.J., Hoskin, P.W.O., Watson, E.B., Cherniak, D.J., & Mariano, A.N., 2001: Rare earth elements in synthetic zircon: Part 1. synthesis, and rare earth element and phosphorus doping. *American Mineralogist 86,* 667-680.

Hanchar, J.M. & Watson, E.B., 2003: Zircon Saturation Thermometry. *In* J. M. Hanchar & P. W. O. Hoskin (eds.): Reviews in mineralogy and geochemistry 53, 89-112. Mineralogical Society of America, Washington.

Hanchar, J.M., & van Westrenen, W., 2007: Rare earth element behavior in zircon-melt systems. *Elements 3,* 37-42.

Harley, S.L., & Kelly, N.M. 2007. Zircon: Tiny but timely. *Elements 3,* 13-18.

Hawkesworth, C.J., Dhuime, B., Pietranik, A.B., Cawood, P.A., Kemp, A.I.S., & Storey, C.D., 2010: The generation and evolution of the continental crust. *Journal of the Geological Society 167,* 229-248.

Heaman, L.M., Bowins, R., & Crocket, J., 1990:. The chemical composition of igneous zircon suites: Implications for geochemical tracer studies. *Geochimica et Cosmochimica Acta 54,* 1597-1607.

Hellstrom, J., Paton, C., Woodhead. J. & Hergt, J., 2008: Appendix A9: Iolite: Software for spatially resolved LA-(QUAD and MC)-ICP-MS Analysis. In: P. Sylvester (editor) *Laser Ablation-ICP-MS in the Earth Sciences: Current Practices and Outstanding Issues 40,* 328-333.

Henderson, G., & Pulvertaft, T.C.R., 1987: The lithostratigraphy and structure of a Lower Proterozoic dome and nappe complex. Descriptive text to 1:100 000 sheets Mârmorilik 71 V. 2 Syd, Nûgâtsiaq 71 V.2 Nord and Pangnertôq 72 V.2 Syd, 72 pp. Copenhagen: Grønlands Geologiske Undersøgelse.

Hickling, N.L., Phair, G., Moore, R., Rose, H. J., Jr. 1970. Boulder Creek Batholith, Colorado. Part I: Allanite and its bearing upon age patterns. *Geological Society of America Bulletin 81,* 1973-1993.

Hinton, R.W. & Upton, B.G.J., 1991: The chemistry of zircon: Variations within and between large crystals

from syenite and alkali basalt xenoliths. *Geochimica et Cosmochimica Acta 55*, 3287-3302.

Hirdes, W., Davis, D.W. & Eisenlohr, B.N., 1992: Reassessment of Proterozoic granitoid ages in Ghana on the basis of U/Pb zircon and monazite dating. *Precambrian Research 56*, 89-96.

Hirdes, W. & Davis, D.W., 1998: First U-Pb zircon age extrusive volcanism in the Birimian Supergroup of Ghana, West Africa. *Journal of African Earth Sciences 27*, 291-294.

Hoffman, P.F., 1990: Dynamics of the tectonic assembly of northeast Laurentia in geon 18 (1.9–1.8 Ga). *Geoscience Canada 17*, 222– 226.

Hoskin, P.W.O., & Ireland, T.R., 2000: Rare earth element chemistry of zircon and its use as a provenance indicator. *Geology 28*, 627-630.

Hoskin, P.W.O., Kinny, P.D., Wyborn, D., & Chappell, B.W., 2000: Identifying accessory mineral saturation during differentiation in granitoid magmas: An integrated approach. *Journal of Petrology 41*, 1365-1396.

Hoskin, P.W.O., & Black, L.P., 2000: Metamorphic zircon formation by solid-state recrystallization of protolith igneous zircon. *Journal of Metamorphic Geology 18*, 423-439.

Hoskin, P.W.O. & Schaltegger, U., 2003: The composition of zircon and igneous and metamorphic petrogenesis. *In* J. M. Hanchar & P. W. O. Hoskin (eds.): Reviews in mineralogy and geochemistry 53, 27-62. Mineralogical Society of America, Washington.

Hoskin, P.W.O., 2005: Trace-element composition of hydrothermal zircon and the alteration of Hadean zircon from the Jack Hills, Australia. *Geochimica et Cosmochimica Acta 69*, 637-648.

Huang, H., Polat, A., & Fryer, B.J., 2013: Origin of Archean tonalite-trondhjemite-granodiorite (TTG) suites and granites in the Fiskenæsset region, southern West Greenland: Implications for continental growth. *Gondwana Research 23*, 452-470.

Iizuka, T., Horie, K., Komiya, T., Maruyama, S., Hirata, T., Hidaka, H., & Windley, B.F., 2006: 4.2 Ga zircon xenocryst in an Acasta Gneiss from northwestern Canada: Evidence for early continental crust. *Geology 34*, 245-248.

Iizuka, T., McCulloch, M.T., Komiya, T., Shibuya, T., Ohta, K., Ozawa, H., Sugimura, E., & Collerson, K.D., 2010: Monazite geochronology and geochemistry of meta-sediments in the Narryer Gneiss Complex, Western Australia: Constraints on the tectonothermal history and provenance. *Contributions to Mineralogy and Petrology 160*, 803-823.

Jennings, E.S., Marschall, H.R., Hawkesworth, C.J., & Storey, C.D., 2011: Characterization of magma from inclusions in zircon: Apatite and biotite work well, feldspar less so. *Geology 39*, 863-866.

Jochum, K.P., & Nohl, U., 2008: Reference materials in geochemistry and environmental research and the GeoReM database. *Chemical Geology 253*, 50-53.

John, J.W. 2003: Oxygen Isotopes in Zircon. *In* J. M. Hanchar & P. W. O. Hoskin (eds.): Reviews in mineralogy and geochemistry 53, 343-385. Mineralogical Society of America, Washington.

Kalsbeek, F., 1981: The northward extent of the Archaean basement of Greenland – a review of Rb-Sr whole-rock ages. *Precambrian Research 14*, 203–219.

Kalsbeek, F., 2001: Geochemical comparison between Archaean and Proterozoic orthogneisses from the Nagsugtoqidian Orogen, West Greenland. *Precambrian Research 105*, 165-181.

Kelemen, P.B., Hanghøj, K., & Greene, A.R., 2003.: One View of the Geochemistry of Subduction-related Magmatic Arcs, with an Emphasis on Primitive Andesite and Lower Crust. *In* R.L. Rudnick (ed.): Treatise on Geochemistry 3, 593-659. Elsevier Ltd.

Kemp, A.I.S. & Hawkesworth, C.J., 2003: Granitic Perspectives on the Generation and Secular Evolution of the Continental Crust. *In* R.L. Rudnick (ed.): Treatise on Geochemistry, 433-463. Elsevier Ltd.

Kinny, P.D. & Maas, R., 2003: Lu-Hf and Sm-Nd isotope systems in zircon. *In* J. M. Hanchar & P. W. O. Hoskin (eds.): Reviews in mineralogy and geochemistry 53, 327-341. Mineralogical Society of America, Washington.

Kinny, P.D., Williams, I.S., Froude, D.O., Ireland, T.R., & Compston, W., 1988: Early Archaean zircon ages from orthogneisses and anorthosites at Mount Narryer, Western Australia. *Precambrian Research 38*, 325-341

Kinny, P.D., Wijbrans, J.R., Froude, D.O., Williams, I.S., & Compston, W., 1990: Age constraints on the geological evolution of the Narryer Gneiss Complex, Western Australia. *Australian Journal of Earth Sciences 37*, 51-69

Klein, E.M., 2003. Geochemistry of the Igneous Oceanic Crust. *In* R.L. Rudnick (ed.): Treatise on Geochemistry 3, 433-463. Elsevier Ltd.

Košler, J., Fonneland, H., Sylvester, P., Tubrett, M., & Pedersen, R., 2002: U-Pb dating of detrital zircons for sediment provenance studies - A comparison of laser ablation ICPMS and SIMS techniques. *Chemical Geology 182,* 605-618.

Košler, J. & Sylvester, P. J., 2003: Present trends and the future of zircon in geochronology: laser ablation ICPMS. *In* J.M. Hanchar & P.W.O. Hoskin (eds.): Reviews in mineralogy and geochemistry 53, 243-275. Mineralogical Society of America, Washington.

Kouamelan, A.N., Delor, C., Peucat, J.J., 1997: Geochronological evidence for reworking of Archean terrains during the Early Proterozoic (2.1 Ga) in the western Côte d'Ivoire (Man Rise – West African Craton). *Precambrian Research 86,* 177–199.

Kramers, J., Frei, R., Newville, M., Kober, B., & Villa, I., 2009: On the valency state of radiogenic lead in zircon and its consequences. *Chemical Geology 261,* 3-10.

Kröner, A., & Layer, P.W., 1992: Crust formation and plate motion in the early Archean. *Science 256,* 1405 -1411.

Leube, A., Hirdes, W., Mauer, R. & Kesse, G.O., 1990: The early Proterozoic Birimian Supergroup of Ghana and some aspects of its associated gold mineralization. *Precambrian Research 46,* 139-165.

Lompo, M., 2009: Geodynamic evolution of the 2.25–2.0 Ga Palaeoproterozoic magmatic rocks in the Man -Leo Shield of the West African Craton. A model of subsidence of an oceanic plateau. *In* S.M. Reddy, R. Mazumder, D.A.D. Evans & A.S. Collins (eds.): *Paleoproterozoic Supercontinents and Global Evolution*. Geological Society of London, Special Publications 323, 231-254.

Longerich, H.P. & Diegor, W., 2001: Introduction to mass spectrometry. *In* P. Sylvester (ed.), Laser Ablation ICPMS in the Earth Sciences, Short course series volume 29, Mineralogical Association of Canada, 243 pp.

Maas, R., Kinny, P.D., Williams, I.S., Froude, D.O., & Compston, W., 1992: The Earth's oldest known crust: A geochronological and geochemical study of 3900-4200 MA old detrital zircons from Mt. Narryer and Jack Hills, Western australia. G*eochimica et Cosmochimica Acta 56,* 1281-1300.

Marsellos, A.E., & Garver, J.I., 2010: Radiation damage and uranium concentration in zircon as assessed by Raman spectroscopy and neutron irradiation. *American Mineralogist 95,* 1192-1201.

Martin, H., & Moyen, J.F., 2002: Secular changes in TTG composition as markers of the progressive cooling of the Earth. *Geology 30,* 319–322.

Marsh, J.H., Grew, E.D., Gerbi, C.C., & Yates, M.G., 2012: The Petrogenesis of the Garnet Menzerite-(Y) in Granulite Facies Rocks of the Parry Sound Domain, Grenville Province, Ontario. *The Canadian Mineralogist 50,* 73-99.

McFarlane, C.R.M., & McCulloch, M.T., 2007: Coupling of in-situ Sm-Nd systematics and U-Pb dating of monazite and allanite with applications to crustal evolution studies. *Chemical Geology 245,* 45-60.

Mole, D.R., Fiorentini, M.L., Thebaud, N., McCuaig, T.C., Cassidy, K.F., Kirkland, C.L., Wingate, M.T.D., Romano, S.S., Doublier, M.P. & Belousova, E.A., 2012: Spatio-temporal constraints on lithospheric development in the southwest-central Yilgarn Craton, Western Australia. *Australian Journal of Earth Sciences 59,* 625-656.

Moresi, L. & Solomatov, V., 1998: Mantle convection with a brittle lithosphere: thoughts on the global tectonic styles of the Earth and Venus. *Geophys. J. Int. 133,* 669–682.

Moyen, J.-F., 2011: The composite Archaean grey gneisses: Petrological significance, and evidence for a non-unique tectonic setting for Archaean crustal growth. *Lithos 123,* 21-36.

Moyen, J., & Martin, H., 2012: Forty years of TTG research. *Lithos 148,* 312-336.

Murali, A.V., Parthasarathy, R., Mahadevan, T.M., & Das, S., 1983: Trace element characteristics, REE patterns and partition coefficients of zircon from different geological environments – A case study on Indian zircons. *Geochimica et Cosmochimica Acta 47,* 2047-2052.

Myers, J.S., & Williams, I.R., 1985: Early Precambrian crustal evolution at Mount Narryer, Western Australia. *Precambrian Research 27,* 153-163.

Myers, J.S., 1988: Early Archaean Narryer Gneiss Complex, Yilgarn Craton, Western Australia. *Precambrian Research 38,* 297-307.

Nagasawa, H., 1971: Partitioning of Eu and Sr between coexisting plagioclase and K-feldspar. *Earth and Planetary Science Letters 13,* 139-144.

Nelson, D.R., 2001: An assessment of the determination of depositional ages for Precambrian clastic sedimentary rocks by U-Pb dating of detrital zircons. *Sediment Geol. 141–142,* 37–60.

Nutman, A.P., Kinny, P.D., Compston, W., & Williams, I.S., 1991: SHRIMP U-Pb zircon geochronology of the Narryer Gneiss Complex, Western Australia. *Precambrian Research 52,* 275-300.

Nutman, A.P., Bennett, V.C., Kinny, P.D., & Price, R., 1993: Large-scale crustal structure on the northwestern Yilgarn Craton, Western Australia: evidence from Nd isotopic data and zircon geochronology. *Tectonics 12,* 971–981.

Næraa, T., Scherstén, A., Rosing, M.T., Kemp, A.I.S., Hoffmann, J.E., Kokfelt, T.F., & Whitehouse, M.J. 2012: Hafnium isotope evidence for a transition in the dynamics of continental growth 3.2 Gyr ago. *Nature 485,* 627-630.

Occhipinti, S.A., Sheppard, S., Tyler, I.M., Nelson, D.R., 1999: Deformation and metamorphism during the c. 2000 Ma Glenburgh Orogeny and c. 1800 Ma Capricorn Orogeny. *In* Watt, G.R., Evans, D.A.D. (Eds.), Two Billion Years of Tectonics and Mineralisation. Geol. Soc. Aust. Perth Abstr. 56, 26– 29.

Paton, C., Hellstrom, J.C., Paul, P., Woodhead, J.D. & Hergt, J.M., 2011: Iolite: Freeware for the visualisation and processing of mass spectrometic data. *Journal of Analytical Atomic Spectrometry 26,* 2508-2518.

Pettke, T., Audétat, A., Schaltegger, U., & Heinrich, C.A., 2005: Magmatic-to-hydrothermal crystallization in the W-Sn mineralized Mole Granite (NSW, Australia). Part II: Evolving zircon and thorite trace element chemistry. *Chemical Geology 220,* 191-213.

Pidgeon, R.T., & Wilde, S.A., 1998: The interpretation of complex zircon U-Pb systems in Archaean granitoids and gneisses from the Jack Hills, Narryer Gneiss Terrane, Western Australia. *Precambrian Research 91*, 309–332.

Pidgeon, R.T., & Nemchin, A.A., 2006: High abundance of early Archean grains and the age distribution of detrital zircons in a sillimanite-bearing quartzite from Mt. Narryer, Western Australia. *Precambrian Research 150*, 201–220.

Pupin, J.P., 1980: Zircon and granite petrology. *Contributions to Mineralogy and Petrology 73,* 207-220.

Rayner, N., Stern, R.A., & Carr, S.D., 2005: Grain-scale variations in trace element composition of fluid -altered zircon, Acasta Gneiss Complex, Northwestern Canada. *Contributions to Mineralogy and Petrology 148,* 721-734.

Rollinson, H.R. 1993: *Using geochemical data: evaluation, presentation, interpretation.* Pearson, 352 pp.

Rubatto, D., 2002: Zircon trace element geochemistry: Partitioning with garnet and the link between U-Pb ages and metamorphism. *Chemical Geology 184,* 123-138.

Rubatto, D., & Hermann, J., 2007: Experimental zircon/melt and zircon/garnet trace element partitioning and implications for the geochronology of crustal rocks. *Chemical Geology 241,* 38-61.

Salah, I.A., Liegeois, J.-P. & Pouclet, A., 1996: Evolution d'un arc insulaire océanique birimien précoce au Liptako nigérin (Sirba): géologie, géochronologie et géochimie. *Journal of African Earth Sciences 22,* 235-254.

Scherstén, A., Sønderholm, M., & Steenfelt, A., 2007: Provenance of West Greenland Cretaceous and Paleocene sandstones and stream sediment samples based on U-Pb dating of detrital zircon: data and results. Rapport Grønlands Geologiske Undersøgelse 21.

Scott, D.J., 1999: U-Pb geochronology of the eastern Hall Peninsula, southern Baffin Island, Canada: a northern link between the Archean of West Greenland and the Paleoproterozoic Torngat Orogen of northern Labrador. *Precambrian Research 93,* 5–26.

Seitz, F., 1949: On the disordering of solids by action of fast massive particles. *Discussions of the Faraday Society 5,* 271-282.

Shannon, R.D., 1976: Revised effective ionic radii and systematic studies of interatomic distances in halides and chalcogenides. *Acta Crystallographica Section A 32,* 751-767.

Sisson, T.W. & Bacon, C.R., 1992: Garnet High-Silica Rhyolite Trace-Element Partition-Coefficients Measured by Ion Microprobe. *Geochimica et Cosmochimica Acta 56,* 2133-2136.

Söderlund, U. & Johansson, L., 2002: A simple way to extract baddeleyite. Geochemistry, Geophysics, Geosystems 3, doi:10.1029/2001GC000212.

Soumaila, A., Henry, P. & Rossy , M., 2004: Contexte de mise en place des roches basiques de la ceinture de roches vertes birimienne de Diagorou-Darbani (Liptako, Niger, Afrique de l'Ouest): plateau océanique ou environnement d'arc/bassin arriére-arc océanique. *Comptes Rendus Geoscience 336,* 1137-1147.

Spandler, C., Hermann, J., & Rubatto, D., 2004: Exsolution of thortveitite, yttrialite, and xenotime during low-temperature recrystallization of zircon from New Caledonia, and their significance for trace

element incorporation in zircon. *American Mineralogist 89*, 1795-1806.

Speer, J. A., 1982: The actinide orthosilicates. *In* Ribbe, P.H. (ed.) Reviews in Mineralogy 5, 113-135.

Steenfelt, A., Garde, A., Moyen J.-F., 2005: Mantle wedge involvement in the petrogenesis of Archaean grey gneisses in West Greenland. *Lithos 79*, 207-228.

Steiger, R.H. & Jäger, E., 1977: Subcommission on geochronology: Convention on the use of decay constants in geo- and cosmochronology. *Earth and Planetary Science Letters 36*, 359-362

Sylvester, P.J. & Attoh, K., 1992: Lithostratigraphy and composition of 2.1 Ga greenstone belts of the West African Craton and their bearing on crustal evolution and the Archean-Proterozoic boundary. *Journal of Geology 100*, 377-393.

Szilas, K., Van Hinsberg, V., Kisters, A.F.M., Hoffmann, J.E., Windley, B.F., Kokfelt, T.F., Scherstén, A., Frei, R., Rosing, M.T., & Münker, C., 2013: Remnants of arc-related Mesoarchaean oceanic crust in the Tartoq Group of SW Greenland. *Gondwana Research 23*, 436-451.

Taylor, P.N., Moorbarth, S., Leube, A. & Hirdes, W., 1992: Early Proterozoic crustal evolution in the Birimian of Ghana: constraints from geochronology and isotope geochemistry. *Precambrian Research 56*, 97-111.

Taylor, H.E. 2001: *Inductively coupled plasma-mass spectrometry: Practices and techniques.* San Diego, California: Academic Press, pp. 294.

Thomas, J.B., Bodnar, R.J., Shimizu, N., & Chesner, C.A. 2003: Melt inclusions in zircon. *In* J. M. Hanchar & P. W. O. Hoskin (eds.): Reviews in mineralogy and geochemistry 53, 63-87. Mineralogical Society of America, Washington.

Thrane, K., Baker, J., Connelly, J., & Nutman, A., 2005: Age, petrogenesis and metamorphism of the syn-collisional Prøven Igneous Complex, West Greenland. *Contributions to Mineralogy and Petrology 149*, 541-555.

Tiepolo, M., Oberti, R. & Vannucci, R., 2002: Trace-element incorporation in titanite: Constraints from experimentally determined solid/liquid partition coefficients. *Chemical Geology 191,* 105-119.

Trail, D., Bruce Watson, E., & Tailby, N.D., 2012: Ce and Eu anomalies in zircon as proxies for the oxidation state of magmas. *Geochimica Et Cosmochimica Acta 97*, 70-87.

Valley, J.W., 2003: Oxygen Isotopes in Zircon. In: J.M. Hanchar & P.W.O. Hoskin (Eds.): Reviews in mineralogy and geochemistry 53, 343-385. Mineralogical Society of America, Washington.

Van Kranendonk, M.J., St-Onge, M.R., Henderson, J.R., 1993: Paleoproterozoic tectonic assembly of Northeast Laurentia through multiple indications. *Precambrian Research 63*, 325–347.

Vidal, M., Alric, G., 1994: The Palaeoproterozoic (Birimian) of Haute-Comoé, in the West African Craton in Côte d'Ivoire: a transtensional back-arc basin. *Precambrian Research 65*, 207–229.

Villaseca, C., Martín Romera, C., De la Rosa, J., & Barbero, L., 2003: Residence and redistribution of REE, Y, Zr, Th and U during granulite-facies metamorphism: Behaviour of accessory and major phases in peraluminous granulites of central Spain. *Chemical Geology 200*, 293-323.

Watkins, A.P., Iliffe, J.E., Sharp, W.E., 1993: The effects of extensional and transpressional tectonics upon the development of Birimian sedimentary facies in Ghana, W. Africa: evidence from the Bomfa/Beposo District, near Konongo. *Journal of African Earth Sciences 17*, 457-478.

Watson, E.B., 1996: Surface enrichment and trace- element uptake during crystal growth. *Geochimica et Cosmochimica Acta 60, 5013–5020.*

Watson, E.B., Cherniak, D.J., Hanchar, J.M., Harrison, T.M., & Wark, D.A., 1997: The incorporation of Pb into zircon. *Chemical Geology 141*, 19-31.

Whitehouse, M.J., Kamber, B.S., 2002: On the overabundance of light rare earth elements in terrestrial zircons and its implications for Earth's earliest magmatic differentiation. *Earth and Planetary Science Letters 6442*, 1–14.

Wilde, S.A., Valley, J.W., Peck, W.H., & Graham, C.M., 2001: Evidence from detrital zircons for the existence of continental crust and oceans on the earth 4.4 Gyr ago. *Nature 409*, 175-178.

Williams, I.R., & Myers, J.S., 1987: Archaean geology of the Mount Narryer region, Western Australia. *Geological Survey of Australia. Report 22.*

Winter, J.D., 2010: *Principles of Igneous and Metamorphic Petrology*, 2nd edition. Pearson Education, 720 pp.

Woodhead, J.A.. Rossman, G.R., & Thomas, A.P., 1991: Hydrous species in zircon. *American Mineralogist 76*, 1533-1546.

Appendix A

Table 1: Birimian sample PK105. LA-ICP-MS zircon analysis results (in ppm).

	PK 105 - 4	PK 105 - 5	PK 105 - 2	PK 105 - 1	PK 105 - 3	PK 105 - 15	PK 105 - 16	PK 105 - 17	PK 105 - 18
P	108	67	108	221	60.3	56.2	164	143	300
Ca	2490	3680	1840	5710	4510	2460	11480	2770	8070
Ti	16.9	35	51	19	11	82	420	94	75
V	1.93	2.81	3.95	2.9	1.02	4.9	16.6	6	4.4
Sr	32	35	40	73	51	25.1	127	30.1	74
Y	950	910	950	1470	890	790	1830	850	890
Nb	5.13	6.8	5.9	2.94	5.2	4.67	23.1	8.2	7.4
La	22.9	49	30	25	70	39	490	450	94
Ce	141	160	205	270	264	255	1040	780	368
Pr	13.6	21.3	38	16.5	35.5	39	123	81	37.8
Nd	95	113	350	101	251	257	560	440	195
Sm	46	34.1	93	45.9	52	63	152	238	45
Eu	53	10.6	149	21.9	36	95	74	75	34.7
Gd	54	47	82	97	47	58	171	177	54.8
Tb	11.1	8	11.9	18.9	6.6	9.4	26.8	13.7	10.2
Dy	102	77	98	184	63	77	239	100	88
Ho	30.9	21	28	48	22.9	23	54	21.1	26.7
Er	118	107	113	175	104	98	206	91	113
Tm	33.2	25.2	27	40.6	26.8	27.2	40.9	22.1	29.5
Yb	379	295	291	434	300	306	407	256	333
Lu	51.2	61	38.4	57.7	51.3	58.9	52.6	34.4	46.2
Hf	8600	9800	8200	7200	9950	11600	8200	7970	9500
Ta	1.6	1.57	1.01	0.85	1.98	1.3	2.81	1.38	1.9
206Pb	499	610	353	460	458	389	465	427	565
207Pb	83	93	73	67	79	61.5	77	78	84
Th	313	282	238	600	313	176	1630	240	268
U	490	550	431	680	460	436	963	459	730
Eu/Eu*	3.25	0.81	5.22	1.00	2.23	4.81	1.40	1.12	2.14
Ce/Ce*	1.92	1.19	1.46	3.20	1.27	1.57	1.02	0.98	1.49

Ca = $^{43}Ca + {}^{44}Ca$

Eu/Eu* = $Eu_N/(0.5(Sm_N \times Gd_N))$. Ce/Ce* =$Ce_N/(0.5(La_N \times Ce_N))$.

	PK 105 - 4	PK 105 - 5	PK 105 - 2	PK 105 - 1	PK 105 - 3	PK 105 - 15	PK 105 - 16	PK 105 - 17	PK 105 - 18
P	108	67	108	221	60.3	56.2	164	143	300
Ca	2490	3680	1840	5710	4510	2460	11480	2770	8070
Ti	16.9	35	51	19	11	82	420	94	75
V	1.93	2.81	3.95	2.9	1.02	4.9	16.6	6	4.4
Sr	32	35	40	73	51	25.1	127	30.1	74
Y	950	910	950	1470	890	790	1830	850	890
Nb	5.13	6.8	5.9	2.94	5.2	4.67	23.1	8.2	7.4
La	22.9	49	30	25	70	39	490	450	94
Ce	141	160	205	270	264	255	1040	780	368
Pr	13.6	21.3	38	16.5	35.5	39	123	81	37.8
Nd	95	113	350	101	251	257	560	440	195
Sm	46	34.1	93	45.9	52	63	152	238	45
Eu	53	10.6	149	21.9	36	95	74	75	34.7
Gd	54	47	82	97	47	58	171	177	54.8
Tb	11.1	8	11.9	18.9	6.6	9.4	26.8	13.7	10.2
Dy	102	77	98	184	63	77	239	100	88
Ho	30.9	21	28	48	22.9	23	54	21.1	26.7
Er	118	107	113	175	104	98	206	91	113
Tm	33.2	25.2	27	40.6	26.8	27.2	40.9	22.1	29.5
Yb	379	295	291	434	300	306	407	256	333
Lu	51.2	61	38.4	57.7	51.3	58.9	52.6	34.4	46.2
Hf	8600	9800	8200	7200	9950	11600	8200	7970	9500
Ta	1.6	1.57	1.01	0.85	1.98	1.3	2.81	1.38	1.9
206Pb	499	610	353	460	458	389	465	427	565
207Pb	83	93	73	67	79	61.5	77	78	84
Th	313	282	238	600	313	176	1630	240	268
U	490	550	431	680	460	436	963	459	730
Eu/Eu*	3.25	0.81	5.22	1.00	2.23	4.81	1.40	1.12	2.14
Ce/Ce*	1.92	1.19	1.46	3.20	1.27	1.57	1.02	0.98	1.49

		laser_traces_02							
PK 105 - 10	**PK 105 - 9**	**2**	**PK 105 - 11**	**PK 105 - 7**	**PK 105 - 8**	**PK 105 - 24**	**PK 105 - 22**	**PK 105 - 21**	**PK 105 - 20**
100	105	113	129	69.3	44	410	57.3	61	65
3540	1760	5810	4180	7180	740	10500	3590	2220	2170
54	9.1	18.6	153	121	12.4	56	69	38	65
7.2	1.03	1.12	5.6	4.7	0.3	10.1	5.9	3.4	4.6
35	22.3	59.6	33.5	54.3	5.8	111	33.2	23.4	25.2
1410	720	1520	1370	1460	836	1310	860	750	940
9.1	3.82	6.3	9.6	7.4	3.78	10.1	4.6	4.9	4.48
49	4.3	73	44	123	5.1	88	134	70	27.3
290	53	175	193	267	51	630	347	227	170
34	3.6	9.4	28.2	32	1.84	89	47.7	37	20.3
227	27	48	201	198	13.3	464	357	224	176
134	15.8	20	120	86	10.2	96	98	60	89
33	8.3	15.7	42.5	25.9	6	64	49.6	23.9	71
263	24.2	49.9	210	168	29.5	99	86	53	78
31.2	6.07	12.4	29	32	6.8	18.4	10.8	7.9	10.4
204	67.5	129	186	192	73	153	82	66	84
43	21.7	45	47.7	40.4	20.8	41.2	26.3	20.9	25.3
140	94.9	199	177	149	101	158	120	94	125
37.3	24.7	47.4	36.8	32	25.4	35.8	29.3	26	29.4
406	275	473	348	335	305	366	317	305	319
59	36	80	51.3	64	43.9	50.9	55.3	47.2	61
9500	8100	8910	8300	10200	9900	8100	10800	9870	11600
1.17	1.08	1.04	1.79	1.69	1.84	2.33	1.26	1.97	1.21
471	521	455	423	514	412	920	610	469	478
77	78	67	70.9	77.2	62	143	119	73.1	78.4
350	174	465	247	477	143	324	178	255	229
540	439	422	463	577	264	920	480	392	506
0.54	1.30	1.52	0.82	0.66	1.06	2.01	1.65	1.30	2.61
1.71	3.24	1.61	1.32	1.02	4.01	1.71	1.04	1.07	1.74

PK 105 - 6	PK 105 - 23
212	85.8
2960	6970
26.5	45.4
0.85	6.4
21.2	63.9
850	1150
5.4	7.68
17.7	143
79.9	540
7.9	72
43.5	442
12.5	77
6.23	62.7
22.39	74
5.4	12.3
62.9	115
23.5	36.1
115.6	142
32.3	35.7
334	371
63.3	59
13000	12100
2.5	1.61
565	740
81	106
203	429
474	665
1.14	2.54
1.63	1.28

Table 2: Birimian sample ASGH028A. LA-ICP-MS zircon analysis results (in ppm).

	ASGH 028A - 1	ASGH 028A - 2	ASGH 028A - 3	ASGH 028A - 5	ASGH 028A - 6	ASGH 028A - 7	ASGH 028A - 8	ASGH 028A - 9	ASGH 028A - 10	ASGH 028A - 14
P	520	690	137	99	350	291	610	203	100	210
Ca	5270	6400	1360	306	4020	9470	7370	2000	290	1110
Ti	38	71	12.7	8.4	32.2	830	472	176	230	22
V	1.06	5.3	0.92	0.64	1.61	22	3.37	8.4	0.47	0.75
Sr	2.34	12.7	8.4	0.96	7.5	53	19.6	7.9	1.12	6.2
Y	1040	3900	1160	860	1010	4700	2710	2980	545	2170
Nb	2.71	7.5	5.2	2.17	4.07	29.2	13.1	10.4	2.61	5.4
La	10	222	25.2	3.4	17	165	98	69	2.48	3.3
Ce	32.9	190	43.1	16.3	57	510	161	129	11.2	42
Pr	5.6	73	8.5	1.7	7.7	98	37.4	27.7	1.15	3.8
Nd	33	292	66	6.7	38.7	460	203	141	6.5	30
Sm	14.2	64	23	3.9	19	239	84	48	3.19	20.8
Eu	2.7	9.8	5.1	0.57	2.99	53	14.1	11	0.66	2.83
Gd	40	149	36	16.7	38.1	463	151	117	13.2	44
Tb	10.2	38	8.2	6.4	9.6	91	31.6	27.8	4.7	15.5
Dy	97.7	350	86	83	93	620	281	256	48.2	171
Ho	31.1	92	39	25.6	26.9	141	75	73	18.7	70
Er	165	318	160	115	135	530	277	264	96	317
Tm	47	75	44	32.6	38.8	116	62	53	26.8	75
Yb	536	681	490	404	505	1220	571	590	352	820
Lu	78	118.6	62	63	54.1	178	76	90	44.4	103
Hf	8300	9980	8100	10300	8300	8400	8400	9200	8300	8140
Ta	1.65	2.36	3.01	1.91	1.14	3.41	2.15	2.64	1.84	5.2
206Pb	238	229	430	201	247	370	421	241	241	439
207Pb	39.5	29.6	60	26	35.4	64	53	29.8	33.7	49.8
Th	84	85	77	36.5	71	518	155	61	34	124
U	222	153	242	135	191	600	322	176	175	294
Eu/Eu*	0.35	0.31	0.54	0.22	0.34	0.49	0.38	0.45	0.31	0.29
Ce/Ce*	1.06	0.36	0.71	1.63	1.20	0.97	0.64	0.71	1.60	2.85

$Ca = {}^{43}Ca + {}^{44}Ca$

$Eu/Eu^* = Eu_N/(0.5(Sm_N \times Gd_N))$. $Ce/Ce^* = Ce_N/(0.5(La_N \times Ce_N))$.

	ASGH028A-1	ASGH028A-2	ASGH028A-3	ASGH028A-5	ASGH028A-6	ASGH028A-7	ASGH028A-8	ASGH028A-9	ASGH028A-10	ASGH028A-14
P	520	690	137	99	350	291	610	203	100	210
Ca	5270	6400	1360	306	4020	9470	7370	2000	290	1110
Ti	38	71	12.7	8.4	32.2	830	472	176	230	22
V	1.06	5.3	0.92	0.64	1.61	22	3.37	8.4	0.47	0.75
Sr	2.34	12.7	8.4	0.96	7.5	53	19.6	7.9	1.12	6.2
Y	1040	3900	1160	860	1010	4700	2710	2980	545	2170
Nb	2.71	7.5	5.2	2.17	4.07	29.2	13.1	10.4	2.61	5.4
La	10	222	25.2	3.4	17	165	98	69	2.48	3.3
Ce	32.9	190	43.1	16.3	57	510	161	129	11.2	42
Pr	5.6	73	8.5	1.7	7.7	98	37.4	27.7	1.15	3.8
Nd	33	292	66	6.7	38.7	460	203	141	6.5	30
Sm	14.2	64	23	3.9	19	239	84	48	3.19	20.8
Eu	2.7	9.8	5.1	0.57	2.99	53	14.1	11	0.66	2.83
Gd	40	149	36	16.7	38.1	463	151	117	13.2	44
Tb	10.2	38	8.2	6.4	9.6	91	31.6	27.8	4.7	15.5
Dy	97.7	350	86	83	93	620	281	256	48.2	171
Ho	31.1	92	39	25.6	26.9	141	75	73	18.7	70
Er	165	318	160	115	135	530	277	264	96	317
Tm	47	75	44	32.6	38.8	116	62	53	26.8	75
Yb	536	681	490	404	505	1220	571	590	352	820
Lu	78	118.6	62	63	54.1	178	76	90	44.4	103
Hf	8300	9980	8100	10300	8300	8400	8400	9200	8300	8140
Ta	1.65	2.36	3.01	1.91	1.14	3.41	2.15	2.64	1.84	5.2
206Pb	238	229	430	201	247	370	421	241	241	439
207Pb	39.5	29.6	60	26	35.4	64	53	29.8	33.7	49.8
Th	84	85	77	36.5	71	518	155	61	34	124
U	222	153	242	135	191	600	322	176	175	294
Eu/Eu*	0.35	0.31	0.54	0.22	0.34	0.49	0.38	0.45	0.31	0.29
Ce/Ce*	1.06	0.36	0.71	1.63	1.20	0.97	0.64	0.71	1.60	2.85

ASGH028A - 22	laser_traces_ 097	laser_traces_ 098	laser_traces_ 099	ASGH028A - 18	ASGH028A - 21	laser_traces_ 102	laser_traces_ 039	ASGH028A - 4	laser_traces_ 044	ASGH028A - 17
177	123	112	305	126	284	75	213	403	233	498
9700	101000	85000	16900	790	1920	13500	2580	1180	3290	1410
73	1040	331	1030	4.6	151	310	250	660	15.5	77
1.75	12.7	13.9	4.6	0.77	3.48	4.9	1.35	6.8	0.58	7.3
65	780	710	134	6.6	14.2	200	14.4	8.7	8.7	8.1
4200	22500	17900	6000	1910	1880	3950	1500	3100	1560	4130
9.7	109	89	109	3.55	9.2	6.3	5.62	16.4	3.8	5.58
78	1160	800	86	5	51	283	19.1	50	17	62
191	2160	2120	291	28.5	135	680	73	143	44.1	100
37	470	308	63	4.1	29	88	8.6	28.4	8	22.7
222	3400	2620	317	20	146	510	57	147	46	145
89	1210	970	126	10.4	54	290	31.5	78	20.7	75
15.6	195	150	23.8	2.4	11.7	50	5.1	12.1	4.06	14.5
159	1360	1170	184	30.2	86	420	56	150	46.2	169
41	209	177	50	9.2	23.5	75	13.3	34.2	11.7	35.9
375	2200	1180	590	149	246	428	146	343	134	376
116	560	370	179	42.6	57	93	44.5	101	48.9	111
510	1850	1640	670	183	215	400	226	440	230	468
120	355	319	204	46	48.1	103	52	96.3	58.3	93
1100	3350	3050	2110	620	580	1030	539	933	652	880
181	473	395	313	79.3	78	140	77	118	102	132
12300	12800	16500	13000	11200	7200	10200	11500	9800	11000	11200
3.7	31.7	47	70	2.35	1.66	2.3	1.35	2.84	2.16	1.53
720	900	770	6400	376	294	420	274	500	332	284
95	96	70	730	41.9	34.2	57	41.4	78	46.1	44
364	1600	1870	2030	64.7	87	300	124	380	88	183
455	2980	2750	2750	238	168	1100	197	430	218	216
0.40	0.46	0.43	0.48	0.41	0.52	0.44	0.37	0.34	0.40	0.39
0.86	0.70	1.03	0.95	1.52	0.84	1.04	1.37	0.91	0.91	0.64

laser_traces_097	laser_traces_098	laser_traces_099
123	112	305
101000	85000	16900
1040	331	1030
12.7	13.9	4.6
780	710	134
22500	17900	6000
109	89	109
1160	800	86
2160	2120	291
470	308	63
3400	2620	317
1210	970	126
195	150	23.8
1360	1170	184
209	177	50
2200	1180	590
560	370	179
1850	1640	670
355	319	204
3350	3050	2110
473	395	313
12800	16500	13000
31.7	47	70
900	770	6400
96	70	730
1600	1870	2030
2980	2750	2750
0.46	0.43	0.48
0.70	1.03	0.95

Table 3: Birimian sample ASGH030A. LA-ICP-MS zircon analysis results (in ppm).

	ASGH030A - 1	ASGH030A - 3	ASGH030A - 2	ASGH030A - 5	ASGH030A - 6	ASGH030A - 4	ASGH030A - 7	ASGH030A - 8	ASGH030A - 9	ASGH030A - 10
P	116	290	108	148	276	164	109.9	173	185	158
Ca	150	300	1420	63	600	790	197	62	530	169
TI			20		26	23	10	13.9	12	11
V	1.48	0.24	0.99	1.02	1.56	0.51	1.45	1.29	1.53	0.45
Sr	0.86	1.01	17.4	0.43	1.73	3.9	0.6	0.54	0.79	0.7
Y	1630	1440	2170	631	3400	1640	1630	1500	1650	1650
Nb	1.43	2.58	4.6	0.86	5	1.64	3.79	2.5	2.76	2.1
La	0.079	1.41	0.61	0.229	2.19	5.6	0.57	0.124	0.41	0.24
Ce	10.4	8.3	4.99	6.04	29	10.8	14.3	10.46	7.36	9
Pr	0.186	2.5	0.205	0.223	2.52	0.94	0.58	0.141	0.267	0.255
Nd	1.8	12	1.49	1.21	15.5	3.3	7.4	1	3.22	2.49
Sm	5.6	5.9	2.9	3.6	10.8	2.2	10.2	1.9	3.84	4.8
Eu	2.78	0.93	1.3	1.29	2.28	0.85	2.96	0.83	1.53	1.13
Gd	32.1	14.4	15.9	21.2	33	19.3	30.4	24.9	26.5	39
Tb	10.2	8	6	7.6	13.3	9.4	9.5	11	9.1	20.7
Dy	116	117	188	59.2	270	119	98	114	116	168
Ho	49	44	72	18.3	96	40	44	38.7	49.7	51
Er	242	202	282	90	360	189	369	139	305	175
Tm	66	46	57	43	80	44	116	28.2	84	40
Yb	880	370	650	660	950	450	1150	470	894	360
Lu	149	57	70.3	96	151	80	150	84	137	84
Hf	9100	9400	9980	6610	15200	7800	10000	5460	8800	7700
Ta	0.96	3.5	2.18	1.18	3.9	1.61	2.09	1.49	1.15	1.34
206Pb	177	370	760	69	560	287	298	116	149	133
207Pb	30.1	46	119	15.6	66	41	74	11.8	31.5	17.1
Th	88	69	122	30	83	53	119	16.3	39.4	25.7
U	159	203	299	139	268	199	203	154	99	161
Eu/Eu*	0.63	0.31	0.59	0.45	0.37	0.40	0.51	0.37	0.46	0.25
Ce/Ce*	20.65	1.06	3.40	6.43	2.97	1.13	5.99	19.04	5.35	8.76

$Ca = {}^{43}Ca + {}^{44}Ca$

$Eu/Eu^* = Eu_N/(0.5(Sm_N \times Gd_N))$. $Ce/Ce^* = Ce_N/(0.5(La_N \times Ce_N))$.

	ASGH030A-1	ASGH030A-3	ASGH030A-2	ASGH030A-5	ASGH030A-6	ASGH030A-4	ASGH030A-7	ASGH030A-8	ASGH030A-9	ASGH030A-10
P	116	290	108	148	276	164	109.9	173	185	158
Ca	150	300	1420	63	600	790	197	62	530	169
Tl			20		26	23	10	13.9	12	11
V	1.48	0.24	0.99	1.02	1.56	0.51	1.45	1.29	1.53	0.45
Sr	0.86	1.01	17.4	0.43	1.73	3.9	0.6	0.54	0.79	0.7
Y	1630	1440	2170	631	3400	1640	1630	1500	1650	1650
Nb	1.43	2.58	4.6	0.86	5	1.64	3.79	2.5	2.76	2.1
La	0.079	1.41	0.61	0.229	2.19	5.6	0.57	0.124	0.41	0.24
Ce	10.4	8.3	4.99	6.04	29	10.8	14.3	10.46	7.36	9
Pr	0.186	2.5	0.205	0.223	2.52	0.94	0.58	0.141	0.267	0.255
Nd	1.8	12	1.49	1.21	15.5	3.3	7.4	1	3.22	2.49
Sm	5.6	5.9	2.9	3.6	10.8	2.2	10.2	1.9	3.84	4.8
Eu	2.78	0.93	1.3	1.29	2.28	0.85	2.96	0.83	1.53	1.13
Gd	32.1	14.4	15.9	21.2	33	19.3	30.4	24.9	26.5	39
Tb	10.2	8	6	7.6	13.3	9.4	9.5	11	9.1	20.7
Dy	116	117	188	59.2	270	119	98	114	116	168
Ho	49	44	72	18.3	96	40	44	38.7	49.7	51
Er	242	202	282	90	360	189	369	139	305	175
Tm	66	46	57	43	80	44	116	28.2	84	40
Yb	880	370	650	660	950	450	1150	470	894	360
Lu	149	57	70.3	96	151	80	150	84	137	84
Hf	9100	9400	9980	6610	15200	7800	10000	5460	8800	7700
Ta	0.96	3.5	2.18	1.18	3.9	1.61	2.09	1.49	1.15	1.34
206Pb	177	370	760	69	560	287	298	116	149	133
207Pb	30.1	46	119	15.6	66	41	74	11.8	31.5	17.1
Th	88	69	122	30	83	53	119	16.3	39.4	25.7
U	159	203	299	139	268	199	203	154	99	161
Eu/Eu*	0.63	0.31	0.59	0.45	0.37	0.40	0.51	0.37	0.46	0.25
Ce/Ce*	20.65	1.06	3.40	6.43	2.97	1.13	5.99	19.04	5.35	8.76

laser_traces_021	laser_traces_022	ASGH030A-21	ASGH030A-22	ASGH030A-25	laser_traces_026	laser_traces_027	ASGH030A-23	ASGH030A-24	laser_traces_061	laser_traces_062
126	262	132	330	214	278	190	337	480	311	214
130	620	160	830	1230	4770	450	400	2810	750	780
2.4	11.7	10	31	68	14	9	17.4	19.6	7.7	4.2
0.29	0.42	1.18	1.28	0.78	5.1	1.25	2.16	2.6	1.83	0.71
0.53	3.1	0.79	2.28	1.12	3.4	0.9	1.6	18.8	0.73	1.72
1450	1340	900	3060	1860	6100	1710	2920	3400	2430	1120
2.61	1.68	1.11	5.6	4.3	11.2	5	3.79	9.6	3.2	2.76
0.2	6.1	0.53	3.6	0.93	5.8	0.52	4	5.7	0.67	9
6.3	29	13.7	29.1	8.8	27.2	10.4	27.5	62	15.7	51
0.27	4.5	0.59	4.5	0.44	4	0.64	2.02	5.4	0.69	6.5
2.02	17.2	5.5	33	5.2	40	5.6	13.5	51	8.3	51
2.9	7.1	8.9	17.9	7.1	29.2	3.7	15	30.6	11.5	36
0.68	1.97	2.86	4.1	1.86	7.7	0.88	4.86	9.6	3.8	7.6
13	33	29.6	44	27.5	78	13.4	67.4	89	57	49
6.6	10.2	7.1	15.5	15.6	20.5	8	18.7	25	16.8	9.6
117	104	68	268	161	450	145	269	330	195	106
42	35	19.4	93	59	188	49	107	110	74	43
185	136	91	395	289	880	201	488	480	357	193
44.7	30	45	83	65	227	43	123	117	86	50
479	390	690	890	640	2040	430	1390	1120	970	590
73	64	98	100	75	222	51	188	129	153	89
12500	5820	8200	10000	8300	9900	5000	8600	11500	9300	11100
2.77	1.05	1.69	2.57	1.35	2.12	1.24	1.68	1.84	1.7	1.91
362	179	162	590	360	1340	350	263	426	266	308
51	22.5	28.7	84	53	184	42	47.5	77	41.3	51.1
29.8	16.3	57	94	43.6	263	24.3	95	230	63	52
168	135	230	240	171	394	121	162	470	143	243
0.34	0.39	0.54	0.45	0.41	0.49	0.38	0.47	0.56	0.45	0.55
6.53	1.33	5.90	1.74	3.31	1.36	4.34	2.33	2.69	5.56	1.60

laser_traces_021	laser_traces_022
126	262
130	620
2.4	11.7
0.29	0.42
0.53	3.1
1450	1340
2.61	1.68
0.2	6.1
6.3	29
0.27	4.5
2.02	17.2
2.9	7.1
0.68	1.97
13	33
6.6	10.2
117	104
42	35
185	136
44.7	30
479	390
73	64
12500	5820
2.77	1.05
362	179
51	22.5
29.8	16.3
168	135
0.34	0.39
6.53	1.33

Table 4: Birimian sample ASGH082A. LA-ICP-MS zircon analysis results (in ppm).

	ASGH 082A - 1	ASGH 082A - 2	ASGH 082A - 3	ASGH 082A - 4	ASGH 082A - 5	ASGH 082A - 6	ASGH 082A - 7	ASGH 082A - 8	ASGH 082A - 9	ASGH 082A - 10
P	149	178	179	1700	102	133	267	190	136	430
Ca	2710	2650	3870	10800	121	1130	12500	5570	2480	6220
Ti	13	6	8	5.9	2.2	3	10	3		1
V	0.59	0.28	0.28		0.279	0.21	0.25	0.249	0.44	0.93
Sr	5.5	3.4	7.7	4.8	1.46	2.91	31.9	39.1	3.43	14.2
Y	1330	642	1510	930	603	940	3110	1260	1170	2200
Nb	2.87	2.54	3.33	1.78	1.03	2.83	6.6	2.97	2.75	4.6
La	2.69	0.97	2.07	3.8	0.69	6.1	16.8	26.3	1.67	15.6
Ce	22.8	11	29.3	24.9	12.7	26.8	40.9	98	19.3	74
Pr	3.6	0.27	5.2	2.35	0.76	2.37	7.5	20.4	1.66	22.4
Nd	35	2.61	57	15.7	3.34	22.4	40.3	107	19.3	145
Sm	20.8	3.86	21.7	10.2	3.32	10.3	12.1	30	18.1	37
Eu	3.15	0.58	3.5	2.2	0.58	1.5	1.5	5.5	2.01	3.9
Gd	45.5	14.6	36.3	32.4	20.8	31.2	33.7	44	33.1	41
Tb	13	4.89	9.6	8.7	7.45	9	12	11.4	9.2	14
Dy	149	56.7	136	99	61.4	81.3	206	119	124	229
Ho	52	26.6	49	30.2	18.8	33.6	89	38.5	50	80
Er	236	167	232	160	71	189	358	163	247	334
Tm	51	53.2	53.6	52	22.3	53.3	94	39	67.6	73
Yb	525	584	600	530	406	636	900	440	687	730
Lu	76	68.2	63.5	74	50.1	68.8	135	72	76.1	73
Hf	10700	9110	8700	9900	6990	8160	14600	8400	8180	9000
Ta	2.08	1.94	2.07	2.12	1.49	1.16	4.7	2.99	1.21	2.37
206Pb	470	650	740	360	191	396	1560	530	670	1210
207Pb	66	121	93.2	54	26.3	72.7	218	70	118	139
Th	139	210	188.4	103	71	162	440	237	212	255
U	315	512	388	271	287	359	800	630	341	610
Eu/Eu*	0.31	0.24	0.38	0.37	0.21	0.26	0.23	0.46	0.25	0.31
Ce/Ce*	1.76	5.17	2.15	2.01	4.22	1.70	0.88	1.02	2.79	0.95

$Ca = {}^{43}Ca + {}^{44}Ca$

$Eu/Eu^* = Eu_N/(0.5(Sm_N \times Gd_N))$. $Ce/Ce^* = Ce_N/(0.5(La_N \times Ce_N))$.

ASGH 082A - 5	ASGH 082A - 6	ASGH 082A - 7	ASGH 082A - 8	ASGH 082A - 9	ASGH 082A - 10	ASGH 082A - 11	ASGH 082A - 12	ASGH 082A - 13	ASGH 082A - 14	ASGH 082A - 15
102	133	267	190	136	430	740	199	158	116	750
121	1130	12500	5570	2480	6220	9700	2240	1030	1660	12400
2.2	3	10	3		1	3		210	15	26.1
0.279	0.21	0.25	0.249	0.44	0.93	0.65	0.23	2.3	0.45	0.07
1.46	2.91	31.9	39.1	3.43	14.2	8.4	3.17	1.66	8.5	15
603	940	3110	1260	1170	2200	1100	1080	519	1120	2350
1.03	2.83	6.6	2.97	2.75	4.6	2.71	1.82	1.62	3.21	3.76
0.69	6.1	16.8	26.3	1.67	15.6	11.3	2.4	1.53	9.8	14.2
12.7	26.8	40.9	98	19.3	74	65	20.6	14.5	54	89
0.76	2.37	7.5	20.4	1.66	22.4	16.7	4	1.71	11	17.8
3.34	22.4	40.3	107	19.3	145	119	20.1	15.5	74	136
3.32	10.3	12.1	30	18.1	37	44	11.8	12.2	22.3	34
0.58	1.5	1.5	5.5	2.01	3.9	6.5	1.31	1.7	3.35	8.9
20.8	31.2	33.7	44	33.1	41	45.1	22.8	24.6	42.1	55
7.45	9	12	11.4	9.2	14	8.9	8.7	5.86	11.5	15.1
61.4	81.3	206	119	124	229	113	117	57.2	122	221
18.8	33.6	89	38.5	50	80	34.7	34.2	22	39.1	75
71	189	358	163	247	334	142	145	111	157	316
22.3	53.3	94	39	67.6	73	33.7	34.5	31.1	35.7	67
406	636	900	440	687	730	384	388	365	430	620
50.1	68.8	135	72	76.1	73	42.2	46.1	40.5	56	95
6990	8160	14600	8400	8180	9000	8100	7070	6780	8300	12400
1.49	1.16	4.7	2.99	1.21	2.37	2.02	1.08	0.73	2.49	2.95
191	396	1560	530	670	1210	423	360	239	450	680
26.3	72.7	218	70	118	139	54	47.3	40.1	60	81
71	162	440	237	212	255	71	91	65.4	114	234
287	359	800	630	341	610	254	221	187	410	397
0.21	0.26	0.23	0.46	0.25	0.31	0.45	0.24	0.30	0.33	0.63
4.22	1.70	0.88	1.02	2.79	0.95	1.14	1.60	2.16	1.25	1.35

ASGH 082A - 25	ASGH 082A - 26	ASGH 082A - 27	laser_traces_83	ASGH 082A - 28	ASGH 082A - 29
1350	179	2600	390	800	137
8700	3490	21300	2700	7980	530
	46.2	37	2	8.4	10.3
0.194	0.54	0.88	0.85	0.19	0.117
1.86	19.7	20.6	3.29	11.7	0.203
1260	1550	1440	1510	1750	570
2.58	3.47	4.47	2.15	2.91	1.31
4.4	24.3	21.4	1.61	3.58	0.069
18.8	131	109	16.2	18	8.9
2.42	28.6	21	1.79	1.43	0.23
18.8	241	164	15	11.5	2.5
9.2	107	96	11.8	6.96	2.82
1.33	11.4	10.5	1.21	1.27	1.09
27.8	99	129	34.3	28.5	11.8
8.9	14.8	18.1	10.6	9.6	3.28
137	142	140	137	132	43.9
46	50	42.1	49.2	49.5	18.2
210	242	187	230	255	93.3
47.1	59.3	44.7	53.8	61.9	23.5
520	557	446	546	599	300
66	92	75	79	106	47.7
7900	11800	10700	10800	13000	8500
1.47	2.08	3	1.55	2.57	0.92
387	390	338	337	628	162
60	55.6	47.4	52.1	92	25.1
117	182	119	132	178	57.6
245	421	317	199	402	110
0.25	0.34	0.29	0.18	0.28	0.58
1.39	1.20	1.24	2.30	1.91	17.00

Table 5: Birimian sample ASGH084A. LA-ICP-MS zircon analysis results (in ppm).

	laser_traces_055	ASGH 084A - 2	ASGH 084A - 3	ASGH 084A - 4	ASGH 084A - 5	ASGH 084A - 6	ASGH 084A - 9	ASGH 084A - 8	ASGH 084A - 7	laser_traces_065
P	76	67	269	94	380	125	97	186	710	80
Ca	256	220	2860	270	1120	340	580	1890	5900	3460
Ti	7	8.4	218	0	1.3	20.7	25	89	101	93
V		0.29	23.2	0.16	0.3	1.25	1.2	4.21	17	1.22
Sr	0.165	0.81	11.1	0.66	2.2	0.64	1.28	14.6	39	77
Y	247	322	1390	570	430	302	490	1000	1260	742
Nb	0.74	0.86	4.9	1.32	0.73	0.76	1.48	1.9	4.6	2.79
La		0.5	101	0.69	5.1	0.78	10	88	72	94
Ce	5.1	9.2	1000	17.7	29	12.5	86	700	1030	470
Pr	0.021	0.7	191	1.8	2.8	1.88	14.5	135	166	92
Nd	0.51	6.8	2160	10.5	18.5	15.2	135	780	1000	520
Sm	1.95	3.7	434	3.5	9.2	5.9	39	155	550	124
Eu	0.66	0.96	70	1.11	2.95	1.53	7.2	22	92	27.7
Gd	5.8	7.5	203	13.3	16.2	8.1	40	117	430	136
Tb	1.83	2.09	21.9	4.3	3.66	2.65	6	17.9	45	20.7
Dy	17.3	22.2	150	45.5	34.8	33.2	48	113	187	126
Ho	7.4	9	40.2	15.7	11.4	11	15.6	28.8	33.1	26.6
Er	49.8	49	151	70	52	44.9	67	104	123	92
Tm	17.7	15.6	39.3	18	15.5	10.6	19.1	26.1	29	21.9
Yb	233	224	455	232	252	158	254	295	440	299
Lu	33.8	33.2	59	45.3	43.2	23.6	38.3	60	72	50
Hf	6870	7940	8700	8100	7900	8200	7880	9200	10100	8500
Ta	0.29	0.17	0.92	1.46	0.94	0.252	0.3	1.06	0.78	1.24
206Pb	85	111	274	182	143	88	139	238	253	333
207Pb	18.7	16.1	44	22.4	17.4	12.2	20.5	35.5	67	41
Th	28.7	27.6	126	46.9	35.1	21.5	41	99	180	80
U	73	90	362	163	103	68	108	262	530	440
Eu/Eu*	0.60	0.56	0.72	0.50	0.74	0.68	0.56	0.50	0.58	0.65
Ce/Ce*		3.74	1.73	3.82	1.85	2.48	1.72	1.55	2.27	1.22

$Ca = {}^{43}Ca + {}^{44}Ca$

$Eu/Eu^* = Eu_N/(0.5(Sm_N \times Gd_N))$. $Ce/Ce^* = Ce_N/(0.5(La_N \times Ce_N))$.

ASGH084A-9	ASGH084A-8	ASGH084A-7	laser_traces_065	ASGH084A-11	ASGH084A-10	ASGH084A-12	ASGH084A-13	ASGH084A-15	ASGH084A-16a	ASGH084A-16b
97	186	710	80	89	82.5	75	115	79	108	82
580	1890	5900	3460	320	250	263	530	279	3050	2040
25	89	101	93			6	19	3	122	60
1.2	4.21	17	1.22	1.76	0.072	0.04	1.85	0.14	16.1	8
1.28	14.6	39	77	1.57	0.75	0.47	1.77	0.76	28.8	18.8
490	1000	1260	742	459	293	357	590	426	1630	963
1.48	1.9	4.6	2.79	0.96	0.59	0.79	1.28	1.26	5.8	3.24
10	88	72	94	3.6	4.2	0.62	8.2	1.98	76	50.5
86	700	1030	470	31.5	37	12.1	92	21.5	750	469
14.5	135	166	92	5.3	4.8	1.26	16.6	1.65	146	94
135	780	1000	520	40	22	10.5	119	9.9	1300	650
39	155	550	124	21	3.7	6.1	38.4	3.2	614	327
7.2	22	92	27.7	3.6	0.96	1.31	7.6	0.74	176	82
40	117	430	136	20.1	6.5	9.7	38.1	9.1	493	298
6	17.9	45	20.7	4.59	2.39	2.5	6	2.86	66.1	41.3
48	113	187	126	42.3	24.1	28.4	47.5	33.1	365	182
15.6	28.8	33.1	26.6	12.7	8.4	10.7	15.4	12.2	53.2	29.4
67	104	123	92	60.1	34.7	52.1	75	60.1	143	78
19.1	26.1	29	21.9	19.2	9.4	15.5	21.9	18.6	28.2	17
254	295	440	299	279	146	213	330	243	259	193
38.3	60	72	50	42.9	26.3	32.7	48	37.3	38.6	27.8
7880	9200	10100	8500	7930	7130	7500	9500	8500	8100	7900
0.3	1.06	0.78	1.24	0.57	0.69	0.21	0.53	0.62	0.55	0.38
139	238	253	333	194	125	131	262	214	211	201
20.5	35.5	67	41	28.2	14.7	18.5	33.8	28.7	32	27.9
41	99	180	80	60	21.4	26.6	73	67	69	46.4
108	262	530	440	140	96	98	220	158	453	407
0.56	0.50	0.58	0.65	0.54	0.60	0.52	0.61	0.42	0.98	0.80
1.72	1.55	2.27	1.22	1.74	1.98	3.29	1.90	2.86	1.71	1.64

ASGH084A - 16a	ASGH084A - 16b	ASGH084A - 19	ASGH084A - 20	ASGH084A - 21	ASGH084A - 1	laser_traces_087	laser_traces_088	ASGH084A - 23	laser_traces_093	ASGH084A - 24
108	82	114	204	83	190	2300	139	117	134	790
3050	2040	3720	780	234	370	11600	252	290	300	4410
122	60	137	90	3	25.9	0.8	12.6	8.7	8.7	410
16.1	8	6.3	3.8	0.23	1.26	0.26	0.45	0.156	0.038	21
28.8	18.8	26.1	1.72	0.69	1.09	9	0.4	0.44	0.43	20.6
1630	963	2600	584	390	790	324	446	461	533	2550
5.8	3.24	6.8	1.37	0.79	1.83	0.84	1.28	1.25	1.04	9.2
76	50.5	81	10.8	1.37	2.2	10.5	0.44	0.14	0.45	158
750	469	546	67	14.4	33.7	23	10.9	10.23	11.1	1540
146	94	151	10.8	1.6	4.5	2.3	0.91	0.209	0.51	289
1300	650	1140	85	6.9	40	13.5	6.7	2.6	6.7	2780
614	327	544	49.3	3.6	24.3	2.7	4.9	2.54	4.6	980
176	82	90	11.7	1.24	3.8	0.99	1.3	0.98	1.28	202
493	298	394	61	9.9	24.8	7	8.9	8.6	11	645
66.1	41.3	73	11.8	3.13	6.31	2.04	2.92	3.03	3.46	73
365	182	560	75	33	65.2	29.7	36.7	37.9	41.6	397
53.2	29.4	99	18.7	12.2	24.4	10.7	14.6	15.4	15.7	83
143	78	312	65.7	65.6	122	57.4	76	79.1	86.3	279
28.2	17	64	19.3	18.7	32.6	16.6	21.6	21.9	22.7	59
259	193	608	269	255	392	189	261	268	296	532
38.6	27.8	85	41.5	37.3	64.5	29.5	41.7	41.5	45.4	76
8100	7900	12400	9000	7510	10400	9830	9200	9900	9510	9800
0.55	0.38	1	0.2	0.39	0.52	0.48	0.191	0.86	0.34	1.51
211	201	480	108	149	224	136	129	154	157	352
32	27.9	58	15.8	21.8	33.3	19.6	17.7	22.3	24	52.7
69	46.4	186	63	45.1	87.5	35.2	44.9	50	53.3	320
453	407	590	155	107	157	79.3	87	92.4	107	542
0.98	0.80	0.59	0.65	0.64	0.47	0.70	0.60	0.64	0.55	0.78
1.71	1.64	1.19	1.49	2.34	2.58	1.13	4.15	14.39	5.58	1.73

ASGH084A - 19	ASGH084A - 20	ASGH084A - 21	ASGH084A - 1	laser_traces_ 087	laser_traces_ 088
114	204	83	190	2300	139
3720	780	234	370	11600	252
137	90	3	25.9	0.8	12.6
6.3	3.8	0.23	1.26	0.26	0.45
26.1	1.72	0.69	1.09	9	0.4
2600	584	390	790	324	446
6.8	1.37	0.79	1.83	0.84	1.28
81	10.8	1.37	2.2	10.5	0.44
546	67	14.4	33.7	23	10.9
151	10.8	1.6	4.5	2.3	0.91
1140	85	6.9	40	13.5	6.7
544	49.3	3.6	24.3	2.7	4.9
90	11.7	1.24	3.8	0.99	1.3
394	61	9.9	24.8	7	8.9
73	11.8	3.13	6.31	2.04	2.92
560	75	33	65.2	29.7	36.7
99	18.7	12.2	24.4	10.7	14.6
312	65.7	65.6	122	57.4	76
64	19.3	18.7	32.6	16.6	21.6
608	269	255	392	189	261
85	41.5	37.3	64.5	29.5	41.7
12400	9000	7510	10400	9830	9200
1	0.2	0.39	0.52	0.48	0.191
480	108	149	224	136	129
58	15.8	21.8	33.3	19.6	17.7
186	63	45.1	87.5	35.2	44.9
590	155	107	157	79.3	87
0.59	0.65	0.64	0.47	0.70	0.60
1.19	1.49	2.34	2.58	1.13	4.15

Table 6: West Greenland detrital zircon (Archean)- LA-ICP-MS analysis results (in ppm).

Sample locality	**Disko, Kingigtoq**									
Sample	**486707_144**	**486727_59**	**486707_140**	**486727_70**	**486727_49**	**486732_87**	**486746_169**	**486718_160**	**486707_151**	**486707_143**
P	190.7	119.52	107.27	109.1	89.06	3843.57	217.66	370.2	289.76	376.52
Ti	9.42	8.66	6.7	6.3	8.36	233.78	15.52	13.71	11.81	9.54
V	2.44	0.174	3.44	0.49	0.142	10.02	0.49	1.11	2.08	1.04
Sr	0.315	0.389	0.216	0.306	0.266	83.95	0.81	2.57	0.348	0.47
Y	870.08	198.98	956.86	351.28	184.58	4810.34	332.31	640.56	2132.98	679.59
Nb	1.94	0.959	1.19	1.06	1.82	5.06	1.58	1.95	3.53	1.66
La	0.1017	0.069	0.0453	0.0109	0.0121	29.9	0.609	0.798	0.1099	0.275
Ce	40.95	4.19	36.96	13.39	24.84	134.59	15.55	21.74	25.54	6.93
Pr	0.612	0.137	0.443	0.0364	0.0408	30.89	0.315	1.34	0.832	0.42
Nd	8.56	1.315	7.71	0.717	0.498	238.8	3.49	10.66	13.2	3.13
Sm	11.01	1.71	10.67	1.02	0.724	178.66	3.38	8.87	20.32	3.73
Eu	1.71	0.65	4.54	0.524	0.229	104.07	0.86	3.83	7.32	1.51
Gd	36.67	4.75	37.59	6.4	3.33	368.59	10.08	21.24	84.65	15.62
Tb	9.14	1.45	8.34	2	1.084	85.64	3.02	6.34	21.91	4.98
Dy	95.26	15.69	85.42	25.25	13.89	733.62	33.59	64.19	230.68	64.01
Ho	30.06	6.36	27.69	10.02	5.51	173.36	10.22	19.27	71.49	20.61
Er	122.25	31.56	121.39	52.18	30.64	584.93	44.42	87.72	295.6	89.9
Tm	22.63	7.33	23.72	12.67	7.63	96.14	9.05	18.19	55.77	17.99
Yb	198.37	78.34	203.22	140.61	87.62	733.09	86.27	177.07	467.62	160.86
Lu	37.46	17.71	36.66	32.54	21.45	118.57	17.99	37.68	88.69	32.38
Hf	9367.49	9148.18	6542.55	11188.98	10627.01	11109.68	8468.68	10446.31	8238.69	16445.21
Ta	0.463	0.892	0.163	1.002	0.984	1.68	0.787	1.04	0.737	0.574
Pb	29.43	4.59	7.85	15.61	12.02	24.91	16.81	45.93	34.09	3.7
Th	128.28	14.65	31.74	55.4	44.6	112.39	52.25	173.95	132.55	15.45
U	69.09	41.05	41.36	104.27	76.64	333.77	57.86	206.44	101.05	73.24
Eu/Eu*	0.26	0.70	0.69	0.63	0.45	1.24	0.45	0.85	0.54	0.60
Ce/Ce*	39.51	10.37	62.80	161.80	269.08	1.07	8.55	5.06	20.33	4.91

$Ca = {}^{43}Ca + {}^{44}Ca$

$Eu/Eu^* = Eu_N/(0.5(Sm_N \times Gd_N))$. $Ce/Ce^* = Ce_N/(0.5(La_N \times Ce_N))$.

Sample locality	Disko, Kingigtoq									
Sample	**486707_144**	**486727_59**	**486707_140**	**486727_70**	**486727_49**	**486732_87**	**486746_169**	**486718_160**	**486707_151**	**486707_143**
P	190.7	119.52	107.27	109.1	89.06	3843.57	217.66	370.2	289.76	376.52
Ti	9.42	8.66	6.7	6.3	8.36	233.78	15.52	13.71	11.81	9.54
V	2.44	0.174	3.44	0.49	0.142	10.02	0.49	1.11	2.08	1.04
Sr	0.315	0.389	0.216	0.306	0.266	83.95	0.81	2.57	0.348	0.47
Y	870.08	198.98	956.86	351.28	184.58	4810.34	332.31	640.56	2132.98	679.59
Nb	1.94	0.959	1.19	1.06	1.82	5.06	1.58	1.95	3.53	1.66
La	0.1017	0.069	0.0453	0.0109	0.0121	29.9	0.609	0.798	0.1099	0.275
Ce	40.95	4.19	36.96	13.39	24.84	134.59	15.55	21.74	25.54	6.93
Pr	0.612	0.137	0.443	0.0364	0.0408	30.89	0.315	1.34	0.832	0.42
Nd	8.56	1.315	7.71	0.717	0.498	238.8	3.49	10.66	13.2	3.13
Sm	11.01	1.71	10.67	1.02	0.724	178.66	3.38	8.87	20.32	3.73
Eu	1.71	0.65	4.54	0.524	0.229	104.07	0.86	3.83	7.32	1.51
Gd	36.67	4.75	37.59	6.4	3.33	368.59	10.08	21.24	84.65	15.62
Tb	9.14	1.45	8.34	2	1.084	85.64	3.02	6.34	21.91	4.98
Dy	95.26	15.69	85.42	25.25	13.89	733.62	33.59	64.19	230.68	64.01
Ho	30.06	6.36	27.69	10.02	5.51	173.36	10.22	19.27	71.49	20.61
Er	122.25	31.56	121.39	52.18	30.64	584.93	44.42	87.72	295.6	89.9
Tm	22.63	7.33	23.72	12.67	7.63	96.14	9.05	18.19	55.77	17.99
Yb	198.37	78.34	203.22	140.61	87.62	733.09	86.27	177.07	467.62	160.86
Lu	37.46	17.71	36.66	32.54	21.45	118.57	17.99	37.68	88.69	32.38
Hf	9367.49	9148.18	6542.55	11188.98	10627.01	11109.68	8468.68	10446.31	8238.69	16445.21
Ta	0.463	0.892	0.163	1.002	0.984	1.68	0.787	1.04	0.737	0.574
Pb	29.43	4.59	7.85	15.61	12.02	24.91	16.81	45.93	34.09	3.7
Th	128.28	14.65	31.74	55.4	44.6	112.39	52.25	173.95	132.55	15.45
U	69.09	41.05	41.36	104.27	76.64	333.77	57.86	206.44	101.05	73.24
Eu/Eu*	0.26	0.70	0.69	0.63	0.45	1.24	0.45	0.85	0.54	0.60
Ce/Ce*	39.51	10.37	62.80	161.80	269.08	1.07	8.55	5.06	20.33	4.91

486707_141	486727_36	486727_48	486727_72	486727_52	486732_84	486722_190	486732_88	486732_103	486727_57	486727_50
185.61	535.11	204.66	564.37	311.5	285.21	330.91	297.5	277.91	259.31	301.36
12.93	32.07	10.86	63.37	8.87	31.26	27.73	15.89	9.14	10.91	3.95
0.216	1.29	0.204	1.75	1.11	1.27	1.22	0.666	0.26	0.621	0.181
0.186	5.61	0.824	6.07	2.37	4.64	1.22	1.18	2.65	0.858	0.48
572.94	1149.85	531.45	394.76	1148.27	533.28	873.68	795.69	623.64	1107.58	800.03
3.69	1.94	1.013	0.831	1.47	1.29	1.84	2.78	1.58	1.57	2.01
0.0339	1.803	0.1006	2.46	0.491	0.898	0.11	0.27	0.433	0.1108	0.0088
51.68	38.56	10.86	16.46	9.15	21.16	48.59	16.18	7.96	11.23	16.88
0.12	3.82	0.312	3.5	1.289	1.78	0.22	0.428	0.789	0.395	0.0612
2.01	32.01	3.28	28.16	12.04	14.13	3.56	3.82	8.02	5.14	1.121
3.52	27.68	3.93	24.81	12.87	11.7	5.9	5.4	7.42	7.04	2.17
0.433	15.37	1.78	12.01	5.22	6.47	2.06	1.2	3	1.6	0.319
15.31	65.42	12.73	46.83	40.9	26.42	29.7	24.58	18.22	30.94	14.67
4.35	15.01	3.64	8.31	10.94	6.36	7.85	6.8	6.05	9.05	4.86
52.84	141.33	43.56	60.58	117.76	65.7	90.15	80.84	61.88	106.27	67.13
18.21	38.85	16.18	13.08	39.05	16.79	29.87	27.72	21.36	36.44	25.49
81.31	155.99	83.18	40.8	173.35	68.1	127.96	121.81	86.1	160.25	129.64
17.3	29.03	19.31	6.59	33.18	14.16	25.44	24.8	17.62	32.71	28.45
163.94	252.1	195.3	50.17	290.56	130.53	224.67	218.71	165.13	281.63	268.32
34.94	48.33	44.03	7.98	59.5	26.51	46.55	42.59	32.67	55.67	57.18
15257.79	9480.83	8393.83	10334.7	8704.75	9258.78	8334.24	9850.98	16129	9362.7	10647.29
2.26	1.042	0.939	0.674	0.815	0.849	0.371	1.36	0.689	1.103	1.145
26.99	42.47	15.17	30.92	13.73	22.16	22.3	25.42	9.79	13.76	10.34
104.27	139.62	76.08	128.12	49.46	79.54	74.29	91.39	37.09	44.8	33.66
85.11	208.09	177.98	236.63	68.06	197.86	62.11	113.14	116.56	60.01	37.02
0.18	1.10	0.77	1.08	0.70	1.13	0.48	0.32	0.79	0.33	0.17
195.02	3.54	14.75	1.35	2.77	4.03	75.18	11.46	3.28	12.92	175.07

486707_148	486727_09	486732_121	486732_85	486718_166	486722_188	486727_20	486727_67	486732_123	486727_44	486727_14
153.63	215.49	266.6	700.92	242.64	124.91	115.9	223.67	227.33	121.46	127.39
6.24	8.09	1.55	39.38	7.29	2.87	9.35	9.84	14.56	9.8	5.74
0.159	0.299	0.56	1.63	0.23	0.396	0.238	0.578	0.67	0.544	0.209
0.223	0.682	0.99	11.81	0.33	0.218	0.492	1.38	0.69	0.928	0.267
376.96	344.19	1371.1	1284.56	450.41	372.83	316.96	413.09	1020.02	241.65	186.74
1.35	1.21	1.73	2.4	1.77	0.99	3.01	0.948	1.83	0.972	1.053
0.0322	0.1075	0.227	3.22	0.0183	0.0137	0.048	0.357	0.108	0.224	0.0099
14.14	6.72	18.04	48.57	13.66	7.49	50.06	7.99	11.78	13.45	9.43
0.0537	0.239	0.861	6.7	0.0557	0.0395	0.151	0.566	0.353	0.31	0.0383
0.684	2.41	10.43	53.17	0.801	0.654	1.9	4.89	3.97	2.8	0.591
1.52	2.36	13.12	40.51	1.83	1.32	2.13	4.17	4.69	2.36	1.26
0.423	1.33	1.13	14.71	0.36	0.474	0.664	2.23	1.07	1.147	0.41
8.49	8.13	45.03	74.65	8.01	6.9	8	12.5	28.35	7.2	6.69
2.51	2.54	12.45	17.25	2.67	2.37	2.29	3.33	8.49	1.88	1.509
31.36	29.13	140.13	153.85	37.05	29.62	26.59	37.8	104.35	22.59	17.91
11.62	10.54	46.32	42.66	14.48	11.26	9.41	13.21	35.83	7.72	6.29
56.29	54.55	199.04	167.62	72.01	53.88	44.77	65.15	152.74	38.14	29.46
12.34	11.96	38.35	31.88	17.37	12.5	10.58	14.22	29.5	8.65	6.48
123.46	122.37	320.44	293.56	167.84	127.83	108.27	145.18	268.07	92.16	63.74
26.08	27.66	61.93	56.44	35.24	29.98	24.28	33.36	51.83	20.24	13.69
10849.92	9062.15	8136.16	10236.54	11978.2	10834.88	10430.68	10116.23	11732.15	9920.96	9866.95
0.497	0.547	0.593	1.39	1.03	0.607	1.88	0.692	0.372	0.95	0.818
11.27	8.06	13.35	30.39	12.29	18.33	34.5	9.41	16.88	21.51	10.79
41.03	21.86	67.69	119.59	46.35	68.25	129.19	30.76	56.54	71.72	37.03
55.84	54.61	46.83	237.43	106.69	72.71	71.68	82.89	51.25	78.78	139.54
0.36	0.93	0.14	0.82	0.29	0.48	0.49	0.94	0.28	0.85	0.43
81.84	10.09	9.82	2.52	102.98	77.49	141.52	4.28	14.52	12.28	116.56

486727_44	486727_14	486746_172	486727_51	486718_163	486732_93	486727_60	486727_12	486727_19	486727_61	486713_193
121.46	127.39	289.75	205.59	188.08	237.19	1650.45	201.96	157.81	566.38	223.54
9.8	5.74	6.41	9.17	15.12	7.73	215.51	7.15	10.95	62.34	11.95
0.544	0.209	2.14	0.978	0.287	0.272	10.82	<0.081	1.11	2.26	0.183
0.928	0.267	0.6	1.066	0.254	0.861	43.49	0.878	0.316	9.97	0.236
241.65	186.74	811.6	768.18	473.03	600.39	2255.29	396.42	544.64	1017.77	402.66
0.972	1.053	1.15	1.48	1.78	2.72	3.7	1.44	1.009	2.76	0.89
0.224	0.0099	0.205	0.234	0.0092	0.1157	18.04	0.1145	0.0696	2.55	0.003
13.45	9.43	5.34	14.58	12.48	20.11	226.24	16.39	17.15	33.27	15.59
0.31	0.0383	0.315	0.77	0.0724	0.289	30.28	0.185	0.474	5.56	0.0739
2.8	0.591	2.94	8.31	1.08	2.98	264.39	1.65	5.96	47.07	1.27
2.36	1.26	3.58	8.84	1.74	3.87	168.29	2.45	6.62	42	2.38
1.147	0.41	1.92	2.64	0.258	0.926	120.04	0.711	2.15	22.79	0.34
7.2	6.69	14.14	27.34	11.61	16.05	239.89	10.16	21.65	70.62	10.26
1.88	1.509	4.58	6.83	3.49	4.84	47.5	3.03	5.15	15.11	2.98
22.59	17.91	66.01	76.53	44.49	55.38	358.34	34.25	54.09	131.15	35.93
7.72	6.29	24.65	26.48	15.94	18.52	79.72	12.2	17.97	33.12	12.53
38.14	29.46	130.57	122.25	71.25	84.78	268.73	58.64	77.59	123.5	58.75
8.65	6.48	30.82	25.59	14.88	17.43	47.74	12.65	15.72	25.08	12.21
92.16	63.74	322.25	250.96	134.79	163.42	390.9	120.41	140.29	233.45	119.38
20.24	13.69	71.21	51.53	27.88	33.26	72.87	25.48	29.96	47.94	25.51
9920.96	9866.95	8517.95	10035.42	8925.68	10029.66	8942.38	10042.22	7559.31	11414.02	9452.39
0.95	0.818	0.304	1.111	0.43	1.51	0.945	1.002	0.624	1.79	0.182
21.51	10.79	7.12	16.11	10.29	37.14	20.53	12.62	19.14	17.22	7.8
71.72	37.03	29.89	58.08	41.52	143.66	79.23	40.26	64.96	75.15	27.09
78.78	139.54	60.15	104.21	33.31	150.4	257.32	68.71	42.8	183.85	37.54
0.85	0.43	0.83	0.52	0.18	0.36	1.83	0.44	0.55	1.28	0.21
12.28	116.56	5.06	8.27	116.39	26.47	2.33	27.10	22.73	2.13	252.01

486727_37	486732_79	486732_83	486727_34	486727_33	486746_182	486732_111	486727_62	486727_63	486732_81	486727_55
220.65	113.71	188.71	358.8	2267.8	402.4	124.21	157.41	186.32	329.8	254.61
2.06	6.25	6.01	23.23	178.71	29.37	4.34	9.8	11.35	12.51	48.53
0.248	0.055	1.15	2.32	6.11	0.46	0.66	0.829	0.183	0.362	0.586
0.528	0.497	0.301	3.66	35.28	4.07	2.7	0.539	0.411	0.374	0.83
875.12	195.01	530.84	785.68	2691.71	726.11	183.35	589.37	408.57	834.94	702.8
1.82	0.744	1.11	2.33	3.54	1.23	1.03	3.25	1.58	1.7	2.28
0.173	0.0069	0.00338	0.882	9.17	1.27	0.216	0.0688	0.0657	0.0571	0.205
21.02	6.62	10.04	13.82	82.41	17.62	5.34	53.03	39.94	34.6	4.56
0.234	0.0313	0.0619	1.63	18.75	1.83	0.309	0.228	0.28	0.212	0.346
3	0.47	1.205	12.77	153.25	14	2.32	2.58	3.68	2.87	3.99
5.71	0.95	2.59	11.42	121.66	10.13	2.08	3.79	3.96	4.81	5.02
1.6	0.392	0.709	5.94	69.35	7.23	0.96	0.965	1.38	1.24	0.986
25.6	3.89	12.87	30.51	228.66	29.04	5	13.53	12.39	20.39	20.1
7.16	1.229	4	8.04	47.83	7.46	1.36	4.21	3.43	6.04	6.01
82.64	15.78	48.97	80.62	390.78	77.02	15.5	53.03	36.71	76.22	70.61
28.26	5.99	18.87	25.6	90.25	20.96	5.5	18.65	12.85	28.44	24.17
131.95	30.73	88.69	110.17	310.9	89.64	26.52	92.15	59.84	131.49	106.09
27.18	7.25	18.89	22.1	55.1	19.07	6.3	21.29	13.16	28.11	21.57
255.27	74.99	181.98	201.47	443.89	177.32	66.07	205.72	127.33	256.32	194.26
54.62	18	39.22	41.73	80.37	35.95	16.18	42.99	27.24	52.79	39.15
10221.38	8308.37	8952.3	9481.87	9942.96	9780.22	12841.79	10108.94	10179.56	8661.88	9314.39
1.316	0.63	0.808	1.55	1.26	0.418	1.4	1.61	0.909	0.807	1.048
48.19	3.6	7.48	10.83	50.27	15.08	8.37	10.16	19.95	19.27	8.56
168.05	9.94	24.31	36.36	165.23	60.5	27.33	42.64	79.2	63.17	50.47
221.86	14.06	38.58	142.48	364.03	77.56	78.49	42.21	91.72	66.37	191.45
0.40	0.62	0.38	0.97	1.27	1.29	0.91	0.41	0.60	0.38	0.30
25.14	108.42	167.06	2.77	1.51	2.78	4.97	101.91	70.88	75.69	4.12

486732_81	486727_55	486727_38	486718_157	486732_104	486707_135	486722_191	486732_107	486732_99	486746_176	486732_80
329.8	254.61	123.99	578.5	697.34	485.87	564.47	211.77	9135.2	822.88	190.91
12.51	48.53	28.22	370.16	42.46	12.74	51.4	11.84	436.79	7.24	11.28
0.362	0.586	0.103	6.61	2.94	0.51	2.48	1.31	16.88	<0.081	0.075
0.374	0.83	0.515	3.55	13.08	2.03	12.7	0.292	198.02	1.02	0.261
834.94	702.8	174.45	1171.33	2765.17	958.4	1082.62	848.11	8961.8	1880.19	682.83
1.7	2.28	1.16	2.51	2.34	1.52	1.69	1.19	6.64	4.05	1.51
0.0571	0.205	0.0441	2.89	3.91	1.85	2.39	0.0373	31.29	0.183	0.008
34.6	4.56	13.17	30.1	39.16	21.91	28.92	23.49	214.74	14.38	7.38
0.212	0.346	0.088	3.75	6.22	3.59	5.16	0.438	52.95	0.349	0.1078
2.87	3.99	1.03	26.25	51.09	28.16	41.89	6.77	402.18	3.42	1.59
4.81	5.02	1.39	19.24	39.87	17.41	37.2	8.8	329.38	5.96	2.67
1.24	0.986	0.614	6.46	18.19	6.4	22.4	1.64	156.59	1.03	0.922
20.39	20.1	5.33	41.01	97.42	40.38	70.38	31.44	671.82	35.18	13.01
6.04	6.01	1.42	11.85	26.93	9.78	16.54	8	158.95	12.87	4.05
76.22	70.61	15.9	121.32	289.54	97.77	140.64	86.81	1337.09	162.31	53.8
28.44	24.17	5.29	37.84	88.09	31.39	35.95	27.58	306.08	61.32	21.53
131.49	106.09	26.28	162.27	371.33	134.87	141.21	118.16	1017.57	288.04	111.5
28.11	21.57	5.82	34.75	71.31	27.47	27.01	23.12	165.9	59.83	25.08
256.32	194.26	56.88	323.31	602.74	262.77	253.75	208.06	1300.22	551.3	249.3
52.79	39.15	12.88	68.83	116.7	54.91	51.81	40.82	198.88	107.69	57.78
8661.88	9314.39	9371.84	10543.08	8467.95	10776.66	9691.49	10270.89	11123.19	12651.12	7391.62
0.807	1.048	1.02	0.593	0.879	0.494	0.555	0.436	1.48	1.56	1.014
19.27	8.56	18.63	21.05	29.02	16.33	17.97	24.58	75.25	31.2	7.92
63.17	50.47	67.69	62.59	119.66	62.8	80.19	85.95	209.73	120.07	25.76
66.37	191.45	84.68	193.11	160.36	125.66	145.42	66.66	525.88	138.3	62.97
0.38	0.30	0.69	0.70	0.89	0.74	1.34	0.30	1.02	0.22	0.48
75.69	4.12	50.88	2.20	1.91	2.05	1.98	44.23	1.27	13.70	60.49

486746_176	486732_80	486739_130	486727_69	486718_164	486746_170	486727_27	486727_64	486718_156	486727_31	486727_13
822.88	190.91	325.28	209.8	165.86	336.57	872.01	185.4	424.76	97.58	193.43
7.24	11.28	29.29	5.45	10.19	29.87	79.1	19.22	16.83	8.84	12.49
<0.081	0.075	1.05	0.621	0.318	0.95	2.9	1.43	0.58	0.211	0.342
1.02	0.261	5.58	0.457	0.394	6.58	15.64	1.15	6.49	0.815	0.903
1880.19	682.83	551.89	918.92	418.62	831.21	1213.59	471.39	1167.74	197.11	186.52
4.05	1.51	1.4	0.96	1.07	1.69	2.2	1.68	1.52	1.177	0.801
0.183	0.008	1.112	0.034	0.0992	1.78	4.19	0.406	0.125	0.1379	0.1131
14.38	7.38	17.42	6.12	7.06	27.51	41.39	31.09	44.44	19.47	11.48
0.349	0.1078	1.65	0.168	0.256	3.05	6.78	0.901	0.626	0.292	0.215
3.42	1.59	12.36	2.53	2.71	23.26	59.29	7.77	9.99	2.56	2.4
5.96	2.67	11.04	4.64	3.16	17.8	42.58	7.76	11.13	2.06	2.17
1.03	0.922	5.34	1.074	1.51	8.7	26.36	3.67	4	1.215	1.177
35.18	13.01	20.78	27.05	11.23	40.04	92.79	18.86	44.5	6.51	6.99
12.87	4.05	5.1	8.04	3.08	9.48	21.13	4.5	10.89	1.87	1.77
162.31	53.8	52.09	93.19	38.13	95.33	171.05	46.58	117	18.83	17.62
61.32	21.53	18.41	31.28	12.73	27.95	43.56	14.92	39.84	6.48	5.91
288.04	111.5	79.4	131.05	61.54	114.8	151.62	68.25	172.01	28.93	28.47
59.83	25.08	17.92	25.4	14.06	22.6	27.45	13.86	34.61	6.73	6.51
551.3	249.3	184.54	223.01	137.14	191.7	241.73	135.67	314.87	64.26	65.66
107.69	57.78	42.71	44.75	30.84	39.77	45.97	29.78	63.53	13.67	15.05
12651.12	7391.62	9914.13	8486.52	7740.81	9770.78	12178.19	10143.05	7944.53	9700.81	8258.88
1.56	1.014	0.605	0.929	0.284	0.456	1.173	0.933	0.195	0.764	0.818
31.2	7.92	16.42	10.91	12.09	15.53	17.8	27.19	32.51	11.61	6.28
120.07	25.76	53.42	36.62	44.14	76.1	78.64	97.43	115.25	38.63	24.47
138.3	62.97	132.32	52.61	59.95	98.08	150.32	153.96	73.26	64.88	63.13
0.22	0.48	1.08	0.29	0.78	1.00	1.28	0.93	0.55	1.01	0.92
13.70	60.49	3.10	19.49	10.66	2.84	1.87	12.37	38.24	23.35	17.72

486722_183	486722_189	486727_26	486727_40	486713_192	486727_47	486739_133	486727_08	486732_75	486732_97	486732_106
2164.77	359.54	165.84	109.86	243.05	369.93	194.47	274.01	108.88	425.58	147.69
146.84	20.34	15.26	8.48	1.9	23.51	15.49	19.42	8.15	9.8	4.64
5.83	3.75	0.185	0.418	1.23	1.05	3.76	0.913	0.33	3.27	0.4
57.98	3.01	0.778	0.97	0.348	3.08	1.44	0.632	0.263	3.39	0.361
3137.67	1174.9	589.76	376.22	847.97	494.74	1326.71	757.81	407.58	1319.94	687.09
3.48	1.43	4.16	0.963	0.84	1.78	1.41	1.403	1.74	2.39	1.15
8.63	0.487	0.239	0.288	0.0094	0.74	0.26	0.0721	0.0097	0.631	0.0293
84.21	10.85	67.51	17.57	6.8	25.04	12.07	14.41	15.62	7.83	5.17
18.72	1.34	0.384	0.487	0.086	1.451	0.671	0.325	0.0546	1.091	0.0626
159.2	12.62	3.93	4.8	1.76	11.19	6.07	3.9	0.724	9.59	1.23
131.39	15.03	4.71	4.88	3.96	9.72	6.56	4.96	1.45	6.64	1.95
60.74	6.26	1.108	2.2	0.507	6.18	2.24	1.232	0.394	4.57	0.558
250.01	47.41	15.55	15.34	19.7	26.97	28.36	19.75	6.93	31.65	13.77
59.62	12.18	4.38	3.75	5.99	5.5	9.36	5.87	2.3	9.66	4.52
481.2	127.5	52.77	37.72	77.52	56.64	113.75	68.75	28.38	119.38	58.99
112.88	38.16	18.45	12.06	27.59	16.35	41.98	24.28	11.07	42.14	22.38
376.21	155.95	87.52	54.54	123.96	72	192.39	112.87	59.75	201.81	109.38
69.02	32.48	18.79	11.93	24.77	14.95	39.47	22.99	13.65	41.36	22.8
586.08	287.37	176.08	112.17	222.98	146.85	364.54	208.1	140.2	376.54	216.62
103.39	56.5	34.55	23.52	45.52	31.2	74.95	42.47	32.58	78.79	44.81
11370.36	8272.14	9043.74	7935.02	8500.29	10675.16	8449.3	9163.15	10955.32	8779.29	9722.7
1.34	0.547	1.91	0.932	0.402	1.17	0.34	0.789	1.57	0.818	0.292
23.86	11.54	19.22	8.52	11.49	56.61	23.9	16.01	12.93	10.17	10.11
174.86	38.92	71.34	30.28	39.2	198.84	81	52.46	40.78	31.69	32.65
312.53	64.06	76.32	41.8	44.19	176.61	74.85	64.8	67.2	44.79	59.23
1.02	0.72	0.40	0.78	0.18	1.17	0.50	0.38	0.38	0.96	0.33
1.59	3.23	53.64	11.29	57.56	5.82	6.96	22.66	163.36	2.27	29.05

		Disko; Atanikerdluk								
486727_71	**486713_200**	**486748_133**	**486754_195**	**486754_190**	**486748_134**	**486761_80**	**486767_25**	**486754_216**	**486748_143**	**486748_153**
217.26	511.67	184.98	188.22	90.98	202.82	277.49	472.16	128.67	296.02	218.33
13.53	11.91	1445.79	12.85	30.32	7.98	109.11	91.84	11.4	41.17	71.79
1	0.85	13.4	0.65	0.8	0.216	1.59	1.84	0.103	3.36	0.85
0.35	1.98	3.11	0.435	0.746	0.442	5.55	6.32	0.466	10.96	2.62
753.01	1492.23	1099.15	514.85	562.28	854.19	648.26	718.34	667.58	733.98	782.04
1.034	2.14	3.2	1.3	2.39	3.35	2.74	2.2	1.54	1.81	2.05
0.011	0.715	0.52	0.0524	0.328	0.0295	3.07	1.273	0.0724	2.2	0.671
10.39	14.57	19.78	8.14	50.67	21.24	28	17.16	17.36	29.85	38.07
0.14	1.062	0.868	0.087	0.472	0.0898	2.87	2.23	0.261	4.91	1.9
2.75	12.63	9.77	1.43	6.36	1.407	21.21	16.77	4.06	41.07	18.63
4.78	15.58	10.4	3.17	8.05	3.4	14.51	12.52	4.01	27.19	16.04
1	8.18	2.62	0.456	2.05	0.362	4.17	4.76	0.73	9.23	5.33
22.43	56.84	31.95	16.68	20.25	17.72	32.18	31.4	18.45	46.75	39.64
6.64	14.39	9.35	4.59	4.6	5.73	6.96	8.34	5.47	9.53	8.4
75.5	152.18	103.49	53.37	48.56	69.21	67.24	81.05	60.02	83.64	78.01
25.06	47.11	34.54	16.77	15.32	24.93	21.67	24.15	22.28	19.95	22.86
111.36	194.33	145.21	74.93	66.76	114.09	89.58	103.53	99.05	79.65	88.31
21.53	39.18	28.6	15.44	13.76	23.6	17.52	21.11	20.24	16.23	17.41
192.93	346.26	261.72	134.53	128.17	216.81	151.15	193.07	189.45	151.67	149.12
37.56	72.6	51.71	26.79	26.95	43.53	29.47	37.51	38.06	32.03	29.12
9412.45	8868.55	9287.83	10039.37	9180.23	11017.86	8434.11	11053.45	10656.87	11157.43	8751.77
0.861	0.398	0.858	0.504	0.833	1.171	1.219	1.44	0.837	1.1	0.358
9.89	24.43	11.01	6.07	14.03	28.53	14.66	19.67	21	8.73	17.98
32.06	65.29	47.6	26.29	55.84	122.22	60.18	88.24	85.62	68.76	80.61
36.19	72.51	50.39	35.29	94.51	115.55	96.6	267.87	98.58	114.25	70.55
0.30	0.84	0.44	0.19	0.49	0.14	0.59	0.73	0.26	0.79	0.65
63.72	4.02	7.09	29.02	31.00	99.32	2.27	2.45	30.40	2.19	8.12

486754_200	486761_111	486772_52	486761_76	486748_120	486748_142	486772_60	486761_84	486772_47	486748_141	486748_156
244.61	739.24	302.43	253.97	294.59	148.55	212.95	524.55	250.72	130.49	95.01
28.32	97.96	73.55	24.68	9.95	10.06	14.23	93.7	3.42	6.22	6.3
1.61	3.24	2.55	<0.107	0.82	0.15	0.191	2.28	0.072	0.668	0.191
6.04	23.1	1.41	1.16	0.694	0.613	0.366	9.14	0.27	0.537	0.291
485.74	663.56	863.15	1229.98	1227.87	339.76	543.37	889.87	602.35	904.13	190.04
1.294	1.6	3.1	2.1	3.31	1.38	2.32	4.32	1.6	2.64	1.46
1.74	6.47	0.496	0.22	0.0471	0.0312	0.0251	2.16	0.0134	0.0317	0.0123
20.91	51.33	28.8	24.18	32.2	25.8	19.83	41.13	13.03	46.76	16.24
3.12	10.89	0.87	0.815	0.346	0.141	0.159	5	0.0608	0.333	0.0418
26.52	81.05	6.56	10.16	5.34	1.5	2.19	42.01	0.903	5.41	0.815
17.71	51.89	6.9	10.52	8.69	2.67	4.04	29.43	2.86	7.37	1.14
8.37	17.25	2	1.99	1.51	0.984	0.579	8.06	0.582	1.37	0.181
31.47	66.16	23.35	44.47	31.13	9.97	16.36	50.48	16.58	25.74	4.38
6.25	12.87	6.42	12.08	9.09	2.59	4.75	10.96	5.11	6.86	1.095
53.28	97.14	78.19	140.71	102.04	29.9	50.62	107.04	59.24	73.58	14.15
14	22.59	28.74	43.62	34.12	10.03	16.8	30.5	20.05	24.91	5.02
54.15	77.76	138.61	177.49	144.14	44.64	75.39	127.24	91.28	113.12	25.71
10.92	15.15	32.88	33.22	29.09	9.44	15.23	24.56	19.21	24.98	6.33
99.13	130.93	328.55	293.41	261.71	90.32	134.4	213.16	175.61	238.09	64.51
22.11	22.84	72.59	54.08	52.24	18.71	26.52	40.88	36.35	49.17	15.01
11103.74	8557.75	13005.07	10761.7	9904.03	8449.75	10450.98	12267.95	9704.37	9495.4	10428.62
0.521	0.729	1.83	1.47	1.31	0.459	1.107	2.09	1.193	0.797	0.896
8.15	11.42	57.83	20.62	22.23	3.28	33.67	47.56	28.24	23.6	21.56
36.58	86.78	230.83	89.61	90.27	17.44	120.85	183.17	102.63	97.19	85.8
191.13	141.11	205.45	133.24	68.5	13.91	129.35	233.37	125.12	60.43	39.44
1.08	0.90	0.48	0.28	0.28	0.58	0.22	0.64	0.26	0.30	0.25
2.16	1.47	10.55	13.74	60.71	93.62	75.55	3.01	109.87	109.54	172.38

486748_156	486767_35	486767_11	486754_189	486767_15	486748_117	486754_196	486748_118	486748_140	486767_27	486754_168
95.01	248.06	153.1	694.39	638.18	277.51	91.48	199.9	612.36	2156.03	103.61
6.3	31.47	20.8	226.87	54.19	11.32	3.27	84.87	52.63	193.42	17.2
0.191	0.203	0.443	4.97	2.42	0.24	0.351	1	2.14	8	0.54
0.291	0.73	1.29	12.83	14.31	2.54	0.312	1.65	16.54	56.69	0.65
190.04	587.05	487.95	1255.23	1204.73	748.94	281.42	549.76	1505.34	2702.98	563.59
1.46	1.96	1.14	2.53	1.87	1.66	1.25	1.28	2.64	3.47	1.67
0.0123	0.1156	0.14	3.35	2.37	0.397	0.0182	0.146	2.05	9.26	0.092
16.24	45.85	20.21	43.11	29.74	11.34	7.1	16.15	44.54	69.05	4.35
0.0418	0.436	0.564	5.77	4.21	0.789	0.0357	0.324	4.39	15.57	0.132
0.815	5.12	6.41	44.23	32.27	8.3	0.486	3.57	36.83	118.96	1.58
1.14	6.83	8.05	30.89	25.35	6.22	1.15	6.01	33.39	90.29	2.36
0.181	1.48	1.71	11.52	10.41	2.12	0.405	1.48	13.41	40.07	0.69
4.38	21.44	19.1	60.5	56.99	26.56	5.31	14.8	72.55	177.26	12.07
1.095	5.64	4.33	13.68	13.77	6.42	1.49	3.61	17.11	43.22	3.69
14.15	60.4	47.12	123.26	141.12	72.57	18.47	42.39	187.49	379	51
5.02	19.85	15.73	33.05	40.1	24.57	7	14.55	37.33	89.34	17.99
25.71	85.59	76.01	132.37	163.11	106.3	39.06	74.07	133.28	316.73	81.85
6.33	17.93	17.07	25.2	33.53	21.48	8.89	16.95	25.29	55.53	18.82
64.51	165.46	166.98	220.04	311.28	197.1	104.11	180.56	202.41	456.97	231.06
15.01	33.22	33.92	42.97	61.87	40.98	25.46	40.61	37.1	77.83	37.53
10428.62	7636.08	8977.77	10909.52	10342.41	11043.8	10213.73	9409.94	11002.95	13258.11	12469.13
0.896	0.955	0.665	0.985	1.085	0.805	0.598	0.56	0.795	1.51	0.99
21.56	13.73	11.44	22.88	12.72	13.5	5.67	17.85	39.07	26.9	7.04
85.8	54.08	41.01	157.93	70.65	55.49	22.46	65.87	184.94	144.58	27.1
39.44	33.21	54.27	94.22	158.21	111.99	51.3	84	204.01	242.43	58.18
0.25	0.37	0.42	0.81	0.84	0.50	0.50	0.48	0.83	0.97	0.40
172.38	49.15	17.31	2.36	2.27	4.88	67.04	17.87	3.57	1.38	9.50

486767_27	486754_168	486754_204	486767_38	486767_39	486772_48	486761_86	486761_109	486754_163	486767_23	486748_119
2156.03	103.61	213.51	320.35	1529.04	554.69	216.96	145.61	144.7	275.09	127.99
193.42	17.2	17.9	16.63	857.75	55.07	8.42	9.02	11.76	5.76	34.55
8	0.54	0.452	0.691	11.51	2.93	0.23	0.89	3.81	0.078	0.59
56.69	0.65	1.39	3.01	36.4	4.42	0.77	0.337	0.79	0.537	1.06
2702.98	563.59	727.39	456.93	1544.08	2029.88	988.7	528.83	270.09	761.96	501.67
3.47	1.67	1.61	2.33	2.67	6.06	1.82	0.995	1.35	2.05	1.94
9.26	0.092	0.456	0.545	14.81	1.88	0.102	0.0462	0.0449	0.299	0.128
69.05	4.35	11.83	39.72	167.7	42.72	16.16	11.22	22.17	11.08	10.14
15.57	0.132	0.838	1.56	20.56	2.49	0.466	0.1167	0.115	0.226	0.185
118.96	1.58	7.53	13.7	164.89	22.04	6.05	1.74	1.136	3.14	2.19
90.29	2.36	7.04	7.73	91.51	24.29	6.48	2.53	1.61	4.6	2.06
40.07	0.69	1.94	1.84	30.64	6.98	1.4	1.316	0.615	0.577	0.675
177.26	12.07	23.37	17.71	146.86	82.94	34.18	11.82	7.85	22.55	11.51
43.22	3.69	6.39	4.64	27.27	22.09	8.96	3.34	1.9	6.64	3.24
379	51	64.97	46.26	222.71	230.8	96.23	40.69	24.45	77.87	41.28
89.34	17.99	21.92	15.57	50.61	70.58	33.63	14.69	8.1	26	14.69
316.73	81.85	92.19	68.06	167.39	288.05	145.17	70.82	38.63	111.3	67.71
55.53	18.82	18.84	14.36	32.27	54.95	30.5	16.03	8.41	22.37	14.15
456.97	231.06	163.7	138.05	282.2	469.16	265.05	157.87	82.23	197.45	131.49
77.83	37.53	31.91	26.58	51.33	86.17	48.99	36.9	18.2	37.98	25.91
13258.11	12469.13	8400.84	9742.12	12489.07	8461.73	9889.34	7143.18	16320.47	8768.88	10544.18
1.51	0.99	0.846	1.29	0.888	1.66	0.747	0.357	1.16	1.224	0.992
26.9	7.04	15.47	45.38	19.54	41.38	19.73	13.73	11.91	18.18	18.14
144.58	27.1	61.65	172.04	144.5	147.91	73.22	51.94	38.94	71.27	37.31
242.43	58.18	84.39	100.27	178.21	130.11	84.72	27.95	25.64	106.1	62.39
0.97	0.40	0.46	0.48	0.81	0.48	0.29	0.74	0.53	0.17	0.42
1.38	9.50	4.61	10.37	2.31	4.75	17.84	36.78	74.26	10.26	15.86

486754_201	486754_208	486772_56	486767_12	486767_24	486772_61	486748_139	486761_70	486754_217	486754_172	486767_37
695.47	197.68	936.2	347.71	348.67	305.97	2264.47	1217.58	2230.83	3046.75	411.63
118.79	83.65	43.8	17.9	10.26	31.72	284.6	97.37	216.26	878.98	35.54
5.56	2.11	2.42	0.497	1.11	1.55	9.89	4.02	7.1	11.88	2.38
19.69	1.92	9.03	2.69	1.26	1.88	125.56	41.4	64.89	74.74	7.44
1053.68	1175.41	1729.95	816.01	1438.81	1145.49	5001.52	1261.17	4316.81	3511.29	2101.24
2.61	1.62	2.09	2.98	3.31	1.76	7.47	1.98	5.8	4.9	2.91
7.6	0.747	3.26	0.635	0.463	0.441	18.45	8.22	17.55	28.34	1.8
153.24	19.23	33.18	22.31	38.09	11.79	164.27	73.24	121.45	151.9	32.05
35.88	0.795	4.72	1.187	0.662	0.731	30.7	13.72	25.39	36.04	4.4
265.23	7.99	35.27	10.22	7.59	5.4	244.19	109.74	210.79	263.19	34.53
84.15	7.84	29.03	8.22	9.18	5.14	164	72.44	145.33	184.04	28.03
40.89	3.4	11.25	2.3	2.66	1.63	69.3	24.84	63.17	82.51	10.28
100.59	39.23	73.92	23.2	38	22.96	326.56	111.35	283.37	306.29	87.82
18.88	10.36	19.87	6.55	11.31	7.72	73.45	21.79	60.96	65.52	23.1
140.64	123	188.18	70.99	135.01	97.27	619.15	171.62	501.94	507.93	238.82
33.23	42.34	55.4	24.22	48.44	36.84	144.7	42.41	130.51	110.5	77.5
121.14	181.62	228.91	110.82	216.57	179.2	484.31	164.84	476.97	345.93	308.98
24.17	37.03	45.22	24.33	45.73	40.9	81.62	32.7	85.34	58	59.67
230.71	332.7	404.62	232.35	418.28	412.38	716.02	298.47	703.77	453.1	538.56
44.14	66.32	78.02	47.46	82.14	81.39	110.22	59.25	125.57	74.23	94.87
9477.28	9102.5	11103.96	9856.72	10517.66	9213.72	9624.02	11215.69	8389.12	9423.79	9441.23
1.306	0.987	1.52	1.8	1.88	1.53	1.14	1.42	1.39	0.873	1.65
15	25.06	25.34	20.56	36.22	19.53	23.62	26.35	40.3	11.98	27.27
70.18	93.72	117.61	77.39	136.03	66.82	206.38	180.23	1031.39	90.15	116.7
128.77	61.02	187.45	105.96	182.4	153.51	228.01	323.13	274.92	228.53	188.15
1.36	0.59	0.74	0.51	0.44	0.46	0.92	0.85	0.95	1.06	0.63
2.23	6.01	2.04	6.18	16.56	5.00	1.66	1.66	1.38	1.14	2.74

486767_37	486754_169	486767_44	486748_127	486754_202	486754_206	486748_123	486761_73	486761_83	486761_105	486767_46
411.63	159.51	1111.57	182.92	2509.24	171.73	1988.92	208.49	167.88	683.52	299.61
35.54	9.41	66.98	153.79	531.96	14.72	279.55	61.46	90.19	103.34	445.25
2.38	0.081	3.73	1.65	9.34	0.881	9.52	0.73	1.07	5.4	4.86
7.44	0.582	21.61	1.6	76.87	2.89	72.59	3.62	1.1	13.61	4.7
2101.24	263.83	1086.6	618.88	4272.2	341.8	4030.02	408.63	512.33	1076.09	803.68
2.91	1.112	1.62	1.49	5.2	1.616	5.12	1.4	1.66	1.51	3.13
1.8	0.0586	4.36	0.199	24.04	0.829	10.48	0.963	0.249	3.04	0.466
32.05	10.96	71.12	6.2	177.17	5.97	93.79	15.15	22.34	30.55	12.03
4.4	0.148	8.14	0.278	35.11	0.853	22.24	1.76	0.569	5.78	0.489
34.53	1.429	70.97	2.88	261.66	6.75	173.7	15.85	5.09	44.59	4.47
28.03	1.94	43.31	3.04	189.3	5.06	138.63	12.13	5.13	37.71	5.94
10.28	0.609	14.39	1.21	80.83	2.16	59.44	3.64	1.41	15.52	1.68
87.82	7.86	72.01	14.08	335.96	12.51	273.89	13.5	18.06	47.75	19.18
23.1	2.15	16.39	4.49	69.26	3.17	62.81	3.67	4.59	11.93	6.68
238.82	22.6	141.29	51.9	547.41	32.26	525.75	39.57	48.36	101.39	71.11
77.5	7.51	35.63	18.25	122.92	10.26	117.18	12.21	16.33	28.64	25.3
308.98	33.03	125.06	85.6	423.74	45.5	381.55	61.84	73.2	131.54	112.55
59.67	7.08	23.89	18.57	75.37	9.99	64	14.88	15.95	26.74	24.1
538.56	64.74	207.68	176.89	640.99	98.36	507.22	151.7	149.34	262.22	216.87
94.87	13.66	38.9	38.82	112.02	20.63	79.89	32.96	29.42	53.77	44.53
9441.23	8419.74	10091.13	12585.43	13289.03	8469.48	9088.96	10929.69	9368.49	9345.33	7998.61
1.65	0.483	1.092	1.22	1.46	1.188	0.747	0.585	0.783	0.218	1.32
27.27	9.23	24.34	8.68	30.6	5.34	16.92	11.23	22.45	11.95	15.8
116.7	31.64	119.21	37.62	258.78	21.19	154.34	43.92	82.18	51.41	48.96
188.15	36.14	124.91	60.76	274.49	57.96	242.48	94.49	98.21	107.54	72.14
0.63	0.48	0.79	0.57	0.98	0.83	0.93	0.87	0.45	1.12	0.48
2.74	28.33	2.87	6.34	1.47	1.71	1.48	2.80	14.28	1.75	6.07

486761_93	486761_87	486761_81	486761_99	486761_103	486761_75	486754_188	486767_33	486761_106	486754_215	486761_67
5114.23	527.53	573.89	383.5	171.08	348.11	150.73	317.8	893.45	363.31	282.28
574.7	35.71	63.74	36.12	9.91	20.64	7.38	13.23	126.54	33.27	26.67
25.16	0.66	5.09	2.08	0.132	0.63	0.282	0.319	6.91	3.43	1.04
208.62	14.55	10.16	15.34	1.46	3.35	0.334	1.67	53.16	7.17	2.08
5738.85	540.5	1676.99	942.51	575.97	1115.86	505.6	826.77	1788.91	1057.9	923.97
8.67	1.18	2.68	2.3	1.3	4.02	1.062	1.36	3.7	1.42	2.01
44.28	2.62	6.9	5.81	0.195	4.12	0.0098	0.221	9.55	2.53	0.407
386.45	21.81	58.11	77.46	9.4	39.38	7.6	4.57	118.83	33.66	15.6
82.98	4.21	10.37	8.49	0.435	2.06	0.0631	0.313	25.09	4.26	0.954
635.32	34.15	71.4	76.91	4.12	14.4	1.131	2.96	183.82	31.91	8.86
455.68	23.12	50.35	37.07	4.45	9.93	1.87	3.78	138.03	25.36	8.07
125.7	7.08	13.72	19.56	0.993	3.15	0.531	1.41	38.39	10.23	2.21
602.5	36.82	86.84	52.05	12.14	32.55	11.21	17.08	248.84	55.93	25.53
113.03	7.51	18.94	8.87	3.79	9.11	3.64	5.46	40.28	12.63	7.57
821.57	64.71	186.4	83.04	45.4	113.73	41.68	71.51	270.19	113.5	86.84
180.2	17.88	57.07	24.92	16.58	40.21	15.08	27.65	61.3	32.74	31.64
604.73	71.07	236.08	111.17	75.34	182.28	70.43	134.54	199.27	129.16	144.11
110.37	14.41	45.9	24.76	16.34	40.35	14.86	29.71	36.7	25.14	29.89
910.86	140.74	407.43	245.9	162.38	369.03	139.68	290.3	317.1	225.88	284.56
152.41	28.18	77.25	51.37	36.16	74.56	30.26	62.83	63.31	45.42	56.72
10857.11	11479.09	9752.72	10824.19	12787.36	11385.7	8882.93	7144.39	13313.38	11188.86	9448.31
2.52	0.991	1.3	0.831	0.976	1.93	0.75	1.089	1.05	0.927	1.144
38.89	10.05	26.43	19.5	10.16	30.88	7.89	3.74	26.51	18.58	19.22
434.55	39.24	167.09	103.52	36.38	123.62	26.66	14.16	110.69	94.56	68.33
624.15	126.74	196.56	97.04	78.16	212.67	44.61	31.06	302.41	105.97	102.72
0.73	0.74	0.63	1.36	0.41	0.54	0.35	0.54	0.63	0.83	0.47
1.53	1.58	1.65	2.65	7.77	3.25	73.56	4.18	1.85	2.47	6.03

486748_151	486767_36	486748_116	486754_191	486754_164	486748_131	486754_181	486761_98	486761_74	486767_31	486754_177
383.99	181.21	359.03	1008.92	129.57	112.75	1800.54	1921.9	655.74	6595.11	269.29
1553.44	4.72	73.35	118.77	4.87	5.3	213.61	309.48	71.45	3142.01	13.86
7.15	0.204	9.77	3.7	0.34	0.38	9.18	11.37	2.49	58.44	0.744
8.88	0.847	22.8	23.9	0.43	0.83	43.91	82.23	31.86	263.23	0.817
1867.51	554.06	1143.19	1862.31	983.34	361.69	2453.42	2930.02	1218.64	7611.63	744.07
4.52	1.76	2.32	2.15	1.01	1.32	2.58	4.65	3.9	16.4	2.94
1.311	0.0818	3.38	6.98	0.0459	0.073	11.13	13.95	7.04	31.67	0.166
30.39	19.27	52.27	55.73	6.08	12.19	86.86	111.04	59.67	241.35	15.27
2.33	0.169	10.33	11.05	0.2	0.211	17.49	27.12	12.87	46.45	0.318
20.45	1.62	91.02	85.16	3.5	1.68	133.59	213.09	99.2	345.87	2.98
18.22	2.3	55.09	61.31	5.72	1.22	100.3	139.41	56.74	269.15	3.84
8.1	0.657	15.26	28.28	0.91	0.579	42.3	43.85	24.69	116.36	0.921
59.6	12.76	89.54	114.85	21.1	6.8	178.55	207.93	77.07	538.49	16.66
15.26	4.08	15.99	25.97	6.78	1.87	40.61	41.52	14.75	128.06	5.17
159.03	49.7	122.72	208	82.58	22.03	343.59	342.13	138.85	1096.67	61.53
50.76	18.76	35.27	50.69	30.55	9.02	81.91	87.23	39.37	259.16	20.84
211.35	90.15	138.22	184.01	145.99	48.81	281.75	333.81	171.11	884.89	96.96
44.12	19.12	29.5	33.52	32.8	12.48	52.45	66.2	35.7	154.68	21.07
386.96	186.24	268.95	293.87	314.74	143.62	428.2	566.68	304.54	1222.95	197.16
77.2	38.75	55.74	53.79	69.17	34.13	78.48	110.71	58.59	192.08	39.78
9411.56	9967.96	10378.04	8854.75	14244.71	12076.76	10483.46	9000.81	11881.81	7753.87	9620.07
0.95	0.967	1.07	0.539	0.4	1.06	0.96	1.261	1.72	2	1.002
21.16	23.85	56.92	22.55	12.96	11.39	31.61	29.58	60.65	27.25	28.37
117.01	75.94	53.88	120.82	33.75	41.75	197.08	217.68	199.05	653.34	98.07
120.55	102.74	123.6	167.06	63.82	125.57	210.8	272.2	301.46	544.85	146.25
0.75	0.37	0.66	1.03	0.25	0.61	0.97	0.79	1.14	0.93	0.35
4.19	39.45	2.13	1.53	15.27	23.64	1.50	1.37	1.51	1.51	16.00

486754_177	486748_147	486772_59	486761_100	486761_96	486754_205	486761_94	486767_43	486772_55	486767_32	486754_184
269.29	287.56	355.33	294.7	187.24	157.64	237.52	1693.4	723.2	5773.37	115.1
13.86	16.51	15	12.61	15.68	7.86	78.6	124.2	137.49	595.58	9.65
0.744	2.03	0.495	1.85	1	0.561	1.08	3.33	5.01	12.31	0.37
0.817	5.25	1.78	1.61	4.52	0.496	2.72	38.84	6.63	172.57	0.94
744.07	1017.75	602.9	1639.31	542.37	702.44	964.89	2279.24	977.8	6006.82	270.17
2.94	1.99	1.29	3.23	1.29	1.108	1.18	3.28	1.79	4.14	1.35
0.166	0.41	0.551	0.261	0.634	0.0815	0.269	6.86	1.87	22.71	0.0338
15.27	13.05	18.02	14.04	15.33	9.85	23.94	59.08	20.38	131.37	4.75
0.318	1.07	1.074	0.726	1.65	0.197	0.544	11.96	2.74	37.82	0.06
2.98	8.79	9.07	7.8	13.46	1.91	5.59	97.57	22.45	288.37	0.717
3.84	7.46	8.05	7.93	9.02	2.61	6.4	69.34	15.05	229.06	0.92
0.921	3.41	3.39	1.44	2.93	0.49	1.48	30.29	6.88	96.97	0.202
16.66	26.21	21.99	30.69	19.75	13.83	19.63	144.64	38.42	442.73	3.35
5.17	7.46	5.71	9.47	4.27	4.36	6.51	33.04	10.28	104.77	1.15
61.53	79.6	60.58	120.76	45.64	54.82	76.18	317.62	99.33	876.48	16.06
20.84	28.55	19.49	43.17	14.72	20.34	27.79	78.82	29.83	200.37	6.52
96.96	130.88	83.76	204.68	67.98	96.13	137.09	299.27	121.21	654.22	37.15
21.07	28.8	18.9	44.72	15.02	20.97	28.44	58.94	23.31	113.3	9.2
197.16	285.98	174.38	412.93	148.82	193.84	276.95	507.77	214.54	877.69	111.12
39.78	63.39	36.13	81.78	31.94	39.86	56.27	95.2	42.72	134.84	26.6
9620.07	8740	9093.03	9245.86	8052.84	10499.84	12229.78	14209.78	11953.9	10020.26	12181.89
1.002	0.804	0.918	1.55	0.379	0.693	0.505	2.06	0.866	1.202	0.6
28.37	12.37	23.69	17.41	10.59	8.21	16.78	17.2	9.85	14.99	13.93
98.07	49.54	79.17	61.19	67.26	29.53	71.36	111.21	34.09	241.6	48.68
146.25	77.58	131.07	76.73	74.66	37.24	71.69	221.85	123.92	427.35	93.34
0.35	0.75	0.78	0.28	0.67	0.25	0.40	0.92	0.87	0.93	0.35
16.00	4.74	5.64	7.76	3.61	18.71	15.06	1.57	2.17	1.08	25.39

486767_43	486772_55	486767_32	486754_184	486748_121	486761_82	486767_19	486748_152	486748_144	486772_57	486754_207
1693.4	723.2	5773.37	115.1	176.63	405.17	91.73	172.97	1253.1	384.15	419.04
124.2	137.49	595.58	9.65	9.49	29.55	7.19	11.31	328.88	19.05	34.42
3.33	5.01	12.31	0.37	0.86	1.41	0.486	1.32	7.61	0.374	0.74
38.84	6.63	172.57	0.94	1.33	8.99	0.7	0.98	34.88	2.23	6.05
2279.24	977.8	6006.82	270.17	726.22	821.06	357.89	1031.31	2323.37	859.72	2869.67
3.28	1.79	4.14	1.35	1.75	1.68	0.676	1.55	4.01	2.26	7.38
6.86	1.87	22.71	0.0338	0.13	1.92	0.0749	0.205	5.06	0.877	1.716
59.08	20.38	131.37	4.75	10.3	25.65	4.34	5.73	43.09	22.38	26
11.96	2.74	37.82	0.06	0.376	3.81	0.256	0.362	9.35	1.56	3.26
97.57	22.45	288.37	0.717	3.56	30.94	2.42	3.88	80	14.44	25.21
69.34	15.05	229.06	0.92	4.13	20.53	2.57	3.73	68.53	11.82	21.72
30.29	6.88	96.97	0.202	1.41	6.88	1.2	1.14	27.46	4.47	9.31
144.64	38.42	442.73	3.35	15.84	37.54	8.83	19.38	132.13	30.55	66.48
33.04	10.28	104.77	1.15	4.96	8.24	2.66	6	29.78	7.9	20.13
317.62	99.33	876.48	16.06	58.61	80.54	31.14	77.7	267.33	86.49	238.74
78.82	29.83	200.37	6.52	21.45	26.11	11.78	27.76	67.28	28.09	84.96
299.27	121.21	654.22	37.15	98.21	119.14	57.01	130.94	242.49	121.84	376.52
58.94	23.31	113.3	9.2	20.68	26.36	13.87	28.06	44.38	24.49	72.04
507.77	214.54	877.69	111.12	192.49	252.52	151.07	258.33	378.84	209.57	621.45
95.2	42.72	134.84	26.6	39.3	55.18	35.79	52.71	64.44	40.41	121.65
14209.78	11953.9	10020.26	12181.89	8634.47	10584	8699.8	9622.23	8427.16	12259.23	10068.19
2.06	0.866	1.202	0.6	0.766	1.056	0.525	0.372	1.25	1.79	2.93
17.2	9.85	14.99	13.93	15.63	16.48	23.67	10.8	18.03	26.32	42.56
111.21	34.09	241.6	48.68	60.13	71.95	76.6	31.96	105.21	79.19	142.03
221.85	123.92	427.35	93.34	93.33	95.39	106.32	41.71	143.9	145.68	193.5
0.92	0.87	0.93	0.35	0.53	0.76	0.77	0.41	0.88	0.72	0.75
1.57	2.17	1.08	25.39	11.21	2.28	7.54	5.06	1.51	4.61	2.65

GRO1080_71	GRO1060_190	GRO1990_08	GRO1600_59	GRO1060_172	GRO2165_27	GRO2165_22	GRO1080_72	GRO1060_166	GRO1600_47	GRO1600_60
133.09	260.17	547.07	108.2	417.75	123.43	169.2	248.64	135.86	299.32	209.1
6.68	4.25	34.49	5.99	244.78	2.47	33.23	7.72	11.73	5.04	2.8
0.525	0.122	2.05	0.176	1.86	<0.065	0.922	0.24	0.2	0.125	0.241
0.704	0.385	43.46	2.16	5.12	0.606	1.147	1.94	4.96	1.241	0.382
394.26	533.32	1044.91	133.08	730.2	401.88	70.84	496.42	339.1	657.21	609.04
1.45	1.61	1.35	0.583	1.93	1.527	0.799	1.521	1.11	1.942	1.586
0.0237	0.0525	0.24	0.0152	0.422	0.00489	0.0583	0.0215	0.084	0.045	0.0255
6.71	6.78	19.19	0.567	10.33	8.96	5.14	13.42	6.66	19.55	21.16
0.0391	0.1048	0.703	0.0179	0.424	0.0356	0.1666	0.151	0.074	0.1255	0.1162
0.483	1.61	8.18	0.21	5.2	0.613	2.69	2.44	1.65	1.676	1.899
0.97	2.46	11.34	0.51	8.59	1.34	4.42	4.68	3.16	3.66	3.34
0.583	1.07	6.04	0.478	2.93	0.28	0.251	2.7	3.86	1.26	0.761
7.8	12.5	41.26	4.85	24.87	8.68	10	18.83	11.35	18.79	16.63
2.63	3.84	13.28	1.446	7.74	2.75	1.536	4.8	2.86	5.79	4.67
32.54	42.21	130.1	16.25	82.37	33.86	10.63	49.23	38.22	64.98	55.26
12.39	14.64	33.59	4.18	23.39	12.5	2.41	16.2	11.22	20.85	18.65
61.22	63.56	119.72	15.68	95.14	61.51	7.71	71.05	48.82	92.11	85.28
14.49	13.01	22.46	2.67	18.43	14.06	1.301	14.91	11.78	19	18.12
146.92	121.39	183.6	21.31	162.06	142.59	9.07	139.56	123.28	171.52	167.71
34.32	24.79	36.23	4.1	28.26	32.31	1.687	29.72	25.61	35.9	33.85
10606.17	9238.52	8314.37	8374.08	10604.19	11084.3	10927.77	10210.01	9338.48	10101.75	10760.54
1.201	0.454	0.762	0.677	0.38	1.363	0.671	0.896	0.338	1.166	1.657
18.96	11.89	18.91	6.5	13.63	38.5	73.52	15.39	7.05	24.43	72.99
76.83	51.65	88.44	24.89	75.77	130.61	298.14	58.29	25.15	85.18	259.96
232.3	67.28	185.82	93.2	72.94	150.89	241.67	115.04	49.4	121.96	205.44
0.65	0.59	0.85	0.93	0.61	0.25	0.12	0.88	1.97	0.46	0.31
53.05	22.00	11.24	8.27	5.88	163.45	12.55	56.69	20.33	62.61	93.56

GRO1080_81	GRO1740_152	GRO1060_171	GRO1080_113	GRO1060_178	GRO1060_182	GRO1060_195	GRO1080_92	GRO1080_131	GRO2165_24	GRO1060_163
103.47	315.21	1138.13	441.59	195.67	149.55	340.75	215.66	147.85	270.12	101.2
7.11	6.95	209.05	47.63	21.26	14.11	19.5	6.9	5.92	32.94	7.76
0.166	0.136	2.57	4.09	0.122	1.08	0.373	0.61	0.298	1.81	0.36
0.359	0.451	24.63	13.04	0.49	2.66	2.96	2.18	0.145	12.05	0.27
223.23	527.26	1714.44	815.92	368.62	468.31	1572.29	506.26	215.83	771.06	333.69
1.163	1.46	3.54	4.28	1.52	1.71	2.46	1.11	0.832	3.01	2.03
0.0058	0.0181	0.33	0.774	0.0264	0.334	0.345	0.0457	0.0028	4.05	0.0761
30.02	15.25	40.95	59.15	12.74	35.51	19.97	30.14	14.13	44.84	27.02
0.0518	0.0756	2.52	1.086	0.132	0.29	0.899	0.294	0.0549	2.84	0.095
0.871	1.5	24.72	12.72	1.91	2.71	11.08	4.19	0.904	17.27	1.16
1.41	3.37	26.61	15.69	2.77	3.41	14.1	7.24	1.81	11.47	1.92
0.295	0.698	15.14	11.7	1.06	1.54	4.23	2.18	0.54	4.28	0.377
5.37	20.98	99.19	39.8	12.07	14.41	58.23	22.93	6.5	33.73	6.02
1.47	5.8	27.55	8.68	3.18	3.4	15.58	5.77	1.516	8.51	2.05
17.96	60.12	247.66	79.91	33.02	40.14	160.08	51.45	18.35	86.38	24.05
6.58	17.76	57.26	25.14	11.28	13.07	50.39	15.53	6.43	26.83	9.26
32.64	59.44	183.91	106.36	49.64	54.09	196.2	64.41	30.87	113.08	46
7.53	9.39	32.4	21.57	10.38	12.67	37.32	13.14	6.35	23.36	10.94
80.02	62.08	249.63	204.73	93.24	109.49	298.67	114.48	63.23	206.5	116.91
17.31	10.09	44.04	41.67	20.37	20.01	55.96	23.94	14.29	40.79	26.18
9270.01	10434.05	11325.48	7377.65	9025.68	7636.12	7917.59	8664.49	8357.32	6941.1	10263.86
0.71	0.277	0.819	0.905	0.471	0.402	0.733	0.365	0.163	1.219	0.588
17.42	8.33	25.92	23.63	24.76	16.09	38.83	23.48	22.46	22.95	12.05
63.88	52.91	140.14	87.49	87.16	40.97	150.96	109.57	76.35	92.28	44.23
28.44	50.38	194.99	124.78	111.86	88.16	115.73	110.48	24.08	86.27	51.62
0.33	0.25	0.90	1.43	0.56	0.67	0.45	0.52	0.48	0.67	0.34
416.85	99.22	10.81	15.53	51.94	27.46	8.63	62.58	274.30	3.18	76.49

GRO1080_94	GRO1080_75	GRO1080_98	GRO1740_135	GRO1600_57	GRO2165_36	GRO1080_80	GRO2165_32	GRO1080_123	GRO1060_180	GRO2165_37
302.2	178.28	152	216.96	176.33	208.56	255.91	956.04	120.43	355	672.05
7.54	6.07	6.41	9.48	78.06	12.5	5.82	67.55	6.67	8.07	27.68
0.217	0.716	<0.102	0.164	2.38	0.69	0.429	0.898	0.172	0.33	1.97
0.88	0.291	0.325	1.73	1.402	6.45	0.234	78.31	0.423	1.8	2.63
572.73	383.09	380.57	838.44	262.94	304.69	811.51	1950.05	368.56	180.2	967.83
2.02	0.919	1.75	2.02	1.116	1.119	2.18	3.17	1.21	0.67	1.178
0.0149	0.0216	0.0068	0.306	0.062	0.234	0.0251	1.02	0.0274	0.336	0.239
5.69	26.94	22.18	11.48	6.24	17.16	23.94	25.82	8.38	4.3	8.89
0.1045	0.18	0.0647	0.527	0.1013	0.164	0.0983	1.72	0.0333	0.15	0.705
1.52	3.55	1.009	4.61	1.213	1.92	1.559	19.97	0.629	0.916	6.41
3.67	5.56	1.82	5.51	2.12	3.48	3.16	33.94	1.98	0.43	6.03
0.569	1.434	0.513	1.22	0.849	2.35	0.886	21.39	0.44	0.292	2.54
16.65	17.55	9.86	28.41	8.52	13.8	17.16	115.48	11.27	3.76	22.48
5.06	4.11	2.8	7.2	2.66	3.48	5.53	32.58	3.06	1.21	7.63
53.11	42.29	32.35	82.5	26.62	35.65	69.26	274.73	36.03	13.94	90.93
18.38	13.11	11.31	28.34	8.22	10.68	26.26	64.1	11.43	5.56	31.63
81.08	55.46	54.99	117.5	35.32	45.74	126.52	219.25	50.16	26.39	132.69
17.09	11.4	11.8	23.55	7.56	10.16	27.74	38.28	10.11	5.51	25.39
158.65	99.67	114.35	201.23	71.95	96.29	266.77	302.92	93.59	57.01	212.82
32.14	20.91	22.09	39.86	14.55	21.51	59.65	52.77	20.53	13.16	41.88
11031.06	8358.43	10243.26	8220.54	7583.42	10220.76	8939.84	9089.19	11311.09	9108.51	9120
0.851	0.852	0.473	0.616	0.552	1.019	1.038	1.233	0.732	0.14	0.843
36.97	21.74	15.15	17.99	27.3	16.24	24.86	33.96	10.31	1.75	14.82
134.42	86.9	55.69	63.38	18.26	53.18	95.06	151.7	37.39	4.24	52.37
181.14	62.87	67.71	115.28	28.37	129.94	62.35	205.24	92.43	23.56	131.18
0.22	0.44	0.37	0.30	0.61	1.04	0.37	1.04	0.28	0.70	0.67
34.71	103.99	254.51	6.88	18.95	21.08	116.00	4.69	66.77	4.61	5.21

GRO2385_39	GRO1740_136	GRO1740_143	GRO2165_25	GRO1080_124	GRO1060_164	GRO1060_175	GRO1060_187	GRO1060_168	GRO1600_52	GRO1060_177
280.3	187.52	1965.24	335.62	324.89	165.09	1069.06	286.56	1230.38	192.7	156.38
119.08	3.88	52.69	13.49	20.16	8.58	113.63	2.04	139.08	6.97	10.01
1.04	0.218	2.08	0.987	0.622	0.14	2.83	0.64	12.21	1.096	0.215
1.83	0.329	68.17	8.1	0.776	0.43	15.34	3.07	45.21	1.196	0.71
420.39	384.87	2906.64	1452.55	652.88	337.99	1663.48	613.24	1957.76	860.48	227.35
0.899	1.76	1.99	2.02	1.46	1.05	1.78	2.62	2.55	3.07	1.4
0.16	0.0078	4.89	0.1974	0.0722	0.0051	0.231	0.107	2.08	0.0343	0.0317
6.16	29.74	29.37	15.69	25.86	9.24	9.77	17.5	20.97	12.9	13.83
0.062	0.0504	2.19	0.483	0.184	0.0274	1.662	0.106	3.58	0.1334	0.124
0.769	0.774	15.96	7.41	2.74	0.376	18.15	0.98	29.33	2.32	0.896
1.49	1.54	23.16	12.1	4.47	1.05	28.54	3.24	35.85	3.94	1.64
0.409	0.233	19.44	2.94	1.031	0.155	18.2	1.88	27.35	0.811	0.554
6.65	8.52	120.9	53.26	17.94	5.95	100.51	10.96	123.52	23.48	5.46
2.71	2.39	37.62	15.34	5.23	1.9	28.76	4.15	39.45	7.14	1.79
35.77	30.27	377.19	162.73	57.55	26.5	244.12	51.61	312.18	82.29	19.29
12.93	11.93	93.85	51.2	20.21	10.36	55.03	16.81	58.67	29.03	6.49
64.65	55.18	324.02	212.07	91.01	47.85	188.27	82.46	161.87	128.28	29.3
14.78	12.29	58.02	40.86	19.11	10.57	32.73	18.86	22.14	25.57	6.34
135.86	119.8	454.76	336.48	173.84	98.56	263.52	191.58	166.18	234.74	68.92
30.24	25.1	78.45	63.32	37.68	20.83	49.57	41.78	24.3	46.03	14.75
9016.88	10889.11	8757.36	8952.13	8638.69	10065.62	9875.88	11597.03	13183.34	9029.74	11461.14
0.732	0.405	0.369	1.142	0.529	0.582	0.283	0.486	0.6	1.278	0.402
11.54	14.28	21.61	33.17	30.23	4.98	6.49	15.97	13.29	18.67	17.46
43.53	52.82	99.9	123.56	113.73	17.79	60.86	60.79	54.29	62.08	66.09
76.13	35.97	266.82	150.53	115.62	21.49	111.45	70.79	352.36	77.7	60.41
0.40	0.20	1.12	0.35	0.35	0.19	1.04	0.96	1.26	0.26	0.57
14.89	361.02	2.16	12.23	54.00	188.13	3.80	39.55	1.85	45.90	53.09

GRO1990_14	GRO2385_43	GRO1080_114	GRO1080_108	GRO1060_157	GRO1990_07	GRO1060_184	GRO1080_121	GRO1990_20	GRO2385_40	GRO1600_56
2384.56	307.09	275.03	147.73	117.22	971.48	166.56	215.49	543.38	853.78	938.46
142.21	15.11	9.21	3.35	7.55	87.73	16.91	13.66	28.93	93.84	56.56
2.25	1.46	0.63	<0.084	<0.15	2.68	0.32	0.269	0.563	2.03	0.58
61.21	4.29	1.65	0.498	1.75	53.52	1.98	0.447	15.24	61.56	27.04
3724.49	710.02	827.16	226.16	314.24	1589.51	351.83	488.68	1358.14	1828.56	1509.47
2.75	1.84	1.84	1.16	1.49	2.3	1.24	1.128	2.06	1.906	2.47
0.702	0.418	0.198	0.0041	0.17	0.272	0.108	0.0121	0.1598	0.836	0.376
22.6	30.6	20.05	5.57	22.87	16.04	12.14	13.77	15.65	29.05	18.76
2.97	0.426	0.278	0.0283	0.067	0.767	0.151	0.0828	0.659	2.005	1.409
26.18	4.61	3.4	0.471	0.805	9.53	1.48	1.62	8.43	24.17	17.77
29.19	6.11	4.65	1.28	1.28	16.74	2.36	2.52	11.12	43.2	29.88
17.9	2.35	0.967	0.389	0.377	12.01	0.64	0.557	5.2	21.53	17.86
110.8	23.13	21.9	5.22	7.77	64.04	9.66	11.7	45.99	113.26	89.88
43	6.04	5.91	1.72	2.32	22.05	2.74	3.34	14.44	28.74	23.68
466.97	68.29	75.81	20.43	25.69	215.6	32.96	39.57	151.36	246.52	191.99
125.98	23.25	26.5	6.8	10.18	54.88	11.73	14.5	47.21	62.37	46.38
468.3	103.56	117.5	32.48	49.52	202.08	56.41	69.41	190.12	228.76	153.36
82.54	21.79	23.22	6.76	11.21	38.95	12.72	15.28	36.13	43.28	29.81
734.4	201.14	211.18	66.26	117.87	315.35	123.57	152.98	304.08	376.77	258.08
125.64	39.38	43.67	14.01	24.43	58.83	23.99	34.38	59.96	73.33	48.81
10789.25	8981.93	9172.39	9719.43	12164.29	6169.76	9254.97	7748.09	8395.3	10166.83	9397.2
1.012	0.942	0.526	0.421	0.387	0.991	0.51	0.277	1.069	1.015	1.029
19.52	17.91	19.95	11.48	14.82	33.99	12.95	17.24	22.27	28.65	13.71
104.58	56.54	66.4	41.01	46.82	60.92	46.89	53.57	74.59	168.63	80.35
319.1	57.7	85.51	86.95	37.26	158.66	78.34	64.25	137.39	196.24	226.76
0.96	0.60	0.29	0.46	0.37	1.12	0.41	0.31	0.70	0.94	1.05
3.77	17.45	20.57	124.46	51.58	8.45	22.88	104.71	11.61	5.40	6.20

GRO1600_56	GRO1080_118	GRO1060_158	GRO1600_45	GRO1080_100	GRO1740_154	GRO1080_132	GRO1060_205	GRO2165_26	GRO2165_28	GRO2165_34
938.46	576.93	640.21	76.55	152.13	671.9	321.41	972.22	943.35	230.43	255.49
56.56	14.7	41.86	6.89	3.61	14.12	10.1	87.36	49.62	3.89	30.14
0.58	0.269	0.99	0.305	0.115	1.39	0.68	5.67	1.13	0.288	0.343
27.04	2.9	11.32	0.491	0.143	11.48	3.67	35.58	36.69	0.781	15.96
1509.47	1184.48	1349.23	265.53	246.28	954.11	672.26	1599.79	2302.6	1380.37	439.91
2.47	2.17	1.55	1.71	0.741	1.15	1.32	2.07	3.3	1.382	1.113
0.376	0.148	0.1357	0.0041	0.0046	0.214	0.575	1.93	0.291	0.031	0.999
18.76	13.47	22.07	3.17	11.38	10.91	13.57	53.47	24.22	3.51	8.25
1.409	0.259	1.047	0.0104	0.0588	0.534	0.252	5.91	0.799	0.195	0.366
17.77	2.87	15.53	0.2	0.901	4.83	2.52	53.24	10.61	3.22	3.11
29.88	5.62	25.74	0.466	1.49	7.74	4.84	42.91	17.79	5.71	5.57
17.86	2.72	14.04	0.174	0.575	4.16	2.09	29.76	9.42	1.409	3.16
89.88	28.6	80.91	3.6	6.59	29.35	20.21	113.34	76.71	33.84	18.58
23.68	8.88	20.21	1.488	2.01	9.2	5.94	28.15	26.44	10.75	6.14
191.99	107.79	170.72	20.35	20.81	100.62	67.43	227.87	276.54	135.03	54.1
46.38	36.32	42.26	8.14	7.73	28.22	22.89	47.29	79.1	48.96	13.95
153.36	171.14	162.05	42.34	35.72	112.9	99.68	150.34	320.28	216.9	57.03
29.81	38.05	32.13	10.01	7.44	22.49	20.83	26.58	62.91	44.38	11.38
258.08	367.47	289.6	101.38	77.29	192.67	190.98	212.33	552.82	401.7	105.9
48.81	79.99	59.11	23.17	16.8	39.45	40.98	38.54	109.88	83.4	24.52
9397.2	10863.27	11204.04	12595.99	8930.09	9801.26	10158.35	10596.96	9543.57	7667.19	9439.56
1.029	0.91	0.358	1.628	0.198	0.242	0.489	0.27	1.568	0.981	0.778
13.71	19.4	22.73	7.13	7.89	9.84	21.07	8.06	35.2	17.91	9.83
80.35	76.58	104.62	22.91	27.46	43.34	77.22	78.43	151.64	61.43	40.84
226.76	132.58	156.76	158.61	44.25	116.23	145.77	368.57	247.03	107.08	91.29
1.05	0.66	0.94	0.41	0.56	0.84	0.65	1.30	0.78	0.31	0.95
6.20	16.56	14.09	116.84	166.54	7.77	8.58	3.81	12.09	10.87	3.28

GRO2165_28	GRO2165_34	GRO1060_192	GRO1080_99	GRO1060_170	GRO1060_203	GRO2165_33	GRO1080_107	GRO1990_19	GRO1080_117	GRO1080_95
230.43	255.49	617.4	249.86	246.37	223.56	2087.49	537.52	550.51	824.78	255.81
3.89	30.14	14.18	9.5	389.5	13.3	87.26	15.15	34.9	27.97	11.15
0.288	0.343	0.217	0.384	7.09	1.31	2.32	0.72	2.24	1.58	0.475
0.781	15.96	2.08	2.47	0.49	2.99	96.74	6.2	9.98	13.58	0.261
1380.37	439.91	1153.09	646.22	390.53	815.18	2764.71	1255.34	1802.52	1225.82	768.55
1.382	1.113	1.91	0.995	1.6	1.02	2.67	2.17	2.26	1.59	1.067
0.031	0.999	0.0841	0.0114	0.0755	0.164	2.89	0.1253	0.59	0.422	0.023
3.51	8.25	7.4	5.97	13.49	15.78	13.93	10.27	29.48	34.04	28.19
0.195	0.366	0.171	0.149	0.067	0.325	2.482	0.661	1.536	1.345	0.325
3.22	3.11	1.83	2.47	0.93	3.08	28.04	7.22	13.59	15.05	5.25
5.71	5.57	3.48	5.72	1.66	5.03	59.51	13.53	14.06	16.75	8.13
1.409	3.16	0.719	2.99	0.467	2.5	37.14	6.1	5.68	7.43	1.45
33.84	18.58	20.51	30.35	8.52	25.67	179.71	51.08	61.77	54.54	30.25
10.75	6.14	7.64	9.03	2.86	8.12	46.4	13.98	18.54	16.93	7.3
135.03	54.1	91.23	78.62	32.76	69.91	391.35	140.93	210.33	171.26	75.92
48.96	13.95	34.1	21.71	11.86	25.92	95.61	41.07	59.19	42.75	24.12
216.9	57.03	160.64	85.51	56.12	114.55	331.81	180.29	245.58	163.97	105.79
44.38	11.38	34.93	16.99	12.06	22.56	58.71	36.85	48.03	29.47	20.89
401.7	105.9	327.84	149.68	113.11	225.6	476.23	333.63	401.52	242.71	186.79
83.4	24.52	67.91	30.63	23.14	46.82	87.75	68.77	77.9	45.49	38.07
7667.19	9439.56	10445.53	10184.3	8562.36	9758.84	8456.11	9286.53	9014.02	10046.68	7799.72
0.981	0.778	0.625	0.237	0.407	0.604	0.781	0.902	1.039	0.453	0.153
17.91	9.83	10.27	8.54	7.39	13.08	9.57	19.97	39.97	28.28	21.64
61.43	40.84	37.81	50.3	24.02	53.65	141.97	81.38	137.05	114.26	71.11
107.08	91.29	94.56	92.86	32.48	79.69	279.22	151.3	169.13	174.98	35.06
0.31	0.95	0.26	0.69	0.38	0.67	1.10	0.71	0.59	0.75	0.28
10.87	3.28	14.85	34.86	45.65	16.45	1.25	8.59	7.45	10.87	78.48

GRO1080_95	GRO1600_49	GRO2165_23	GRO1080_119	GRO1080_106	GRO1080_120	GRO1600_67	GRO2385_44	GRO1740_151	GRO1060_165	GRO1600_61
255.81	789.13	235.53	333.97	154.61	323.82	312.4	215.07	224.63	1623.62	343.72
11.15	42.62	9.3	11.24	8.86	4.22	9.6	8.38	68.17	142.61	8.24
0.475	1.167	0.961	0.168	0.474	0.74	1.12	0.504	1.1	2.72	0.419
0.261	19.59	0.294	1.55	2.07	0.68	2.75	1.146	0.79	52.81	0.332
768.55	1522.77	743.14	674.4	235.48	1012.05	1127.27	376.87	516.07	3656.46	1184.35
1.067	1.554	0.867	1.59	1.146	1.6	1.22	0.828	1.37	4.6	3.85
0.023	0.233	0.009	0.321	0.0234	0.0325	0.0464	0.198	0.0272	4.29	0.0089
28.19	22.89	15.47	21.14	4.76	15.82	16.43	8.41	6.61	49.87	23.59
0.325	1.248	0.1828	0.167	0.0733	0.144	0.299	0.1368	0.0506	4.49	0.1261
5.25	14.24	3.05	1.47	0.972	2.93	4.34	1.029	0.662	42.54	2.3
8.13	22.47	5.75	2.76	2.17	4.82	6.72	1.7	1.51	63.7	4.5
1.45	11.98	1.277	0.72	1.089	0.96	2.17	0.714	0.444	32.46	1.451
30.25	71.22	22.82	16.79	8.32	24.95	31.28	7.31	7.82	207.18	22.45
7.3	21.09	6.49	5.4	2.26	7.52	9.03	2.57	2.46	48.76	7.29
75.92	195.08	74.69	60.25	26.72	87.83	108.32	31.22	33.93	378.06	94.54
24.12	47.45	25.36	20.31	7.24	32.07	35.53	11.41	15.17	92.54	38.17
105.79	167	112.44	91.46	32.25	149.8	152.74	50.97	78.48	344.84	197.67
20.89	30.33	23.24	19.25	7.47	31.79	31.57	11.22	18.76	68.96	44.24
186.79	242.36	210.09	175.31	75.7	307.23	264.34	106.77	194.56	575.63	429.01
38.07	44	42.35	38.16	17.77	67.79	52.46	24.06	45.03	108.54	94.12
7799.72	10334.51	7902.15	10919.73	14328.31	9879.4	9665.49	8143.09	8112.02	11325.11	8969.83
0.153	1.026	0.608	0.273	0.851	0.797	1.268	0.591	0.416	1.16	1.373
21.64	18.86	16.98	18.73	10.77	29.27	20.67	9.95	4.97	22.01	15.82
71.11	83.3	44.72	65.7	44.42	105.85	72.15	34.26	14.29	165.52	52.78
35.06	140.27	33.69	56.98	210.96	120.42	101.61	77.92	34.02	204.26	78.42
0.28	0.92	0.34	0.32	0.78	0.27	0.46	0.62	0.40	0.86	0.44
78.48	10.22	91.80	21.98	27.66	55.66	33.57	12.30	42.88	2.73	169.48

									Grønne Ejland	
GRO1080_122	**GRO1080_111**	**GRO1740_145**	**GRO1600_46**	**GRO1600_50**	**GRO1740_142**	**GRO2165_21**	**GRO1060_191**	**GRO1060_194**	**463377_58**	**463377_26**
297.7	159.62	327.89	148.52	307.61	140.73	57.72	942.79	554.87	198.66	119.05
26.69	10.07	5.56	9.63	12.35	5.88	8.31	45.56	27.73		
0.506	0.261	0.67	0.189	0.46	0.12	0.403	1.73	3.09	0.927	0.083
5.83	0.88	2.89	0.445	8.49	0.85	0.664	9.95	3.78	0.433	0.312
515.3	383.17	1136.75	340.73	424.73	726.63	122.61	3104.83	2811.86	722.17	389.38
1.4	1.23	1.65	0.853	0.94	1.45	0.691	6.85	11.48	0.0276	0.0255
0.177	0.0921	0.1011	0.00175	0.594	0.0228	0.0084	0.582	0.389	0.138	0.0778
12.83	5.42	10.87	3.37	13.82	33.53	2.172	14.03	12.95	8.4	8.37
0.883	0.0444	0.206	0.0153	0.405	0.296	0.0365	1.584	0.336	0.151	0.0749
10.87	0.567	3.09	0.282	3.94	4.92	0.57	15.4	3.6	1.72	0.804
12.02	1.2	4.03	0.89	6.27	8.13	1.43	23.02	8.46	2.65	1.29
5.97	0.303	1.49	0.323	3.33	1.44	0.796	10.59	2.22	0.641	0.373
25.38	5.45	24.91	6.12	24.04	23.79	6.29	97.8	53.59	16.23	6.22
4.93	2.18	8.02	2.06	6.54	6.62	1.588	27.95	18.54	5.29	2.34
47.11	27.77	104.51	28.71	63.77	68.69	14.76	302.33	239.95	63.19	29.71
14.72	11.33	35.22	11.31	15.59	21.49	4.19	92.99	89.54	22.72	12.01
66.19	60.99	165.83	53.66	56.46	95.94	15.3	386.24	407.69	103.33	59.64
14.94	14.15	35.45	11.83	9.94	18.88	2.95	70.63	78.98	21.79	14.11
156.41	140.78	315.46	111.77	88.77	172.68	24.82	583.18	663.19	200.26	147.91
35.28	31.64	65.79	22.62	16.35	33.01	5.24	112.71	133.85	39.65	31.14
7881.25	8754.66	8783.63	9200.77	8084.54	8742.08	9255.69	11366.26	10483.45	10412.85	10905.4
0.378	0.285	0.644	0.772	0.46	0.338	0.715	3.35	4.28	0.864	1.006
17.95	4.05	17.86	3.38	20.81	27.51	19.31	17.28	17.76		
52.15	12.56	59.64	9.71	55.25	81.7	56.79	76.18	47.02	71.02	44.49
75.54	25.85	80.3	20.09	99.18	108.5	140.02	196.82	146.81	134.6	84.66
1.05	0.36	0.45	0.42	0.83	0.32	0.81	0.68	0.32	0.30	0.40
7.81	20.40	18.13	156.75	6.78	98.24	29.86	3.52	8.62	14.01	26.39

463377_21	463377_35	463377_16	463378_139	463378_127	463377_14	463378_143	463378_147	463377_24	463378_152	463377_62
51.37	114.12	136.07	116.55	314.64	170.01	224.18	166.43	142.07	134.66	188.5
			9.35	28.12		16.74	9.38		9.33	
0.151	<0.043	1.6	0.285	0.82	1.341	0.87	0.657	1.478	0.186	1.01
0.349	0.357	1.92	0.49	1.57	1.184	1.52	0.621	1.046	0.306	0.805
191.48	264.6	531.15	405.96	1190.79	897.18	521.08	536.52	444.58	522.91	500.83
0.0277	<0.0058	<0.0074	2.1	2.38	0.165	1.45	2.4	1.103	1.7	0.0412
0.0105	0.0152	2.19	0.259	4.64	0.687	0.994	0.177	0.964	0.085	1.25
7.26	6.35	12.98	17.58	28.97	28.94	17.03	23.72	42.18	15.99	12.96
0.0273	0.0559	0.847	0.123	3.67	0.901	0.856	0.0838	0.62	0.164	1.86
0.294	1.06	5.64	1.24	27.95	8.87	6.69	0.941	4.97	2.08	13.58
0.494	2.71	4.66	1.63	18.27	9.01	4.93	1.58	4.44	2.98	9.83
0.245	0.503	1.61	0.345	6.14	2.28	2.4	0.246	1.51	0.452	5.42
3.51	12.76	16.76	8.42	44.15	34.29	17.88	8.76	15.37	13.77	23.63
1.11	3.19	4.52	2.69	11.44	8.8	4.73	2.85	3.94	3.79	5.47
14.81	29.98	50.21	31.63	114.79	94.91	48.95	39.53	43.13	44.8	53.82
5.65	8.7	16.79	11.52	36.31	30.86	14.36	14.71	14.6	15.53	16.74
28.14	34.93	76.39	54.96	146.74	128.4	60.12	74.92	64.91	69.95	70.58
6.66	6.95	16.44	12.35	30.09	25.91	12.26	17.54	13.56	14.92	14.53
71.81	63.5	159.96	118.91	278.27	236.32	112.76	182.98	129.74	140.2	134.76
15.87	12.82	33.6	24.49	50.33	46.01	22.87	40.82	25.74	29.76	27.17
10288.96	11491.75	10478.24	13584.37	10222.62	11258.68	8495.31	11129.82	9100.47	8395.82	12464.45
0.976	0.718	0.812	1.52	1.23	1.049	0.741	1.152	0.919	0.708	0.714
			6.34	31.63		10.47	25.23		16.43	
31.25	61.03	58.72	26.88	177.9	142.95	46.72	102.71	165.2	70.73	52.38
94.16	294.23	88.18	42.7	218.52	176.86	105.46	67.66	76.68	114.31	104.75
0.57	0.26	0.56	0.28	0.66	0.40	0.78	0.20	0.56	0.22	1.09
103.21	52.43	2.29	23.71	1.69	8.85	4.44	46.88	13.13	32.60	2.05

463378_152	463377_62	463377_37	463378_121	463377_61	463377_63	463378_131	463377_47	463378_164	463378_109	463377_50
134.66	188.5	158.91	281.49	72.74	14.2	752.06	316.93	209.39	153.43	493.23
9.33			15.63			7.77		8.56	1.89	
0.186	1.01	0.849	0.326	0.818	0.184	0.452	0.558	0.252	0.068	1.98
0.306	0.805	0.302	0.565	0.529	0.259	5.42	3.13	0.379	0.334	3.92
522.91	500.83	671.15	960.54	370.49	108.85	307.08	880.44	586.56	668.38	1269.42
1.7	0.0412	0.198	2.82	<0.0199	<0.0056	1.31	0.763	1.51	3.17	0.673
0.085	1.25	0.0102	1.324	2.12	0.0033	1.79	5.2	0.389	0.0324	4.21
15.99	12.96	9.4	26.72	39.44	27.9	28.39	32.64	14.99	12.39	28.52
0.164	1.86	0.102	1.416	1.54	0.0557	1.44	5.77	0.264	0.0817	3.11
2.08	13.58	1.76	10.12	12.53	1	6.91	38.64	2.18	1.34	21.37
2.98	9.83	3.28	8.53	8.55	1.32	3.4	23.74	2.86	2.18	15.35
0.452	5.42	0.378	2.7	3.25	0.658	0.85	13.52	0.48	0.17	6.4
13.77	23.63	18.59	26.74	19.04	4.44	11.09	41.37	12.49	13.87	44.21
3.79	5.47	5.45	7.92	4.02	0.97	2.8	9.21	3.93	4.25	11.36
44.8	53.82	62.37	89.35	38.44	9.2	29.62	89.93	47.31	54.13	122.77
15.53	16.74	21.8	30.44	12	3.03	9.31	28.56	16.28	20.51	40.38
69.95	70.58	94.9	135.47	52.48	12.96	41.17	126.67	75.06	97.08	175.33
14.92	14.53	19.19	29.26	11.26	3.01	8.21	26.95	15.68	20.1	36.44
140.2	134.76	173.17	267.21	112.97	30.79	82.36	259.38	143.18	190.19	339.39
29.76	27.17	34.43	53.76	24.28	7.15	16.89	52.86	29.59	39.85	69.22
8395.82	12464.45	10474.17	11610.33	10612.89	9805.16	9435.54	14160.24	9792.28	9370.23	10537.71
0.708	0.714	0.668	1.017	0.509	0.553	0.639	1.062	0.649	1.221	1.08
16.43			35.52			12.76		21.01	14.58	
70.73	52.38	84.91	166.52	78.04	30.44	61.26	114.31	86.27	60	93.49
114.31	104.75	83.91	147.69	95.24	90.54	68.31	338.91	84.05	96.58	172.37
0.22	1.09	0.15	0.55	0.78	0.83	0.42	1.32	0.25	0.09	0.75
32.60	2.05	70.14	4.70	5.25	495.30	4.26	1.43	11.26	57.96	1.90

463378_120	463378_145	463378_148	463377_27	463378_142	463377_22	463378_122	463377_33	463378_158	463378_118	463378_110
308.57	262.32	129.08	114.81	221.01	99.59	119.05	238.53	101.03	81.14	116.12
7.13	93.5	4.43		28.8		12.17		7.35	5.8	9.5
0.742	2.15	0.283	1.881	1.22	0.346	0.138	0.906	0.367	0.271	<0.055
0.374	0.564	0.456	0.345	1.18	0.511	0.342	5.39	0.75	0.37	0.292
1045.41	722.75	373.52	542.45	667.17	354.69	591.45	1647.49	439.54	329.49	157.81
2.43	2.68	1.36	<0.0045	1.69	0.0294	2.26	1.57	1.6	2.08	0.673
0.0205	1.79	0.0725	0.0242	2.44	0.635	0.1221	0.372	0.17	0.119	0.0059
28.43	13.86	29.47	5.3	26.01	11.25	14.39	21.89	23.58	4.34	6.2
0.184	0.891	0.11	0.0285	3.92	0.835	0.188	0.342	0.229	0.124	0.0346
3.26	5.19	1.32	0.55	31.3	6.74	2.32	4.53	3	0.951	0.644
5.19	4.56	1.55	1.53	27.41	5.3	2.98	6.87	3.34	1.12	1.05
0.647	1.34	0.37	0.315	4.45	2.29	0.334	0.96	0.94	0.493	0.355
23.49	18.13	8.33	10.39	54.67	12.17	14.57	37.1	12.5	5.18	4.87
6.97	5.4	2.34	3.58	10.31	3.01	4.29	11.71	3.29	1.77	1.241
83.05	61.79	29.1	46.37	87.24	31.67	52.29	145.14	35.25	24.44	12.91
29.54	21.16	10.42	17.76	22.64	10.76	18.82	52.47	11.34	9.49	4.64
137.25	93.2	49.57	82.01	85.49	51.44	86.48	240.38	48.95	49.29	21.86
29.66	19.01	11.67	17.85	16.96	11.96	18.22	49.6	10.29	12.34	4.66
279.87	173.81	122.8	167.66	163.59	125.7	171.09	461.95	99.08	137.24	48.65
56.04	36.28	26.77	34.07	34.08	28.01	35.1	89.84	20.27	29.32	10.23
9652.52	11282.88	11322.75	9635.52	12702.42	9621.87	9681.01	10393.35	9193.25	13010.09	8738.72
0.919	1.55	0.802	0.697	0.953	0.672	1.126	1.43	0.368	1.76	0.406
22.14	21.78	19.15		15.63		22.96		14.2	7.56	5.85
91.56	99.08	78.27	19.92	81.9	60.13	97.04	168.47	53.43	30.95	21.52
59.92	159.61	96.11	45.38	135.92	89.96	157.89	162.63	53.73	170.58	34.06
0.18	0.45	0.31	0.24	0.35	0.87	0.15	0.18	0.44	0.63	0.48
111.41	2.64	79.43	48.57	2.02	3.72	22.86	14.77	28.76	8.60	104.44

463378_128	463377_46	463378_140	463377_51	463378_116	463378_163	463378_134	463377_49	463377_11	463377_23	463377_40
179.43	257.94	210.72	499.92	236.31	900.82	185.76	297.89	87.52	325.59	113.53
107.16		6.12		20.91	175.09	26.04				
25.04	1.035	0.836	2.42	0.654	15.02	1.31	0.537	0.083	3.42	3.87
4.6	2.58	0.57	8.61	0.651	5.11	0.78	0.962	0.35	3.69	0.548
368.56	1312.8	767.66	1289.85	1240.51	2284.18	583.54	4940.76	340.5	584.23	355.7
1.3	2.48	2.03	1.148	1.64	4.92	1.69	11.31	0.027	0.235	0.113
2.28	2.89	0.969	9.44	0.788	16.42	0.829	0.802	0.0056	6.79	1.096
13.24	25.23	15.35	65.54	18.02	91.55	12.55	25.38	22.03	34.78	12.14
1.541	2.65	0.589	9.68	1.383	12.81	0.868	1.31	0.0272	7.37	1.28
8.96	19.34	5.1	73.32	11.09	80.45	6.91	14.51	0.565	49.95	8.48
5.69	13.7	4.74	47.76	10.25	51.5	6.4	20.93	1.59	29.15	6.37
1.51	6.81	1.4	21.85	3.77	21.35	2.34	4.46	0.227	16	3.11
13.09	42.71	17.62	88.66	33.35	103.84	16.52	123.23	9.48	50.85	13.12
3.3	11.23	4.86	18.04	9.29	24.52	4.46	38.59	2.8	10.81	3.69
34.28	123.04	61.87	160.41	102.73	233.71	46.65	485.48	32.26	90.91	38.05
10.28	37.48	21.35	43.89	35.1	66.06	16.15	179.05	11.61	21.04	11.43
46.62	147.87	98.21	169.06	156.33	260.6	75.51	769.82	52.46	71.46	50.26
9.11	27.74	21.75	33.72	32.63	50.35	17.93	147.37	11.26	12.58	10.84
89.8	241.5	209.32	302.89	293.87	431.08	202.99	1248.34	110.57	99.88	106.34
18.31	43.81	43.52	56.75	59.98	80.98	49.69	229.95	22.58	15.05	19.86
8709.09	10594.08	13233.18	11415.22	8124.4	8102.33	12900.97	10458.79	11622.37	11685.91	11210.9
0.636	1.66	1.089	1.32	0.723	1.22	0.774	4.23	0.92	0.93	0.926
6.6		15.71		22.27	26.02	14.91				
49.79	108.22	58.09	109.33	105.47	312.96	69.65	182.27	69.69	52.09	45.54
82.48	203.88	71.81	168.11	105.84	185.24	133.08	236.56	73.93	234.43	155.17
0.53	0.86	0.47	1.03	0.62	0.89	0.70	0.27	0.18	1.27	1.04
1.70	2.19	4.89	1.65	4.15	1.52	3.56	5.96	429.62	1.18	2.47

463378_169	463377_15	463378_165	463378_123	463378_108	463378_124	463377_45	463378_144	463377_25	463378_157	463378_129
313.9	498.27	86.31	342.1	215.26	281.53	478.68	225.74	189.29	167.37	220.01
6.17		6.99	35.33	28.19	8.34		12.96		13.28	9.51
0.307	6.74	0.353	3.46	0.8	1.02	0.708	1.36	2.85	0.534	1.14
0.521	3.36	0.636	1.1	0.661	0.68	3.71	1.21	0.521	0.483	0.538
895.62	1142.18	335.24	1371.41	756.28	1178.78	509.47	751.95	1400.11	458.67	894.92
2.28	1.81	1.27	2.01	1.97	1.94	0.0254	2.05	0.244	1.49	2.17
0.798	14.45	0.0664	2.88	1.204	0.712	6.83	0.28	0.279	0.281	0.745
10.61	94.8	6.46	24.46	14.93	12.59	40.6	37.41	12.58	15.97	13.71
0.837	13.98	0.0562	2.77	0.842	0.886	5.59	0.244	0.429	0.307	0.536
8.19	95.23	0.668	19.81	6.37	7.6	36.97	2.56	4.26	2.36	4.62
6.87	52.7	1.16	14.67	4.95	7.73	18.65	3.34	4.81	2.46	4.12
0.756	26.93	0.281	7.21	1.82	1.78	11.03	0.97	2.32	0.771	1.33
17.79	85.67	7.02	41.21	16.58	25.67	33.07	14.3	28.02	9.59	18.95
5	17.9	2.06	11.2	4.95	8.05	6.82	4.02	9.05	2.99	5.67
65.99	154.49	27.72	123.04	59.57	97.13	61.64	53.21	115.82	36.26	70.43
26.57	40.11	10.24	40.24	21.58	34.63	17.31	21.25	44.43	13.23	27.43
136.4	151.79	51.58	175.1	105.99	162.18	67.47	106.68	206.78	61.17	133.13
31.31	30.5	11.2	37.09	23.46	36.02	13.16	24.69	45.16	13.53	29.63
320.85	274.24	113.66	339.74	220.42	345.31	117.43	252.51	438.34	131.86	294.75
70.13	50.91	25.66	69.28	48.02	71.56	22.58	58.35	90.91	27.69	65.46
10648.34	10028.2	10034.23	9606.55	9819.13	10384.31	8774.48	8345.18	9549.78	10655.26	9169.58
1.024	1.369	0.609	0.868	1.019	1.145	0.462	0.753	0.706	0.653	1.028
8.56		7.18	29.63	17.09	19.98		36.73		12.15	28
32.39	117.7	24.58	128.47	69.09	77.84	58.79	140.12	68.3	53.51	114
72.63	163.25	34.51	198.38	107.98	136.57	92.09	100.24	108.34	77.92	159
0.21	1.23	0.30	0.90	0.61	0.39	1.36	0.43	0.61	0.49	0.46
3.12	1.61	25.45	2.08	3.57	3.82	1.58	34.45	8.75	13.09	5.22

463378_129	463377_56	463378_133	463378_155	463377_57	463378_146	463378_160	463377_28	463377_52	463377_39	463378_130
220.01	196.24	199.86	161.31	339.16	206.89	126.41	160.84	340.7	210.38	429.29
9.51		9.26	13.93		13.94	7.6				35.12
1.14	5.79	0.805	1.06	1.569	0.273	0.384	1.013	4.37	0.454	2.03
0.538	9.9	0.325	0.313	0.914	0.444	0.421	1.392	5.26	0.491	3.06
894.92	911.86	693.56	452.38	995.26	696.59	624.99	663.13	2129.12	832.06	1191.22
2.17	0.181	1.96	1.59	0.276	2.93	1.13	<0.0066	1.32	<0.0036	2.36
0.745	3.88	0.0473	0.0527	1.3	0.213	0.0482	0.287	5.21	0.903	18.67
13.71	34.61	26.64	9.99	16.12	33.66	4.14	34.79	104.66	20.98	66.22
0.536	3.26	0.095	0.0671	0.542	0.324	0.0877	0.226	9.95	0.94	9.66
4.62	22.34	1.377	0.866	3.79	2.78	0.966	2.98	71.96	8.22	59.17
4.12	14.72	2.58	1.41	3.54	3.98	2.06	4.5	65.06	7.17	31.39
1.33	5.14	0.658	0.38	0.68	0.779	0.45	1.48	17.95	3.13	6.49
18.95	35.88	14.14	7.14	19.13	17.26	10.23	20.91	111.63	28.31	60.49
5.67	8.63	4.32	2.56	6.17	5.09	3.65	5.84	24.6	7.36	13.86
70.43	90.77	56.24	33.01	81.69	58.03	48.38	64.42	239.61	80.76	128.83
27.43	29.87	21.1	12.85	32.56	19.29	19.27	22.25	72.78	26.34	37.89
133.13	129.22	98.75	64.88	158.83	87.82	93.61	95.46	305.55	111.15	146.02
29.63	26.55	21.7	14.9	34.6	20.02	21.43	19.26	61.39	21.46	28.2
294.75	242.19	206	156.49	335.92	188.33	217.92	171.14	549.65	189.83	242.16
65.46	45.28	43.66	34.43	68.49	36.63	46.88	34.73	106.97	37.18	44.46
9169.58	8368.72	9183.79	9215.61	9170.37	11529.51	10415.78	9116.16	8603.14	10038.21	9740.32
1.028	0.783	0.856	0.854	0.886	0.943	0.656	0.641	1.03	0.55	1.004
28		13.58	15.99		57.4	7.47				21.46
114	113.96	52.38	60.08	81.53	223.93	16.05	121.81	321.1	86.4	157.9
159	83.33	41.15	103.53	135.1	153.65	35.8	76.34	230.12	91.25	137.84
0.46	0.68	0.33	0.37	0.25	0.29	0.30	0.47	0.64	0.67	0.46
5.22	2.34	95.65	40.43	4.62	30.84	15.33	32.88	3.50	5.48	1.19

						Itsaku				
463377_32	**463377_10**	**463377_36**	**463378_156**	**463377_60**	**463378_159**	**463398_24**	**463398_07**	**463398_26**	**463398_21**	**463398_12**
148.61	157.12	212.94	123.38	220.32	223.04	99.95	298.94	365.17	141.96	239.47
			7.35		12.45	8.96	16.39	3.93	4.93	12.93
0.355	1.598	0.976	0.231	0.418	0.331	0.288	0.542	<0.049	0.457	0.424
0.366	0.633	0.673	0.405	0.754	0.612	0.246	1.274	0.256	0.39	0.265
644.11	1168.3	1379.96	361.61	668.28	903.29	222.73	695.5	609.87	590.56	486.15
<0.0034	0.086	0.496	1.47	2.18	1.56	0.99	2.71	2.31	2.6	1.68
0.0353	0.898	0.088	0.2	2.85	1.315	0.0823	0.232	0.0066	0.0063	0.0146
18.32	18.71	9.37	6.59	18.88	16.52	38.07	15.36	22.59	38.46	23.18
0.159	1.5	0.155	0.222	2.94	1.47	0.163	0.392	0.0832	0.1356	0.0838
2.32	11.28	3.11	1.65	20.56	11.02	2.23	3.68	1.618	2.55	1.525
3.65	14.66	5.54	1.76	11.64	8.26	2.81	4.84	4.2	5.13	2.82
1.33	6.47	0.472	0.491	6.75	3.84	0.918	1.66	0.67	0.973	0.469
17.19	55.39	31.36	6.24	25.16	22.94	8.39	19.8	20.35	19.45	13.33
4.78	13.15	10.11	2.08	6	6.44	1.81	5.99	6.37	5.09	3.97
55.65	133.68	125.73	27.04	65.56	77.36	19.4	67.34	66.08	54.32	45.43
19.97	39.89	44.78	10.6	23	27.32	5.95	23.17	19.94	18.12	15.83
93.99	159.62	199.99	53.25	103.23	136.55	29	97.09	82.03	82.91	71.87
20.7	30.79	40.5	12.81	21.91	30.85	5.96	19.25	15.69	18.27	15.19
199.41	271.83	365.88	135.29	206.15	314.44	60.99	168.31	136.93	185.64	144.11
42.15	50.64	69.83	29.19	42.8	67.48	13.67	33.13	26.54	39.07	29.72
8488.52	10916.11	10525.37	10683.03	12034.44	10860.84	9554.37	9083.62	10836.36	9520.01	9428.34
0.528	0.961	1.46	1.054	2.31	0.781	0.681	1.135	1.191	1.343	0.912
			14.45		31.77	19.75	14.09	31.29	31.86	15.18
83.91	71.37	61.26	44.97	46.23	110.75	67.75	58.81	114.31	112.46	52.16
111.9	93.71	78.39	115.89	183.39	157.02	88.31	104.07	149.48	81.99	54.13
0.51	0.69	0.11	0.45	1.21	0.85	0.58	0.52	0.22	0.30	0.23
58.86	3.88	19.31	7.53	1.57	2.86	79.11	12.26	232.02	316.71	159.50

			Upernivik							
463398_08	**463398_11**	**463398_16**	**481914_83**	**481912_35**	**481912_48**	**481912_49**	**481909_103**	**481903_109**	**481913_63**	**481914_84**
443.46	148.21	205.73	240.28	177.02	307.31	89.59	154.37	120.8	696.52	261.29
23.24	7.26	13.71	18.53	7.04	2.4	5.4	7.79	7.49	14.13	3.38
0.95	0.085	0.62	0.287	<0.071	<0.054	0.072	0.449	0.62	0.516	0.482
6.36	0.245	0.319	0.524	0.72	0.316	0.277	0.44	0.338	0.939	0.38
668.69	207.75	616.85	424.62	361.99	733.24	118.38	413.92	354.26	1393.83	655.83
1.81	0.825	1.29	1.33	2.34	2.06	0.585	2.11	1.65	4.76	1.97
1.307	0.0173	0.132	0.0333	0.142	0.0138	0.0282	0.0894	0.0426	0.1138	0.0142
32	23.82	28.59	9.69	33.31	15.65	0.726	22.75	35.45	10	6.84
1.419	0.0596	0.52	0.0811	0.095	0.0672	0.0055	0.247	0.186	0.263	0.0632
11.63	0.756	6	1.097	1.054	1.158	0.105	2.72	1.046	2.66	0.906
11.27	1.23	8.15	1.7	2.19	3.35	0.201	2.95	1.44	4.16	2.19
6.67	0.476	2.68	0.892	0.336	0.7	0.075	0.994	0.379	1.59	0.595
29.68	6.32	23.95	8.57	9.02	18.08	1.51	10.01	7.75	20.8	14.26
7.93	1.721	6.51	2.79	2.68	5.87	0.608	3.13	2.53	8.35	4.51
78.4	19.38	70.72	34.1	34.71	68.37	8.62	33.52	28.43	114.57	56.92
20.82	7.19	22.35	13.16	11.88	24.17	3.62	11.73	10.17	42.37	21.22
82.55	31.71	92.67	62.85	56	111.81	19.27	57.18	44.86	212.44	99.93
16.14	6.5	19.4	14.44	12.16	24.45	4.6	13	9.62	49.03	21.94
149.86	62.78	171.45	140.06	121.71	227.79	49.04	126.79	90.2	468	209
29.09	13.05	34.41	29.28	24.88	48.71	11.55	28.53	19.59	92.7	42.74
8758.11	8308.5	9218.16	10258.52	12648.62	11159.33	8194.77	17091.15	9371.35	11520.33	10200.53
0.807	0.746	0.755	1.354	1.63	1.684	0.737	1.562	0.658	2.84	1.205
26.42	9.67	40.95	2.66	40.62	38.11	10.98	39.13	23.35	30.95	21.06
105.89	31.72	125.23	3.62	143.58	144.24	34.84	170.27	97.33	118.33	86.92
128.04	30.88	107.2	5.77	97.69	318.61	113.02	124.3	48.69	245.57	215.86
1.12	0.52	0.59	0.71	0.23	0.28	0.42	0.56	0.35	0.52	0.33
5.66	178.54	26.26	44.88	69.03	123.69	14.03	36.85	95.85	13.91	54.95

481912_27	481912_47	481912_46	481903_105	481909_107	481909_106	481909_96	481913_61	481914_80	481913_67	481909_105
119.96	339.28	105.25	273.13	223.93	134.91	159.24	312.24	235.05	363.34	480.14
5.28	54.41	5.54	9.26	6.92	16.09	10.73	2.45	15.45	13.99	91.83
0.88	1.17	0.164	1.14	0.453	0.63	0.262	0.6	0.251	0.461	1.66
0.43	0.534	0.351	0.75	5.38	0.387	0.328	0.399	0.474	1.148	7.31
328.56	817.94	328.72	1290.03	800.02	336.62	577.99	896.92	556.73	1026.73	1285.36
0.781	2.71	0.98	1.91	1.8	1.121	1.22	2.09	1.113	2.04	3.04
0.155	0.38	0.0608	0.406	1.481	0.0224	0.0204	0.0692	0.0214	0.306	4.11
8.28	47.19	5.35	9.02	9.51	11.49	6.61	50.37	9.32	11.34	33.32
0.0948	0.803	0.109	0.694	0.701	0.0441	0.119	0.173	0.1096	0.67	7.11
1.245	7.58	1.037	7.23	4.52	0.743	1.373	2.54	1.541	6.03	64.45
1.9	8.51	1.36	8.34	4.1	1.27	2.21	5.02	3.44	7.5	53.88
0.49	3.36	0.398	2.59	1.76	0.248	0.696	0.94	0.893	3.87	28.15
9.77	25.89	6.69	32.18	15.69	6.35	10.95	22.74	14.85	28.71	109.72
2.52	7.35	2.25	9.35	5.04	2.02	3.63	6.84	4.45	8.57	22.62
30.49	84.71	26.41	113.44	64.34	25.73	44.02	82.76	52.75	96.77	171.69
10.6	27.48	9.53	39.06	23.72	9.76	16.82	29.95	18.6	32.61	39.64
46.54	120.03	49.81	172.41	117.3	45.75	82.94	139.76	82.27	149.58	129.76
10.04	24.74	11.15	34.14	25.9	9.69	18.19	29.96	16.86	32.91	21.59
101.17	224.86	111.91	319.26	253.41	94.85	181.99	282.14	154.9	309.39	178.66
22.08	48.21	23.1	59.91	55.94	20.01	39.55	58.61	31.3	66.64	32.38
9768.52	9697.4	9694.92	8812.49	9471.39	9909.52	8202.24	9374.15	8938.58	9073.84	11317.75
0.863	1.67	0.782	1.11	0.905	0.588	0.69	1.251	0.624	0.974	0.858
8.78	84.58	7.81	25.66	13.61	11.46	6.94	33.1	8.66	13.83	12.13
27.25	242.25	28.14	80.27	67.7	45.26	24.15	109.41	30.84	71.98	67.93
43.01	160.41	63.05	89.32	119.71	41.01	45.07	88.51	44.74	127.31	123.6
0.35	0.69	0.40	0.48	0.67	0.27	0.43	0.27	0.38	0.81	1.12
16.44	20.56	15.82	4.09	2.25	87.99	32.29	110.80	46.32	6.03	1.48

481912_27	481912_47	481912_46	481903_105	481909_107	481909_106
119.96	339.28	105.25	273.13	223.93	134.91
5.28	54.41	5.54	9.26	6.92	16.09
0.88	1.17	0.164	1.14	0.453	0.63
0.43	0.534	0.351	0.75	5.38	0.387
328.56	817.94	328.72	1290.03	800.02	336.62
0.781	2.71	0.98	1.91	1.8	1.121
0.155	0.38	0.0608	0.406	1.481	0.0224
8.28	47.19	5.35	9.02	9.51	11.49
0.0948	0.803	0.109	0.694	0.701	0.0441
1.245	7.58	1.037	7.23	4.52	0.743
1.9	8.51	1.36	8.34	4.1	1.27
0.49	3.36	0.398	2.59	1.76	0.248
9.77	25.89	6.69	32.18	15.69	6.35
2.52	7.35	2.25	9.35	5.04	2.02
30.49	84.71	26.41	113.44	64.34	25.73
10.6	27.48	9.53	39.06	23.72	9.76
46.54	120.03	49.81	172.41	117.3	45.75
10.04	24.74	11.15	34.14	25.9	9.69
101.17	224.86	111.91	319.26	253.41	94.85
22.08	48.21	23.1	59.91	55.94	20.01
9768.52	9697.4	9694.92	8812.49	9471.39	9909.52
0.863	1.67	0.782	1.11	0.905	0.588
8.78	84.58	7.81	25.66	13.61	11.46
27.25	242.25	28.14	80.27	67.7	45.26
43.01	160.41	63.05	89.32	119.71	41.01
0.35	0.69	0.40	0.48	0.67	0.27
16.44	20.56	15.82	4.09	2.25	87.99

Table 7: LPrøven Igneous Complex zircon. LA-ICP-MS analysis results (in ppm).

Sample locality	**Itsaku**									
Sample	**463392_79**	**463392_75**	**463391_34**	**463392_32**	**463392_9**	**463391_23**	**463391_14**	**463392_59**	**463392_51**	**463391_48**
P	4626	5124	2373	1908	3046	778	511	1349	900	600
Ti	431.06	41.38	387	227.9	379.06	50	12	171.46	111.92	49
V	31.22	0.327	3.75	5.99	8.44	0.284	0.76	3.87	1.83	1.71
Sr	4.16	9.15	10.65	2.51	2.39	3.5	0.888	1.294	0.918	1.198
Y	4869.34	702.11	3127.58	1715.38	2038.19	587.83	815.5	886.31	989.64	867.58
Nb	11.31	2.11	12.2	4.46	6.1	2.61	1.6	3.55	3	2.62
La	61.05	245.26	23.54	16.56	22.07	38.63	11.59	9.28	5.27	1.564
Ce	201.81	617.75	125.8	69.4	96.08	103.42	33.98	48.28	27.58	13.02
Pr	35.69	79.57	29.33	11.98	16.53	10.63	3.69	8.1	4.44	2.64
Nd	249.12	305.19	202	80.61	107.89	45.68	19.37	54.83	30.97	17.42
Sm	167.07	50.67	132.56	49.74	59.87	12.4	9.83	29.9	19.7	12.92
Eu	77.44	2.03	73.94	19.29	22.48	0.892	0.658	10.72	6.24	5.94
Gd	328	55.36	201.61	97.64	117.09	25.5	31.05	49.86	44.84	28.82
Tb	70.76	9.3	42.74	21.94	26.93	6.26	8.17	11.14	11.26	8.35
Dy	627.84	82.91	354.95	198.02	255.86	64.33	88.73	101.42	108.53	97.1
Ho	156.31	25.2	91.33	52.75	66.79	20.09	27.78	27.38	32.83	30.74
Er	562.32	99.79	311.69	194.02	242.4	84.7	111.95	104.24	129.09	134.52
Tm	101.46	19.16	57.15	34.76	43.78	16.52	21.68	20.05	24.38	26.92
Yb	860.69	167.7	458.14	283.73	351.14	139.34	183.42	177.66	204.79	246.61
Lu	144.39	32.83	74.38	48.75	57.43	26.47	34.55	31.4	37.76	45.32
Hf	9557	9683	10307	10500	10052	8959	8473	11134	10157	7968
Ta	2.270	1.150	1.600	1.378	1.383	1.242	1.020	1.461	1.286	1.143
Pb	47.01	16.61	25.16	19.91	26.84	12.3	18.79	31.04	26.54	14.93
Th	400.13	75.52	157.89	118.04	141.91	64.87	99.74	141.91	123.36	72.33
U	766.93	49.74	326.09	315.73	285.79	66.45	135.56	324.77	231.32	171.74
Eu/Eu*	1.01	0.12	1.38	0.85	0.82	0.15	0.12	0.85	0.64	0.94
Ce/Ce*	1.04	1.06	1.15	1.19	1.21	1.23	1.25	1.34	1.37	1.54

Ca = ^{43}Ca + ^{44}Ca

Eu/Eu* = $Eu_N/(0.5(Sm_N \times Gd_N))$. Ce/Ce* =$Ce_N/(0.5(La_N \times Ce_N))$.

463391_14	463392_59	463392_51	463391_48	463391_44	463391_51	463392_57	463391_22	463391_64	463391_37	463391_25
511	1349	900	600	754	1035	676	1203	1036	1026	1116
12	171.46	111.92	49	196	340	73.02	359	323	326	302
0.76	3.87	1.83	1.71	3.18	4.92	2.31	5.56	5.01	3.28	5.02
0.888	1.294	0.918	1.198	4.27	7.71	0.811	9.5	8.11	6.46	5.91
815.5	886.31	989.64	867.58	986.5	1920.49	1354.73	1566.59	2368.16	1617.4	1338.81
1.6	3.55	3	2.62	6.61	10.75	2.83	10.91	11.26	10.11	8.97
11.59	9.28	5.27	1.564	3.56	5.83	4.99	7.97	6.3	5.92	6
33.98	48.28	27.58	13.02	36.95	60.76	29.79	84.02	72.35	71.03	69.01
3.69	8.1	4.44	2.64	9.03	14.64	3.99	16.92	15.38	15.42	13.96
19.37	54.83	30.97	17.42	65.32	118.75	31.6	125.82	123.56	121.85	101.81
9.83	29.9	19.7	12.92	31.78	70.88	23.87	71.61	74.25	83.67	50.54
0.658	10.72	6.24	5.94	12.53	43.34	4.99	37.33	38.07	35.98	25.11
31.05	49.86	44.84	28.82	58.81	117.69	62.68	102.03	134.14	109.02	88.16
8.17	11.14	11.26	8.35	11.51	22.54	15.59	19.8	28.12	21.35	16.42
88.73	101.42	108.53	97.1	108.53	196.65	152.08	162.36	254.98	184.65	153.15
27.78	27.38	32.83	30.74	29.12	52.04	45.58	41.13	70.12	47.32	40.51
111.95	104.24	129.09	134.52	106.65	188.71	181.25	151.31	262.27	176.24	151.46
21.68	20.05	24.38	26.92	18.84	35.54	34.08	27.77	47.68	32.82	28.54
183.42	177.66	204.79	246.61	146.99	291.55	284.36	233.96	391.97	280.39	235.35
34.55	31.4	37.76	45.32	25.28	53.32	51.14	39.31	70.02	44.47	41.3
8473	11134	10157	7968	10578	9447	10366	10617	8580	9465	9648
1.020	1.461	1.286	1.143	1.279	1.113	1.197	1.723	1.800	1.820	1.830
18.79	31.04	26.54	14.93	41.02	18.33	29.18	43.42	33.72	35.42	48.28
99.74	141.91	123.36	72.33	256.62	135.47	170.67	292.17	246.69	193.09	207.07
135.56	324.77	231.32	171.74	298.11	241.72	196.19	217.53	285.92	327.32	303.41
0.12	0.85	0.64	0.94	0.89	1.45	0.39	1.34	1.17	1.15	1.15
1.25	1.34	1.37	1.54	1.57	1.58	1.61	1.74	1.77	1.79	1.81

463391_64	463391_37	463391_25	463392_71	463392_82	463390_52	463392_70	463392_15	463391_27	463391_46	463392_31
1036	1026	1116	376	550	288	316	489	243	376	482
323	326	302	29.99	71.69	19	8.3	47.41	437	103	68.86
5.01	3.28	5.02	0.673	1.41	-	0.209	1.5	1.65	2.49	2
8.11	6.46	5.91	0.591	0.583	0.464	0.416	0.729	2.09	2.84	0.638
2368.16	1617.4	1338.81	686.54	719.93	877.53	628.31	762.77	517.73	769.28	718.1
11.26	10.11	8.97	2.02	3.29	4.86	2.13	2.1	3.37	2.75	2.34
6.3	5.92	6	4.32	4.28	5.05	2.65	4.3	1.035	2.19	2.67
72.35	71.03	69.01	20.6	27.56	24	12.32	25.62	6.65	24.01	22.2
15.38	15.42	13.96	1.695	3.04	1.879	0.907	2.41	0.642	3.41	2.38
123.56	121.85	101.81	9.28	20.64	12.25	4.7	15.06	5.97	26.25	16.44
74.25	83.67	50.54	6.85	13.79	10.1	3.33	10.53	5.74	17.18	10.6
38.07	35.98	25.11	0.661	4.58	0.503	0.27	2.06	0.747	8.77	3.01
134.14	109.02	88.16	24.3	30.11	33.59	14.29	28.95	19.35	32.71	25.95
28.12	21.35	16.42	6.48	7.72	8.76	4.69	7.78	5.25	7.55	6.86
254.98	184.65	153.15	71.37	77.59	91.98	59.99	80.21	55.95	77.95	73.11
70.12	47.32	40.51	23.71	23.95	30.6	21.14	24.86	17.7	23.58	22.55
262.27	176.24	151.46	101.55	100.21	131.25	94.78	102.7	74.64	98.14	96.1
47.68	32.82	28.54	21.05	19.65	25.38	19.91	19.58	15.23	19.2	18.86
391.97	280.39	235.35	186.83	171.28	218.11	182.5	167.68	131.88	167.09	164.53
70.02	44.47	41.3	33.26	31.14	42.06	37.06	30.74	25.18	29.54	31.83
8580	9465	9648	10607	11282	8738	9786	9114	7667	8745	9630
1.800	1.820	1.830	1.112	1.521	2.19	1.490	1.072	1.148	1.054	1.205
33.72	35.42	48.28	23.28	33.82	12.78	20.41	22.98	12.82	27.78	23.71
246.69	193.09	207.07	102.93	187.77	68.27	109.9	119.68	70.36	104.03	116.59
285.92	327.32	303.41	189.02	238.12	96.75	184.75	167.75	114.26	214.9	241.13
1.17	1.15	1.15	0.16	0.69	0.08	0.12	0.36	0.22	1.13	0.55
1.77	1.79	1.81	1.83	1.84	1.88	1.91	1.92	1.96	2.11	2.12

463390_72	463391_61	463391_38	463392_72	463391_45	463391_57	463392_21	463392_40	463392_25	463392_19	463391_49
348	392	331	330	385	464	476	202	405	296	246
47	55	79	27.96	49	160	41.21	27.55	31.98	37.34	48
0.604	4.07	1.091	0.72	1.18	2.39	2	0.82	0.96	14.75	1.49
1.072	1.89	1.65	0.63	1.269	1.15	0.524	0.889	0.546	0.852	4.4
896.16	797.06	606	591.54	662.9	804.54	856.03	354.27	716.28	555.77	615.79
1.83	2.72	3.71	1.91	2.78	2.75	1.862	2.5	1.76	2.02	1.94
2.3	1.401	1.9	3.42	1.303	0.541	1.725	2.51	1.279	1.554	1.533
15.07	13.8	25.52	20.67	19.84	8.34	18.95	17.89	14.68	15.68	16.01
1.233	1.628	3.94	1.415	2.9	1.039	1.636	0.874	1.154	1.079	1.045
10.68	13.24	29.61	7.42	23.95	9.48	12.26	4.57	10.1	8.94	9.69
10.48	9.49	17.55	4.76	15.79	9.92	9.96	2.79	8.78	5.12	8.6
0.58	4.02	10.19	0.56	5.89	1.87	2.65	0.626	1.93	2.32	2.03
36.65	25.99	30.23	15.1	34.18	32.24	30.01	9.84	27.29	16.81	26.71
9.76	7.17	6.51	4.64	7.38	8.22	8.53	2.65	7.76	4.76	6.98
102.58	79.96	61.26	56.77	72.51	79.9	91.67	33.43	81.37	52.6	70.93
33.35	25.81	17.7	19.12	21.83	25.48	28.98	11.18	24.71	17.59	20.55
136.99	115.59	70.15	90.24	88.88	108.35	123.32	53.6	98.13	74.33	85.95
26.37	25.58	14.07	18.56	17.59	21.63	23.96	11.77	18.76	15.74	17.22
225.1	223.1	122.25	168.54	156.81	202.43	206.64	112.82	167.19	138.4	141.98
42.77	38.85	22.18	31.27	30.7	37.42	37.79	20.74	32.1	24.35	27.5
8245	9343	9007	10392	8724	8651	9575	10615	10172	8759	8259
1.011	1.196	1.296	1.267	1.022	1.390	1.086	1.259	0.850	1.184	1.189
18.66	18.5	20.92	120.03	34.27	18.1	27.09	23.11	28.82	197.67	16.18
101.08	97.08	100.51	129.91	208.89	99.48	138.59	127.16	158.74	90.1	88.98
66.06	192.72	230.6	270.18	179.17	153.11	235.8	316.2	141.42	206.64	103.62
0.09	0.78	1.35	0.20	0.78	0.32	0.47	0.37	0.38	0.76	0.41
2.15	2.20	2.24	2.26	2.46	2.68	2.72	2.91	2.91	2.91	3.04

463390_47	463392_10	463392_11	463390_50	463391_52	463391_40	463392_14	463390_49	463390_12	463390_13	463391_35
357	316	216	211	295	175	331	227	291	272	258
40	30.17	65.95	26	47	19	41.54	49	38	28	547
0.9	1.46	7.82	0.961	0.548	1.19	0.775	0.586	1.14	0.459	3.09
1.035	0.676	3.32	0.688	4.5	0.605	0.382	0.781	0.632	0.594	0.804
1074.53	658.99	453.66	426.94	628.51	502.45	533.34	503.72	947.43	744.87	715.07
2.21	1.71	1.87	2.16	2.85	2.3	2.09	2.96	1.86	2.04	3.01
1.206	0.405	1.216	2.43	1.243	1.148	1.254	0.887	0.583	0.519	0.775
22.14	6.36	11.64	17.98	19.27	13.76	17.43	16.53	13.39	12.6	10.53
2.42	0.586	0.647	0.742	1.604	0.882	1.288	1.608	1.287	1.276	0.587
21.17	6.22	4.39	4.54	13.55	6.25	8.91	14.31	13.57	11.26	6.51
17.15	6.94	3.71	3.51	8.61	5.49	6.43	12.59	13	9.63	7.44
3.87	0.477	0.515	0.274	4.64	1.199	1.616	4.43	2.5	2.52	0.963
50.3	25.16	12.94	14.01	21.92	13.55	17.44	23.7	39.98	29.01	27.6
11.72	6.54	3.68	3.87	5.85	3.95	5.09	6.43	10.3	7.93	7.27
124.1	72.1	43.69	44.13	62.93	46.16	56.7	61.75	105.23	82.6	80.43
37.54	23.14	14.83	14.3	20.34	16.62	18.51	19.06	33.07	26.44	25.62
149.08	94.49	63.3	63.17	86.3	77.29	78.84	76.26	134.68	108.17	103.2
28.53	18.29	12.85	12.91	16.95	16.87	15.7	15.78	25.27	21.75	20.65
237.63	163.89	114.93	113.07	153.24	159.8	136.77	151.04	216.44	183.43	173.94
45.1	29.88	21.89	21.91	28.72	29.78	25.86	26.66	40.36	34	32.66
8287	8571	8435	7851	8411	9521	9942	9044	8964	9124	8994
1.099	1.070	1.107	1.304	1.205	1.194	1.145	1.37	0.763	1.36	1.114
27.8	17.16	17.47	18.57	15.77	17.09	19.02	23.71	13.25	21.1	18
136.74	79.6	86.35	97.06	91.28	91.82	99.07	119.9	69.5	111.27	76.22
144.04	110.74	166.92	124.97	114.31	169.73	190.07	206.64	84.74	181.19	92.66
0.40	0.11	0.23	0.12	1.03	0.43	0.47	0.78	0.34	0.46	0.21
3.12	3.14	3.16	3.22	3.28	3.29	3.30	3.33	3.72	3.73	3.76

463390_13	463391_35	463392_46	463390_35	463392_36	463391_28	463390_34	463388_86	463392_52	463390_63	463390_40
272	258	279	245	333	276	318	270	261	142	197
28	547	26.26	22	56.82	68	41	96.13	36.15	30	96
0.459	3.09	0.55	0.857	0.416	0.981	0.261	14.81	0.88	1.08	2.44
0.594	0.804	0.583	0.411	0.48	1.153	0.335	36.17	0.748	0.547	0.939
744.87	715.07	349.2	1101.95	417.16	450.99	554.72	827.06	431.13	372.21	353.08
2.04	3.01	3.22	1.54	1.96	4.23	3.24	4.5	2.59	2.67	2.33
0.519	0.775	1.18	0.886	1.371	0.903	0.396	1.416	1.298	1.02	0.615
12.6	10.53	15.21	18.43	17.75	14.92	7.68	27.76	15.19	21.33	8.23
1.276	0.587	0.792	1.473	0.869	0.849	0.5	1.82	0.577	1.411	0.321
11.26	6.51	5.33	16.78	6.38	7.23	5.17	12.53	3.7	11.24	2.49
9.63	7.44	5.38	16.91	4.69	5.64	6.92	9.12	2.99	8.34	2.8
2.52	0.963	0.99	1.5	1.164	1.46	0.454	14.19	0.558	1.37	0.348
29.01	27.6	11.13	50.17	13.97	15.26	24.03	24.38	10.5	14.77	10.12
7.93	7.27	3.09	12.62	3.97	3.87	6.21	6.5	3.38	3.63	2.97
82.6	80.43	32.28	129.84	42.69	42.96	64.29	79.4	40.64	37.72	34.96
26.44	25.62	10.72	39.28	13.8	14.76	19.69	26.13	14.38	12.09	11.96
108.17	103.2	51.96	157.29	57.82	67.98	73.66	115.84	67.36	53.22	53.26
21.75	20.65	11.44	30.48	11.62	13.92	14.9	23.24	14.91	11.18	10.71
183.43	173.94	109.08	243.99	104.91	126.28	130.03	212.62	131.62	103.46	96.74
34	32.66	22.15	45.34	20.01	25.58	23.93	38.47	24.54	18.85	18.31
9124	8994	9838	8578	9186	9710	8746	12169	10967	9437	6890
1.36	1.114	1.800	1.043	1.169	2.010	1.177	2.630	1.750	1.5	0.965
21.1	18	19.77	26.98	17.75	14.47	37.17	22.36	29.38	15.14	11.45
111.27	76.22	110.76	155.16	88.69	66.44	194.94	283.57	136.47	99.51	55.55
181.19	92.66	186.45	136.8	143.69	179.26	184.89	798.54	388.76	184.46	97.72
0.46	0.21	0.39	0.16	0.44	0.48	0.11	2.91	0.30	0.38	0.20
3.73	3.76	3.79	3.88	3.91	4.10	4.15	4.16	4.22	4.28	4.46

463391_63	463392_50	463392_49	463392_84	463388_95	463392_48	463392_58	463390_32	463392_74	463392_76	463391_11
254	320	172	285	177	388	488	231	190	217	190
35	31.93	39.86	32.98	19.03	31.42	22.44	32	19.84	19.38	67
0.838	0.417	0.254	0.515	0.511	1.03	1.03	0.56	0.12	0.265	2.09
0.645	0.557	1.91	0.474	0.536	0.603	0.419	0.71	0.301	0.469	1.604
630.98	651.78	397.81	760.28	555.25	598.68	1399.44	435.26	353.03	455.04	530.16
2.16	1.75	2.32	2.48	1.91	2.72	2.11	2.56	2.19	2.01	1.89
0.627	0.402	1.657	0.468	0.647	2.88	0.271	0.948	1.161	0.723	0.416
16.58	7.64	17.59	11.34	11.42	42.09	10.9	20.14	17.58	11.76	11.68
1.244	0.411	0.498	0.727	0.48	1.439	0.993	0.875	0.507	0.356	0.558
9.83	5.07	3.6	8.8	4.03	9.67	13.4	6.94	3.36	2.97	5.53
6.53	4.95	3.48	9.44	4.54	6.33	15.98	6.49	3.14	3.13	5.25
1.67	0.456	0.343	0.884	0.373	2.08	0.633	1.58	0.242	0.269	1.038
20.74	20.93	12.98	31.27	15.45	20.62	58.6	16.61	9.81	12.21	17.53
5.84	6.19	3.49	7.62	4.21	5.47	14.66	4.55	3	3.82	4.8
65.99	70.97	40.83	80.76	51.6	60.98	152.69	50.24	33.29	43.5	54.02
22.03	22.52	13.49	26	17.5	19.59	47.64	16.31	11.51	15.43	17.53
94.87	97.61	58.09	106.72	78.69	86.07	190.51	72.74	49.54	68.13	76.13
19.35	19.23	11.46	21.34	15.97	17.35	36.33	15.32	10.67	13.73	15.04
167.96	180.6	104.6	188.54	140.76	158.67	305.46	144.09	95.63	122.83	132.14
32	31.77	19.18	34.36	26.91	30.88	55.44	26.45	17.97	23.72	25.49
8536	8833	8604	9858	10691	9870	10418	12275	9821	9959	8730
1.310	1.289	1.279	1.081	0.848	1.192	1.156	1.57	1.351	1.349	0.881
18.43	20.15	19.44	17.67	17.5	23.15	44.09	23.35	19.51	17.6	13.75
111.76	100.23	87.64	65.11	105.25	104.93	254.04	112.72	96.06	97.39	76.35
184.43	180.14	131.87	49.68	142.53	127.28	193.47	200.49	181.35	191.65	115.78
0.44	0.14	0.16	0.16	0.14	0.56	0.06	0.47	0.13	0.13	0.33
4.52	4.52	4.66	4.68	4.93	4.98	5.06	5.32	5.52	5.58	5.83

463391_21	463390_56	463390_59	463391_13	463392_63	463392_85	463391_60	463388_94	463392_8	463391_09	463392_23
193	273	223	420	350	308	159	217	198	519	211
65	22	44	19	23.2	28.41	16	15.35	25.1	17	25.56
1.82	0.495	0.279	0.332	0.45	2.11	0.119	2.36	0.504	0.079	0.257
0.74	0.381	0.516	0.39	0.296	0.34	0.405	0.576	0.413	0.415	0.382
628.09	823.9	384.23	892.39	383.01	1261.73	572.55	1031.83	419.48	1107.08	482.09
1.665	1.533	1.421	1.86	1.389	1.98	3.14	2	1.554	1.83	1.99
0.541	0.363	0.428	0.1341	0.428	0.533	0.356	0.381	0.312	0.0782	0.368
21.7	10.95	8.85	7.16	11.72	25.58	10.02	15.05	12.02	5.35	9.4
1.27	0.481	0.252	0.518	0.41	1.389	0.305	0.601	0.467	0.364	0.231
14.25	6.77	2.99	7.9	3.87	17.5	3.03	6.28	3.97	6.1	2.3
14.1	9.14	3.76	11.48	3.83	17.35	4.25	8.06	4.17	9.99	2.95
2.46	1.013	0.607	0.551	0.507	1.59	0.297	0.936	0.654	0.141	0.329
35.02	33.46	14.58	40.04	12.6	63.01	17.58	29.12	13.57	39.77	12.89
7.86	8.93	3.8	9.96	3.3	15.54	5.16	8.31	3.83	10.46	3.73
75.76	92.73	42.55	100.65	38	153.6	57.39	97.41	42.77	113.67	46.58
21.82	29.46	13.77	30.97	13.13	46.73	19.58	32.15	14.29	37.53	15.55
82.69	121.19	59.22	128	61.21	179.59	83.2	137.3	61.51	162.06	68.95
15.51	22.64	11.62	24.59	13.28	32.82	16.36	26.45	13.01	32.58	14.22
125.81	193.28	102.29	214.1	125.66	266.64	142.52	231.62	117.74	274.67	125.51
23.15	35.98	20.36	40.04	27.28	48.98	27.17	44.33	23.39	55.43	23.73
7679	8099	7492	9576	9086	9677	9135	10423	10349	10252	10010
1.019	1.135	0.865	1.134	0.965	1.390	1.760	0.950	0.970	0.910	1.201
35.62	12.82	5.19	33.07	25.26	40.14	13.79	27.77	17.89	32.63	14.87
191.71	63.98	27.35	185.97	113.13	202.67	85.39	185.55	102.64	154.15	79.24
152.02	57.12	29.25	124.08	161.27	216.07	115.93	244.64	199.6	157.8	159.79
0.34	0.18	0.25	0.08	0.22	0.15	0.11	0.19	0.27	0.02	0.16
6.30	6.31	6.49	6.54	6.73	7.16	7.32	7.57	7.58	7.63	7.76

463392_45	463391_12	463390_10	463391_24	463392_20	463392_28	463390_24	463390_71	463390_70	463392_83	463390_33
233	179	139	220	211	265	236	171	252	178	226
12.09	26	19	43	29.68	18.89	23	20	23	621.23	19
0.666	0.386	0.375	0.355	0.307	1.249	0.3	0.34	1.16	2.03	-
0.466	0.519	0.437	0.686	0.342	0.318	0.525	0.463	0.448	0.293	0.38
974.2	459.54	307.15	473.46	325.55	833.86	686.18	405.75	1158.76	353.61	608.56
1.96	1.92	1.49	4.82	1.511	1.83	2.57	2.17	2.18	2.96	2.15
0.548	0.298	0.1526	0.518	0.271	0.315	0.176	0.202	0.232	0.164	0.129
20	8.24	6.67	16.29	9.02	15.63	11.65	10.87	20.38	5.76	9.32
0.68	0.203	0.251	0.435	0.224	0.576	0.485	0.347	1.056	0.1093	0.342
8.71	2.11	1.98	3.83	2.23	6.13	6.33	2.99	13.57	1.409	4.94
11.22	2.87	2.33	3.88	2.48	7.79	7.38	2.72	15.4	2	6.13
0.895	0.299	0.409	0.6	0.416	0.826	0.643	0.443	1.4	0.164	0.73
38.53	13.19	8.35	12.54	9.78	27.2	27.62	11.55	53.82	8.99	21.33
9.88	3.96	2.47	3.88	2.56	7.36	7.32	3.35	12.77	2.84	6.11
104.52	46.51	30.11	45.65	31.13	84.54	73.04	40.78	133.55	32.45	68.32
32.82	16.23	10.55	15.65	10.48	27.52	23.47	14.19	40.09	11.64	21.32
134	69.41	47.59	72.78	47.97	118.96	97	64.15	159.25	52.02	89.04
25.61	14.16	10.86	16.36	9.97	22.64	19.47	13.31	30.14	10.72	18.19
217.75	125.21	97.16	150.05	93.84	196.45	168.22	118.16	249.61	97.55	156.27
39.14	23.85	19.76	30.1	17.92	36.94	29.53	23.23	45.42	19.01	29.03
9400	9598	9961	9581	9913	9040	8914	8694	8235	9554	10077
1.088	1.281	0.864	3.120	0.814	1.256	1.158	1.252	1.04	1.083	1.2
29.08	13.73	14.4	34.56	12.97	29.8	15.23	17.65	21.94	10.95	10.72
162.4	75.15	80.2	142.13	65.95	151.13	86.87	115.16	127.37	68.66	58.6
189.41	138.4	183.56	354.96	108.77	249.75	94.16	205.23	107.29	129.51	64.01
0.13	0.15	0.28	0.26	0.26	0.17	0.14	0.24	0.15	0.12	0.20
7.89	8.06	8.20	8.26	8.81	8.83	9.60	9.88	9.91	10.35	10.68

463391_50	463390_21	463392_26	463391_16	463388_88	463392_12	463390_75	463392_56	463392_44	463391_32	463390_37
186	144	243	189	318	181	163	205	219	207	178
27	21	20.94	25	49.14	24.94	18	21.7	20.18	18	33
0.661	0.379	0.865	0.703	3.19	0.38	0.151	0.112	0.157	0.306	0.272
0.659	0.396	0.299	0.603	1.18	0.27	0.448	0.266	0.345	0.478	0.341
413.47	417.61	841.8	598.73	667.12	401.16	431.37	521.92	572.39	813.79	457.09
2.29	1.8	1.699	2.33	2.64	1.517	2.14	1.77	1.66	4.35	1.76
0.23	0.254	0.197	0.1641	0.288	0.1682	0.131	0.1252	0.1467	0.164	0.1206
14.99	14.25	14.71	12.71	23.38	11.08	7.59	8.07	8.76	13.82	9.15
0.458	0.348	0.475	0.4	0.747	0.278	0.164	0.181	0.178	0.378	0.216
4.04	3.32	7.32	4.15	6.8	2.57	1.55	2.33	2.61	5.54	2.11
4.06	3.52	10.53	4.81	6.82	2.17	1.86	3.63	3.87	7.43	2.57
1.177	0.542	1.162	0.776	2.5	0.392	0.398	0.261	0.267	0.535	0.427
13.08	11.71	34.86	19.09	21.59	10.12	9.65	14.6	17.4	29.9	13.55
3.84	3.59	8.62	5.19	6.34	3.09	3.17	4.46	5.01	7.61	3.66
44.67	40.48	87.32	60.69	70.35	37.95	41.16	51.77	57.77	91.89	45.79
14.33	14.05	27.93	19.89	22.17	13.33	14.44	17.34	19.36	28.83	16.04
62.73	64.82	112.61	86.4	93.79	61.86	70.55	77.89	85.77	118.85	71.92
13.04	13.43	21.36	17.6	19.8	12.48	15.84	15.56	17.28	22.61	15.09
113.41	124.01	181.76	150.82	175.57	111.03	145.06	135.21	150.7	195.54	130.53
22.19	23.5	34.54	29.33	32.91	21.52	30.96	26.01	29.19	36.02	25.49
8792	9108	9325	9400	9584	9293	9129	9510	9763	9519	9512
1.273	1.137	1.207	1.502	1.463	1.175	1.246	1.214	1.231	2.310	1.178
19.23	16.81	15.19	20.54	19.3	16.47	28.42	15.43	16.35	13.94	15.11
106.99	90.2	75.27	118.72	118.4	86.87	159.3	80.03	92.14	81.08	87.29
160.7	171.03	70.08	213.22	251.98	197.44	209.98	139.27	154.29	115.28	169.2
0.49	0.26	0.19	0.25	0.63	0.26	0.29	0.11	0.10	0.11	0.22
11.12	11.54	11.57	11.94	12.13	12.33	12.46	12.90	13.05	13.36	13.64

463392_16	463390_16	463391_33	463392_35	463391_59	463392_37	463390_09	463392_80	463390_76	463390_69	463390_11
200	137	167	142	203	222	186	155	301	139	161
33.65	31	10	19.39	44	32.39	21	15.65	32	31	16
2.22	0.448	0.365	0.237	0.221	0.189	0.231	0.419	0.769	0.157	0.201
0.415	0.34	0.531	0.278	0.467	0.313	0.306	0.34	0.243	0.248	0.381
484.99	372.35	571.24	283.84	473.02	408.06	472.33	358.18	855.95	327.76	618.26
1.91	1.636	7.03	1.501	2.24	1.73	1.722	2.13	2.17	1.69	1.97
0.252	0.0829	0.22	0.229	0.2	0.0757	0.069	0.254	0.0521	0.0562	0.0534
15.73	5.81	13.36	11.09	16.83	6.88	8.24	15.23	11.81	6.95	10.99
0.276	0.1118	0.215	0.1409	0.323	0.131	0.206	0.184	0.499	0.149	0.368
2.8	1.468	2.32	1.429	3.05	1.67	2.43	1.85	7.58	1.523	5.59
3.47	2.24	3.16	1.84	4.18	2.67	3.39	2.37	10.41	2.12	7.46
0.61	0.226	0.362	0.261	0.731	0.246	0.377	0.287	0.68	0.271	0.598
13.73	9.45	15.58	7.48	14.09	11.7	13.44	9.76	37.1	7.86	26.19
3.91	2.84	4.6	2.24	4.13	3.23	3.95	2.84	9.38	2.6	6.62
46.12	35.3	57.25	26.77	45.28	39.59	47.55	35.19	99.21	31.01	68.24
15.66	12.76	20.96	9.2	16.35	14.1	15.78	12.04	31.28	11.48	21.61
68.05	59.03	98.16	41.27	71.07	60.63	71.04	53.33	125.93	50.31	87.47
14.01	12.85	20.75	8.95	14.5	12.31	14.29	11.6	24.44	11.1	16.77
127.8	120.62	198.02	81.65	133.93	117.49	126.25	108.92	204.05	99.43	144.08
24.03	23.9	39.63	16.13	25.69	21.67	24	20.61	39.1	19.69	27.3
9933	9619	10347	10482	9450	10247	8923	10626	7808	8493	9088
1.170	1.024	4.150	1.039	0.996	1.102	0.971	1.348	1.243	1.084	0.991
25.35	11.73	16.2	15.55	26.63	10.5	13.79	19.62	24.5	12.89	10.72
137.42	69.97	89.57	83.58	117.67	54.11	75.09	110.55	132.09	68.2	59.08
232.52	171.03	159.31	177.11	163.47	109.31	129.64	223.67	118.9	155.62	39.45
0.27	0.15	0.16	0.22	0.29	0.13	0.17	0.18	0.11	0.20	0.13
14.36	14.53	14.79	14.86	15.94	16.63	16.63	16.96	17.63	18.28	18.87

463390_09	463392_80	463390_76	463390_69	463390_11	463390_68	463390_51	463390_61	463390_23	463390_26	463390_46
186	155	301	139	161	139	153	188	199	188	135
21	15.65	32	31	16	89	9	19	23	11	15
0.231	0.419	0.769	0.157	0.201	0.284	0.193	0.153	0.334	-	0.193
0.306	0.34	0.243	0.248	0.381	0.283	0.411	0.311	0.603	0.389	0.316
472.33	358.18	855.95	327.76	618.26	267.07	479.19	356.38	549.28	482.47	348.29
1.722	2.13	2.17	1.69	1.97	1.89	2.03	1.596	2.12	1.96	1.718
0.069	0.254	0.0521	0.0562	0.0534	0.1	0.129	0.1226	0.0871	0.1157	0.0555
8.24	15.23	11.81	6.95	10.99	10.8	15.07	9.02	10.05	13.35	7.19
0.206	0.184	0.499	0.149	0.368	0.186	0.26	0.0916	0.157	0.172	0.0974
2.43	1.85	7.58	1.523	5.59	1.89	3.86	1.229	2.16	2.68	1.182
3.39	2.37	10.41	2.12	7.46	2.65	4.22	1.94	3.76	3.98	1.96
0.377	0.287	0.68	0.271	0.598	0.397	0.4	0.185	0.233	0.411	0.153
13.44	9.76	37.1	7.86	26.19	9.66	18.56	9.05	16.85	16.33	8.11
3.95	2.84	9.38	2.6	6.62	2.47	5.04	2.72	4.68	4.62	2.7
47.55	35.19	99.21	31.01	68.24	28.98	58.05	34.7	56.07	49.98	32.73
15.78	12.04	31.28	11.48	21.61	9.23	17.91	12.09	19.09	17.16	11.72
71.04	53.33	125.93	50.31	87.47	40.56	76.72	55.33	82.64	73.89	53.04
14.29	11.6	24.44	11.1	16.77	8.45	15.04	11.97	16.88	14.71	11.29
126.25	108.92	204.05	99.43	144.08	77.32	133.46	108.11	148.92	128.98	103.77
24	20.61	39.1	19.69	27.3	15.22	24.94	21.22	28.57	24.66	20.71
8923	10626	7808	8493	9088	7422	9847	7839	9091	8605	8826
0.971	1.348	1.243	1.084	0.991	1.007	1.124	1.02	1.349	1.063	1.167
13.79	19.62	24.5	12.89	10.72	31.13	18.88	11.63	18.02	12.02	16.82
75.09	110.55	132.09	68.2	59.08	166.38	106.17	67.07	108.86	66.84	85.3
129.64	223.67	118.9	155.62	39.45	141.23	116.51	158.32	182.87	77.08	180.96
0.17	0.18	0.11	0.20	0.13	0.24	0.14	0.13	0.09	0.16	0.12
16.63	16.96	17.63	18.28	18.87	19.06	19.81	20.49	20.69	22.78	23.54

463390_26	463390_46	463390_39	463391_58	463392_24	463392_27	463390_36	463390_20	463392_33	463392_67	463392_22
188	135	173	118	195	185	182	196	112	200	166
11	15	17	22	19.95	19.17	14	17	12.38	23.42	20.91
-	0.193	0.189	0.332	0.244	0.191	0.372	-	0.293	0.192	0.223
0.389	0.316	0.335	0.665	0.341	0.217	0.356	0.268	0.323	0.301	0.339
482.47	348.29	481.85	336.48	469.18	442.32	771.55	433	394.19	501.35	397.91
1.96	1.718	2.02	3.56	1.96	1.767	1.654	1.821	3.04	2.32	1.822
0.1157	0.0555	0.055	0.163	0.0992	0.0443	0.0331	0.0751	0.1122	0.1182	0.067
13.35	7.19	8.23	21.02	12.49	7.73	8.84	11.13	12.64	17.05	10.59
0.172	0.0974	0.128	0.279	0.146	0.1144	0.181	0.126	0.1074	0.184	0.1232
2.68	1.182	2.18	2.86	1.9	1.706	3.11	1.93	1.204	2.56	1.529
3.98	1.96	3.13	2.85	2.93	2.58	5.53	2.74	2.2	3.48	2.34
0.411	0.153	0.29	0.667	0.255	0.284	0.367	0.231	0.162	0.351	0.223
16.33	8.11	13.12	9.28	13.38	12.3	23.5	13.81	7.54	15.49	10.3
4.62	2.7	4.12	2.85	3.77	3.55	6.85	3.69	2.85	4.3	3.28
49.98	32.73	47.98	31.97	45.46	43.49	77.79	42.7	35.52	49.68	37.55
17.16	11.72	16.46	11.54	15.48	15.15	25.89	14.77	12.83	16.63	12.87
73.89	53.04	74.31	53.75	69.92	66.47	109.66	64.19	61.08	71.44	58.77
14.71	11.29	15.68	11.92	14.45	13.79	21.37	13.4	12.99	14.19	11.87
128.98	103.77	141.13	113.54	130.59	123.32	186.98	120.26	114.29	125.93	109.06
24.66	20.71	26.79	23.41	25.37	23.67	34.85	23.07	21.47	23.39	21.7
8605	8826	9708	9283	11249	9632	8519	8741	11248	9523	9873
1.063	1.167	1.404	1.980	1.292	1.126	0.981	1.084	1.840	1.098	1.267
12.02	16.82	19.88	22.65	15.36	14.44	19.01	10.29	24.35	21.65	15.06
66.84	85.3	97.68	115.61	81.65	78.23	109.44	54.39	142.52	115.94	76.76
77.08	180.96	211.4	151.58	198.91	156.47	162.98	74.35	347.07	169.36	157.77
0.16	0.12	0.14	0.40	0.12	0.15	0.10	0.11	0.12	0.15	0.14
22.78	23.54	23.61	23.72	24.98	26.13	27.49	27.54	27.71	27.83	28.05

463390_26	463390_46
188	135
11	15
-	0.193
0.389	0.316
482.47	348.29
1.96	1.718
0.1157	0.0555
13.35	7.19
0.172	0.0974
2.68	1.182
3.98	1.96
0.411	0.153
16.33	8.11
4.62	2.7
49.98	32.73
17.16	11.72
73.89	53.04
14.71	11.29
128.98	103.77
24.66	20.71
8605	8826
1.063	1.167
12.02	16.82
66.84	85.3
77.08	180.96
0.16	0.12
22.78	23.54

Appendix B

Laser ablation LA-SF-ICP-MS analysis

Trace element concentrations were determined on thin sections by isotopic analyses using laser ablation sector-field inductively coupled plasma mass spectrometry (LA-SF-ICP-MS) at the Geological Survey of Denmark and Greenland (GEUS). A UP213 frequency-quintupled Nd:YAG solid state laser system from New Wave Research (Fremont, CA) employing two-volume cell technology was coupled to an ELEMENT 2 double-focusing single-collector magnetic SF-ICP-MS from Thermo-Fisher Scientific. The mass spectrometer was equipped with a Fassel-type quartz torch shielded with a grounded Pt electrode and a quartz bonnet. Operating conditions and data acquisition parameters are listed here on the right.

To ensure stable laser output energy, a laser warm-up time of 15-20 minutes were applied before operation, providing stable laser power and flat craters by a "resonator-flat" laser beam. The mass spectrometer was run for min. one hour before analyses to stabilize the background signal. Prior to loading, samples and standards were carefully cleaned with ethanol to remove surface contamination. After sample insertion the ablation cell was purged with helium carrier gas for a minimum of 15 minutes to minimize gas blank level. Helium was used as carrier gas for the ablated material and was mixed with argon make-up gas ca. 0.5 m before entering the plasma.

The ICP-MS was optimised for dry plasma conditions through continuous linear ablation of the NIST 612 glass standard. The signal-to-noise ratios were maximized for isotopes in the middle and heavy isotopic mass range while opting for low element-oxide production levels by minimising the $^{156}CeO/^{140}Ce$ and $^{254}UO_2/^{238}U$ ratios. Instrumental drift was minimized by using a standard-sample-standard analysis protocol, bracketing 10 sample analyses by 2-4 measurements of the NIST-612 standard. The quality of the standard measurements was controlled by NIST-614 (nominal trace element conc. ~ 1 ppm) and NIST-612 glasses measured as known-unknown during the analytical sequence.

Data were acquired from single spot analysis of 25 or 40 µm, using nominal laser fluence of 10 J/cm^2 and a pulse rate of 10 Hz. Two different analysis conditions using slightly different sampling times were employed to improve precision of a first round of analyses. Spot size and laser output energy was kept constant during individual analysis sequences. Total acquisition time for single analyses were ~83 sec., including 30 sec. gas blank measurement followed by laser ablation for 30 sec. and washout for 20 sec. Factory-supplied software from Thermo-Fisher Scientific was used for the acquisition of the transient data, obtained through pre-set spot locations. Data reduction and determination of concentrations was performed off-line through the software Iolite (Hellstrom et al. 2008, Paton et al. 2011).

LA-SF-ICP-MS operating and data acquisition parameters

Laser system	**New Wave Research UP213 solid state Nd:YAG laser with aperture imaging**
Laser wavelength	213 nm (Nd:YAG)
Laser mode	Q-switched (Nd:YAG)
Nominal pulse width	4 ns (Nd:YAG)
Repetition rate	10 Hz
Spot sizes (diameter)	25 µm (most) and 40 µm (a few analyses)
Energy density on sample	10 J/cm^2 (homogenized energy distribution)
Ablation cell	Standard type (small) volume cell
Ablation cell gas flow rates	330-370 ml/min He
Tubing for gas flow	Tygon S-50 HL (5 mm i.d.)
Laser beam focus	Fixed at sample surface

ICP-MS	**Thermo-Fisher Scientific ELEMENT 2 double-focusing sector-field ICP-MS**
Interface cones	Ni sampler and skimmer cone
Detector type	single-collector discrete dynode electron multiplier
Detector mode	cross-calibrated pulse counting and analogue
Detector vacuum	10^{-7} mbar (during analysis)
Argon gas flow rates (l/min):	
Plasma	16
Auxiliary	0.90
Sample	0.94-0.97
RF power	1115-1120 W
Lenses (V):	
Extraction	-2000
Focus	-870
X-Deflection	4.25
Y-Deflection	-3.50
Shape	107
SEM potential	2375 V

Data acquisition and processing	
Isotopes measured (sampling times in ms in brackets)	^{29}Si (10), ^{31}P (10/20), ^{43}Ca (10), ^{44}Ca (5), ^{49}Ti (10/20), ^{51}V (10/20), ^{88}Sr (10/20), ^{89}Y (10/20), ^{93}Nb (10/20), ^{139}La (20/100), ^{140}Ce (10/20), ^{141}Pr (10/20), ^{146}Nd (10/20), ^{147}Sm (10/30), ^{153}Eu (10), ^{157}Gd (10), ^{159}Tb (10), ^{163}Dy (10), ^{165}Ho (10), ^{166}Er (10), ^{169}Tm (10), ^{172}Yb (10), ^{175}Lu (10), ^{178}Hf (10), ^{181}Ta (10), ^{206}Pb (10), ^{207}Pb (10), ^{232}Th (10), ^{238}U (10)
Settling times	1 ms; 10-34 ms at magnet jumping (7 jumps)
Integration window	10 % except Si (100%) and P,Ca, Ti, V (80 %)
Samples per peak	1
Aquisition mode	Time resolved analysis
Scan type	E-scan
Detection mode	Both
Integration type	Average
Mass resolution	Low (300)
Oxide production rate	Tuned to $\leq$ 0.6% UO_2 ($^{254}UO_2/^{238}U$)
Analysis duration	30 s. blank, 30 s. ablation and 20 s. washout.
Software for data reduction	Iolite vers. 2.2 (Hellstrom et al. 2008)
External standardization	NIST-612
Internal standard isotopes	^{29}Si

Tonny Bernt Thomsen
November 2012
Petrologi og malmgeologi
Geologiske Undersøgelser for Danmark og Grønland (GEUS)

Tidigare skrifter i serien "Examensarbeten i Geologi vid Lunds universitet":

326. Qvarnström, Martin, 2012: An interpretation of oncoid mass-occurrence during the Late Silurian Lau Event, Gotland, Sweden. (15 hp)
327. Ulmius, Jan, 2013: P-T evolution of paragneisses and amphibolites from Romeleåsen, Scania, southernmost Sweden. (45 hp)
328. Hultin Eriksson, Elin, 2013: Resistivitets-mätningar för avgränsning av lak-vattenplym från Kejsarkullens deponis infiltrationsområde. (15 hp)
329. Mozafari Amiri, Nasim, 2013: Field relations, petrography and 40Ar/39Ar cooling ages of hornblende in a part of the eclogite-bearing domain, Sveconorwegian Orogen. (45 hp)
330. Saeed, Muhammad, 2013: Sedimentology and palynofacies analysis of Jurassic rocks Eriksdal, Skåne, Sweden. (45 hp)
331. Khan, Mansoor, 2013: Relation between sediment flux variation and land use patterns along the Swedish Baltic Sea coast. (45 hp)
332. Bernhardson, Martin, 2013: Ice advance-retreat sediment successions along the Logata River, Taymyr Peninsula, Arctic Siberia. (45 hp)
333. Shrestha, Rajendra, 2013: Optically Stimulated Luminescence (OSL) dating of aeolian sediments of Skåne, south Sweden. (45 hp)
334. Fullerton, Wayne, 2013: The Kalgoorlie Gold: A review of factors of formation for a giant gold deposit. (15 hp)
335. Hansson, Anton, 2013: A dendroclimatic study at Store Mosse, South Sweden – climatic and hydrologic impacts on recent Scots Pine (*Pinus sylvestris*) growth dynamics. (45 hp)
336. Nilsson, Lawrence, 2013: The alteration mineralogy of Svartliden, Sweden. (30 hp)
337. Bou-Rabee, Donna, 2013: Investigations of a stalactite from Al Hota cave in Oman and its implications for palaeoclimatic reconstructions. (45 hp)
338. Florén, Sara, 2013: Geologisk guide till Söderåsen – 17 geologiskt intressanta platser att besöka. (15 hp)
339. Kullberg, Sara, 2013: Asbestkontamination av dricksvatten och associerade risker. (15 hp)
340. Kihlén, Robin, 2013: Geofysiska resistivitetsmätingar i Sjöcrona Park, Helsingborg, undersökning av områdets geologiska egenskaper samt 3D modellering i GeoScene3D. (15 hp)
341. Linders, Wictor, 2013: Geofysiska IP-undersökningar och 3D-modellering av geofysiska samt geotekniska resultat i GeoScene3D, Sjöcrona Park, Helsingborg, Sverige. (15 hp)
342. Sidenmark, Jessica, 2013: A reconnaissance study of Rävliden VHMS-deposit, northern Sweden. (15 hp)
343. Adamsson, Linda, 2013: Peat stratigraphical study of hydrological conditions at Stass Mosse, southern Sweden, and the relation to Holocene bog-pine growth. (45 hp)
344. Gunterberg, Linnéa, 2013: Oil occurrences in crystalline basement rocks, southern Norway – comparison with deeply weathered basement rocks in southern Sweden. (15 hp)
345. Peterffy, Olof, 2013: Evidence of epibenthic microbial mats in Early Jurassic (Sinemurian) tidal deposits, Kulla Gunnarstorp, southern Sweden. (15 hp)
346. Sigeman, Hanna, 2013: Early life and its implications for astrobiology – a case study from Bitter Springs Chert, Australia. (15 hp)
347. Glommé, Alexandra, 2013: Texturella studier och analyser av baddeleyitomvandlingar i zirkon, exempel från sydöstra Ghana. (15 hp)
348. Brådenmark, Niklas, 2013: Alunskiffer på Öland – stratigrafi, utbredning, mäktigheter samt kemiska och fysikaliska egenskaper. (15 hp)
349. Jalnefur Andersson, Evelina, 2013: En MIFO fas 1-inventering av fyra potentiellt förorenade områden i Jönköpings län. (15 hp)
350. Eklöv Pettersson, Anna, 2013: Monazit i Obbhult-komplexet: en pilotstudie. (15 hp)
351. Acevedo Suez, Fernando, 2013: The reliability of the first generation infrared refractometers. (15 hp)
352. Murase, Takemi, 2013: Närkes alunskiffer – utbredning, beskaffenhet och oljeinnehåll. (15 hp)
353. Sjöstedt, Tony, 2013: Geoenergi – utvärdering baserad på ekonomiska och drifttekniska resultat av ett passivt geoenergisystem med värmeuttag ur berg

i bostadsrättsföreningen Mandolinen i Lund. (15 hp)

354. Sigfúsdóttir, Thorbjörg, 2013: A sedimentological and stratigraphical study of Veiki moraine in northernmost Sweden. (45 hp)
355. Månsson, Anna, 2013: Hydrogeologisk kartering av Hultan, Sjöbo kommun. (15 hp)
356. Larsson, Emilie, 2013: Identifying the Cretaceous–Paleogene boundary in North Dakota, USA, using portable XRF. (15 hp)
357. Anagnostakis, Stavros, 2013: Upper Cretaceous coprolites from the Münster Basin (northwestern Germany) – a glimpse into the diet of extinct animals. (45 hp)
358. Olsson, Andreas, 2013: Monazite in metasediments from Stensjöstrand: A pilot study. (15 hp)
359. Westman, Malin, 2013: Betydelsen av raka borrhål för större geoenergisystem. (15 hp)
360. Åkesson, Christine, 2013: Pollen analytical and landscape reconstruction study at Lake Storsjön, southern Sweden, over the last 2000 years. (45 hp)
361. Andolfsson, Thomas, 2013: Analyses of thermal conductivity from mineral composition and analyses by use of Thermal Conductivity Scanner: A study of thermal properties in Scanian rock types. (45 hp)
362. Engström, Simon, 2013: Vad kan inneslutningar i zirkon berätta om Varbergscharnockiten, SV Sverige. (15 hp)
363. Jönsson, Ellen, 2013: Bevarat maginnehåll hos mosasaurier. (15 hp)
364. Cederberg, Julia, 2013: U-Pb baddeleyite dating of the Pará de Minas dyke swarm in the São Francisco craton (Brazil) – three generations in a single swarm. (45 hp)
365. Björk, Andreas, 2013: Mineralogisk och malmpetrografisk studie av disseminerade sulfider i rika och fattiga prover från Kleva. (15 hp)
366. Karlsson, Michelle, 2013: En MIFO fas 1-inventering av förorenade områden: Kvarnar med kvicksilverbetning Jönköpings län. (15 hp)
367. Michalchuk, Stephen P., 2013: The Säm fold structure: characterization of folding and metamorphism in a part of the eclogite-granulite region, Sveconorwegian orogen. (45 hp)
368. Praszkier, Aron, 2013: First evidence of Late Cretaceous decapod crustaceans from Åsen, southern Sweden. (15 hp)
369. Alexson, Johanna, 2013: Artificial groundwater recharge – is it possible in Mozambique? (15 hp)
370. Ehlorsson, Ludvig, 2013: Hydrogeologisk kartering av grundvattenmagasinet Åsumsfältet, Sjöbo. (15 hp)
371. Santsalo, Liina, 2013: The Jurassic extinction events and its relation to CO2 levels in the atmosphere: a case study on Early Jurassic fossil leaves. (15 hp)
372. Svantesson, Fredrik, 2013: Alunskiffern i Östergötland – utbredning, mäktigheter, stratigrafi och egenskaper. (15 hp)
373. Iqbal, Faisal Javed, 2013: Paleoecology and sedimentology of the Upper Cretaceous (Campanian), marine strata at Åsen, Kristianstad Basin, Southern Sweden, Scania. (45 hp)
374. Kristinsdóttir, Bára Dröfn, 2013: U-Pb, O and Lu-Hf isotope ratios of detrital zircon from Ghana, West-African Craton – Formation of juvenile, Palaeoproterozoic crust. (45 hp)
375. Grenholm, Mikael, 2014: The Birimian event in the Baoulé Mossi domain (West African Craton) — regional and global context. (45 hp)
376. Hafnadóttir, Marín Ósk, 2014: Understanding igneous processes through zircon trace element systematics: prospects and pitfalls. (45 hp)

LUNDS UNIVERSITET

Geologiska institutionen
Lunds universitet
Sölvegatan 12, 223 62 Lund